

1. LEG 193 SYNTHESIS: ANATOMY OF AN ACTIVE FELSIC-HOSTED HYDROTHERMAL SYSTEM, EASTERN MANUS BASIN, PAPUA NEW GUINEA¹

R.A. Binns,^{2,3} F.J.A.S. Barriga,^{4,5} and D.J. Miller⁶

ABSTRACT

In the Ocean Drilling Program's only foray to an active seafloor hydrothermal system hosted by felsic volcanic rocks at a convergent plate margin, deep penetrations were achieved at two contrasted sites within the PACMANUS field (Manus backarc basin, Papua New Guinea). Just 1.0 km apart, these sites are characterized, respectively, by diffuse low-temperature venting at the seabed (Site 1188, Snowcap site; 1650 meters below sea level [mbsl]) and focused high-temperature venting (Site 1189, Roman Ruins; 1700 mbsl). Shallow holes at a background location remote from known hydrothermal activity (Site 1190) and at a second high-temperature chimney field (Site 1191, Satanic Mills) failed to drill beyond unaltered felsic lavas which at Sites 1188 and 1189 form an impervious cap (as thick as 35 m) to an underlying, pervasively altered lava sequence with occasional volcanoclastic horizons.

To the maximum depth drilled (387 meters below seafloor [mbsf]), alteration assemblages are characterized by clay minerals and ubiquitous disseminated pyrite. Hydrothermal K-feldspar at Site 1189 differentiates it from Site 1188 where, by contrast, several intervals of pyrophyllite-bearing acid sulfate alteration suggest input from magmatic volatiles. At both deeply penetrated sites the dominant silica phase in alteration assemblages changes downhole from opal-A at the transition from overlying unaltered lava to cristobalite and then to quartz. The boundary between the cristobalite and quartz domains is gradational between 60 and 110 mbsf in Hole 1188A under Snowcap

¹Binns, R.A., Barriga, F.J.A.S., and Miller, D.J., 2007. Leg 193 synthesis: anatomy of an active felsic-hosted hydrothermal system, eastern Manus Basin, Papua New Guinea. *In* Barriga, F.J.A.S., Binns, R.A., Miller, D.J., and Herzig, P.M. (Eds.), *Proc. ODP, Sci. Results, 193*: College Station, TX (Ocean Drilling Program), 1–71.

doi:10.2973/odp.proc.sr.193.201.2007
²Division of Exploration and Mining, Commonwealth Scientific and Industrial Research Organisation (CSIRO), PO Box 136, North Ryde, NSW 1670, Australia.

Ray.Binns@csiro.au;
entex@acenet.com.au

³Department of Earth and Marine Sciences, Australian National University, Canberra ACT 0200, Australia.

⁴Creminer, Departamento Geologia, Faculdade de Ciencias, Universidade de Lisboa, Edifício C6, Campo Grande, 1749-016 Lisboa, Portugal.

⁵Museu Nacional de Historia Natural (Mineralogia e Geologia), Rua da Escola Politecnica 58, 1250-102 Lisboa, Portugal.

⁶Integrated Ocean Drilling Program, Texas A&M University, 1000 Discovery Drive, College Station TX 77845-9547, USA.

but is sharper and shallower (~25 mbsf) in Hole 1189A on the fringes of the Roman Ruins field. Hole 1189B, higher on the Roman Ruins mound, intersected a "Stockwork Zone" with abundant quartz \pm pyrite \pm anhydrite veins and breccia infills, from base of casing (31 mbsf) to ~110 mbsf, below which an abrupt change occurred to a "Lower Sequence" with interleaved cristobalite- and quartz-bearing assemblages and common preservation of igneous plagioclase. Only two thin intervals of sulfide-rich mineralization were encountered, both below the Roman Ruins chimney field.

Postcruise volcanic facies analyses based on logging data and cores with well-preserved fabrics, plus assessments of immobile element geochemistry for altered rocks referred against a local database for glassy lavas, establish that Pual Ridge is constructed from numerous lava flows averaging ~15 to 30 m thick and ranging from andesite to rhyodacite in composition, with dacites dominant. Investigations of alteration and mineralization support the concept of a single major hydrothermal event imposed at PACMANUS after accumulation of most of the Pual Ridge volcanic sequence. Different phases within this event, involving pronounced differences in fluid chemistry, created a variety of alteration styles yet to be fully unraveled. Much of the extensive subseafloor alteration may have been completed before uprise of high-temperature vent fluids that formed seabed chimneys.

Prominent alteration-related geochemical differences between Sites 1188 and 1189 include enrichments in potassium, barium, and uranium at Site 1189. Altered wallrocks in the Stockwork Zone of Hole 1189B have lost silica, but Si is more generally conserved at precursor levels. Leaching during hydrothermal alteration did not contribute significant base or precious metals, or barium, to seabed chimney deposits. At both sites hydrothermal alteration involves volume expansion arising from grain-scale dilation imposed by excess pore fluid pressures. Progressive dilation with nonreplacive deposition of sulfides and gangue minerals in open spaces is a dominant process in the two occurrences of subseafloor semimassive sulfide encountered below Roman Ruins.

Fluid inclusions in vein anhydrites provide conclusive evidence of phase separation ("boiling") within the PACMANUS hydrothermal system at temperatures exceeding 360°C, somewhat higher than alteration temperatures computed from oxygen isotope analyses of clay minerals but comparable with oxygen isotope temperature estimates for vein quartz. Strontium isotope characteristics of anhydrites from veins, breccia matrixes, and semimassive sulfides imply deposition from varied mixtures between seawater and high-temperature hydrothermal fluids. The latter are more radiogenic ($^{87}\text{Sr}/^{86}\text{Sr} = 0.7050$) than fresh lavas at Pual Ridge (basaltic andesite to rhyodacite; $^{87}\text{Sr}/^{86}\text{Sr} = 0.7036$) and so include a component of very deeply circulated seawater.

There is circumstantial evidence for a magmatic component in the high-temperature hydrothermal fluid. Hydrothermal alteration of the volcanic sequence at Pual Ridge may have been largely completed before the main mineralizing events. Excess fluid pressures during both alteration and subsequent mineralization suggest a "pressure cooker" model whereby the subseafloor hydrothermal system is largely confined by a cap of impervious volcanics that become sporadically breached by hydrofracturing or tectonic processes to allow seafloor venting and sulfide deposition. Fluid flow within the PACMANUS system, especially that related to seabed venting, is governed by fractures rather than high porosity and permeability of the subseafloor rocks.

A vibrant microbial assemblage exists in the higher parts of the hydrothermal system (to ~130 mbsf). Below this the system appears sterile, but temperature limits for viability have not been established. Cultures at 60° and 90°C are dominated by *Geobacillus* sp. and *Deinococcus* sp., respectively. Whereas mineralized bacterial cells have been observed, seafloor biomineralization appears not to play an important role at PACMANUS.

INTRODUCTION

From earliest Archean time, felsic volcanic sequences and their associated intrusive rocks have been especially favorable hosts for a variety of valuable hydrothermal ore deposits, including massive polymetallic sulfide and porphyry-style copper-gold bodies. Ancient volcanic arcs or backarcs related to subduction at convergent plate margins are commonly the established or inferred geological setting for such mineral occurrences. Investigating hydrothermal activity in analogous modern settings has obvious merit as an approach to understanding ore genesis, a critical requirement for mineral exploration in older sequences.

Rare opportunities for analog research in economic geology arose following discoveries in the late 1970s of hot springs and polymetallic sulfides on the floor of the Galapagos spreading center (Corliss et al., 1979; Malahoff et al., 1983) and shortly thereafter of actively forming “black smoker chimneys” at 21°N on the East Pacific Rise (Francheteau et al., 1979; Spiess et al., 1980). An immediate and, at the time, novel outcome was recognition of hot and buoyant hydrothermal fluids that precipitate metallic sulfides directly where they vent onto the seafloor and mix with cold seawater. The discoveries also stimulated great interest in the associated chemosynthetic microbial communities and macrofauna, as well as the influence of hydrothermal venting on ocean chemistry. With such a diverse range of scientific interest and applications, the Ocean Drilling Program (ODP) developed an early priority for projects that would examine seafloor phenomena and processes below active vent fields. The first ODP expeditions to hydrothermal sites focused on divergent plate boundaries at mid-ocean spreading ridges, where mafic volcanism predominates. During Leg 139 (Mottl, Davis, Fisher, and Slack, 1994) Middle Valley was drilled on the thickly sedimented Juan de Fuca Ridge, northeastern Pacific Ocean. During Leg 158 (Herzig, Humphris, Miller, and Zierenberg, 1998) the Trans-Atlantic Geotraverse (TAG) site on the sediment-starved Mid-Atlantic Ridge was investigated. During Leg 169 (Zierenberg, Fouquet, Miller, and Normark, 2000) Middle Valley was revisited and Escanaba Trough on nearby Gorda Ridge was investigated.

Mineral deposits formed at oceanic spreading centers are usually fated to become lost to the geological record through ultimate subduction. Although major advances of fundamental importance to ore genesis arose from drilling mid-ocean basaltic settings, it was desirable to extend ODP's program to a conceptually more appropriate active hydrothermal site associated with felsic volcanism in a convergent margin tectonic setting. Accordingly, Leg 193 was planned and undertaken at the PACMANUS hydrothermal site, discovered in 1991 (Binns and Scott, 1993) on Pual Ridge, a dacite-dominated neovolcanic edifice in the eastern Manus backarc basin of the Bismarck Sea, Papua New Guinea.

Leg 193 departed from Guam on 14 November 2000, occupied station from 18 November to 29 December, and ended at Townsville (Australia) on 3 January 2001. This synthesis chapter summarizes the plethora of frontier research subsequently conducted at laboratories in Australia, Canada, Germany, Japan, Korea, Norway, Papua New Guinea, United Kingdom, United States, and Portugal by shipboard scientific participants. In addition to work now published, results of unpublished and uncompleted projects are included where known to the authors.

SCIENTIFIC OBJECTIVES

The general goal of Leg 193 was to delineate the subsurface characteristics of the PACMANUS hydrothermal system, particularly the volcanic architecture of Pual Ridge on which it is situated, deep-seated mineralization and alteration patterns, and structural and other characteristics that dictate the nature and flow of hydrothermal fluids. Testing for microbial life within the system and collecting subseafloor hydrothermal fluids were additional objectives.

Specific objectives included the following:

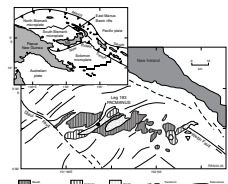
1. Establish whether Pual Ridge, the edifice hosting PACMANUS, was constructed as a “layer cake” sequence of lavas or, alternatively, by inflation of large lava domes or shallow intrusions.
2. Assess the temporal interplay between volcanic and hydrothermal activity, using any older sedimentary, ferruginous oxide, or massive sulfide horizons concealed within the lava sequence.
3. Compare and contrast alteration and mineralization characteristics and processes below sites of focused high-temperature venting and diffuse low-temperature venting, respectively.
4. Sample and delineate the characteristics and sources of hydrothermal fluids within the PACMANUS system.
5. Assess the source or sources of base metals and precious metals and seek explanations for the elevated contents of copper, zinc, silver, and gold in massive sulfide chimneys at the PACMANUS seafloor.
6. Delineate fluid pathways within the system, and establish a hydrologic model from structural patterns, physical properties, and isotope geochemical evidence in fresh and altered bedrocks.
7. Establish the nature and extent of microbial activity and the potential for biomineralization within the hydrothermal system.

Our ability to achieve these objectives was constrained by a number of factors, including poor core recovery, the small number of deep penetrations achieved relative to the evident complexity of the hydrothermal system, and absence or scarcity of certain anticipated phenomena—especially subsurface massive sulfides.

GEOLOGICAL SETTING

The Manus backarc basin, constituting two microplates (North Bismarck and South Bismarck) set between opposed fossil and active subduction zones, lies within the complex zone of oblique convergence between the Australian and Pacific plates (Fig. F1). Northward subduction of the oceanic Solomon microplate beneath the South Bismarck

F1. Tectonic setting and regional seafloor geology of eastern Manus Basin, p. 50.



microplate, where basement formed by earlier Tertiary arc volcanism and backarc spreading, currently occurs along the New Britain Trench with associated eruption of young arc volcanoes along the concave northern side of the island of New Britain. Present-day structure of the basin is dominated by seafloor spreading in the center and extensional rifting in the east, the various segments delineated by sinistral transform faults (Martinez and Taylor, 1996). According to Macpherson et al. (1998, 2000) isotopic evidence in submarine lavas indicates presence of an active mantle plume under the central and western portions of the Manus Basin, but it is unclear to what extent this influenced the eastern portion where Leg 193 was conducted.

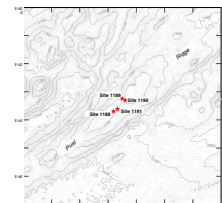
The eastern Manus Basin is a pull-apart rift zone of distributed extension on low-angle normal faults between two transform or transfer faults. An east-west-trending belt of mostly high standing neovolcanic edifices overlying early Tertiary arc volcanic crust and younger Tertiary–Holocene sediment-filled half-grabens links the active ends of the bounding Djuul and Weitin transforms (Fig. F1). Individual edifices are variously dominated by lavas ranging from picritic basalt to dacite-rhyodacite with similar isotopic and trace element geochemistry (Binns et al., 1996, 2002b; Kamenetsky et al., 2001) to subaerial arc volcanoes on the island of New Britain to the south (Woodhead and Johnson, 1993).

Pual Ridge, a linear edifice trending northeast at about the center of this neovolcanic belt, stands some 500–600 m above basaltic andesite- and sediment-floored valleys to the east and west, respectively (Fig. F2). Seafloor outcrops are predominantly dacitic to rhyodacitic in composition near PACMANUS, although consanguineous basaltic andesites and andesites occur as small, isolated cones along the crest and flanks and as more extensive flows on the northwestern flank and southern end of Pual Ridge. The eastern side of Pual Ridge has a terraced morphology resulting from a sequence of subhorizontal dacite flows ~30 m thick that here forms the hanging wall of a major normal fault (Gennerich, 2001). Glassy flows along the crest have negligible to minor sediment cover and vary in structure from lobate or tube flows and sheet flows to block lava with increasingly siliceous character (Waters et al., 1996). Local pockets of hyaloclastite are present, including spalled surficial tube pumice. The lavas of Pual Ridge are vesicular, and conspicuously aphyric or sparsely porphyritic compared to most other eastern Manus volcanic edifices. In the vicinity of PACMANUS, lava compositions tend to fall into three compositional groups whose distributions and topographic relationships suggest individual flows or lava fields from 200 m to 1 km in extent (Fig. F3).

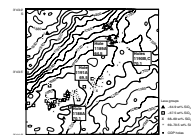
Isolated hydrothermal deposits occur for some 13 km along the crest of Pual Ridge (Binns and Scott, 1993; Scott and Binns, 1995; Binns et al., 1995; Shipboard Scientific Party, 2002a). The more significant active deposits extend for 2 km between two elongate highs on the ridge crest (Fig. F2). These lie between 1650 and 1750 meters below sea level (mbsl) and are collectively named the PACMANUS hydrothermal field after the 1991 discovery expedition (Binns and Scott, 1993).

Three of the five main hydrothermal centers within the PACMANUS field were examined during Leg 193 (Fig. F4). Roman Ruins (1680–1690 mbsl; Site 1189) and Satanic Mills (1685–1695 mbsl; Site 1191) are 100- to 200-m-wide sites of focused high-temperature activity expelling acid fluids (pH = 2.3–3.5) at temperatures commonly above 250°C (Douville et al., 1999). Chimneys venting boiling fluid (356°C) were recently discovered at a site on the southern extension of Satanic Mills (Tivey et al., 2006; Seewald et al., 2006). Sulfide chimneys range to as tall as 20 m

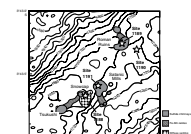
F2. Bathymetric setting of Leg 193 drill sites, p. 51.



F3. Distribution of lava groups in the PACMANUS vicinity, p. 52.



F4. Distribution of hydrothermal deposit types, p. 53.



but are generally 1–3 m high. They rise directly above largely unaltered dacite-rhyodacite lavas or surmount mounds of fallen chimney fragments and Fe oxyhydroxide deposit. Tsukushi (~1665 mbsl) and Rogers Ruins (~1700 mbsl) are additional chimney fields at PACMANUS not examined during Leg 193 (Fig. F4).

By contrast, Snowcap (1635–1645 mbsl; Site 1188) is a broad knoll (10–15 m high × 150 m across) where both fresh and altered volcanic outcrops are interspersed with flat patches of gravely to sandy sediment (containing both altered and fresh volcanic clasts), metalliferous hemipelagic ooze, and dark surficial Mn-Fe oxide crusts. Some active sulfide chimneys occur on the lower western flank of Snowcap. Shimmering low-temperature venting is extensive across the crest, especially at the edges of altered outcrops (measured at 6°C but likely higher locally) and within patches of white to cream-colored microbial mat. Submersible and deep-tow video observations at Snowcap include several instances where younger glassy dacite lava has flowed over altered dacite-rhyodacite outcrops. Dredge samples of the glassy lava fall into the 67.5 wt% SiO₂ youngest category of Figure F3, and one contains a 5-cm xenolith of pyrite-bearing, totally altered dacite (Binns et al., 2002b). Samples of altered rock collected from Snowcap by dredge, grab, and submersible exhibit lapilli-like structures, some with remnant glassy rhyodacite kernels whose vesicle and microlite orientations establish that the parent rock was a coarse hyaloclastite. Alteration is dominated by cristobalite, natroalunite, diaspore, illite-smectite, and native sulfur (Yeats et al., 2000; Binns et al., 2002b). Some samples contain fine networks of pyrite veins. The “acid sulfate” alteration assemblage, including globules and layers of formerly molten sulfur implying disproportionation of SO₂, suggests involvement of magmatic components in the responsible fluids and higher temperatures than those measured at shimmering vents. Minor occurrences of similar alteration have been dredged along with dominant fresh lavas at Satanic Mills and Roman Ruins (Binns and Scott, 1993; Binns et al., 2002b; Giorgetti et al., 2006).

PACMANUS chimneys are particularly rich in chalcopyrite and sphalerite and contain high levels of gold and silver (Parr et al., 1995, 2003; Moss and Scott, 2001; Binns et al., 2002b; Binns, 2004). Barite is the principal gangue mineral, although anhydrite is present in some chimneys. Chimneys at Tsukushi and the western flank of Snowcap tend to be richer in Pb and poorer in Cu and Au than those from Roman Ruins, Satanic Mills, or Rogers Ruins. Elevated contents of “magmatophile” trace elements (As, Sb, Bi, Te, In, Tl, and Mo) unlikely to be sufficiently available by leaching processes suggest involvement of an exsolved magmatic fluid component in the PACMANUS hydrothermal system, and this is supported by low sulfur isotope ratios in chimney sulfides (Binns et al., 2002b). On both criteria the magmatic component is greatest at Satanic Mills and the chimneys fringing Snowcap. Douville et al. (1999) ascribe exceptionally high SO₄, H₂S, and F contents of PACMANUS vent fluids to incorporation of magmatic volatiles into the hydrothermal system. Ishibashi et al. (1996) also infer significant magmatic input from gas compositions in vent fluids.

In addition to occurrences within or linking the chimney fields (Fig. F4), independent patches and spires of Fe-Mn-Si oxide deposit meters to tens of meters across are scattered along the crest of Pual Ridge (Heath et al., 2000; Binns et al., 2002b). Some actively vent shimmering clear fluid measured at temperatures as high as 73°C (BIOACCESS'98 cruise; C.J. Yeats, pers. comm., 1998). The principal constituents are Fe oxyhy-

dioxide and opaline silica, with Mn oxides at the outer surface of some samples. Filamentous microfabrics denote microbial activity during formation.

KEY OUTCOMES OF THE DRILLING LEG

To achieve its objectives the initial strategy for Leg 193 was to drill at three contrasting sites (Fig. F4): (1) the Snowcap field of altered outcrops with low-temperature diffuse venting (Site 1188), (2) the Roman Ruins field of chimneys with high-temperature focused venting (Site 1189) located some 1000 m northeast of Snowcap, and (3) “background” Site 1190, lying remote from known hydrothermal deposits and 240 m east-southeast of Roman Ruins. With these, we expected to establish both lateral and vertical variations in alteration and mineralization patterns in relation to the contrasted seafloor vent styles and a reference section of unaltered volcanic rocks. Only shallow penetration to 17.2 meters below seafloor (mbsf) in fresh rhyodacite was achieved with three holes at “background” Site 1190 (Holes 1190A, 1190B, and 1190C). During a brief time window made available by operations, Hole 1191A was drilled at an additional high-temperature site, the Satanic Mills chimney field (Site 1191; ~300 m north-northeast of Snowcap), but limited penetration (20.1 mbsf) into fresh dacite-rhyodacite with sulfide films and alteration along fractures did not provide the anticipated comparison with Roman Ruins.

The major achievements of Leg 193 were deep-cored penetrations at Sites 1188 and 1189, together with wireline logging and deployment of logging-while-drilling (LWD) in separate holes for each of these sites. At Snowcap (Site 1188), Hole 1188A was cored to 211.6 mbsf, whereas Hole 1188F, located 23 m away, was cored from 218.0 to 386.7 mbsf below 190 m of casing. In combination, these holes penetrated the upper two-thirds of the Pual Ridge volcanic edifice. Hole 1188A was initially drilled through ~35 m of fresh dacite/rhyodacite, a somewhat unexpected thickness considering its proximity to seabed outcrops of altered rock. Drilling then passed rapidly into pervasively altered volcanic rocks that persisted to the base of Hole 1188A and continued throughout the deeper Hole 1188F. Holes 1188C, 1188D, and 1188E were unsuccessful attempts to spud-in the deeper penetration hole. Hole 1188B in the same vicinity commenced as a successful LWD experiment to 72 mbsf, followed by deployment of the advanced diamond core bit that recovered only two samples of cristobalite-bearing altered dacite from hole fill before failing further penetration.

At Roman Ruins (Site 1189), Hole 1189A commenced between sulfide chimneys, and, after initially intersecting a thin unit of fresh dacite (~0.2 m recovered), it penetrated to 125.8 mbsf in pervasively altered volcanic rock. A 6-cm unit of semimassive sulfide was present at 107.7 mbsf (curated depth). In Hole 1189B, drilled beside an active chimney 35 m from Hole 1189A and 8 m higher on the Roman Ruins mound, both soft and hard rocks were encountered during initial hammer-in casing to 31 mbsf, then coring continued to 206.0 mbsf. Core recovery was exceptionally poor (<1%) within a rapidly penetrated “Stockwork Zone” (31–118 mbsf) of pyritic veins and breccias within altered volcanic rocks. The first sample (31.00 mbsf) was an 8-cm piece of semi-massive sulfide. Recovery in Hole 1189B improved (~19%) for a “Lower Sequence” of variably altered volcanic rocks from ~118 to 206.0 mbsf, prominently distinguished from the overlying Stockwork Zone in bore-

hole resistivity imagery by a more widely spaced, blocky fracture pattern. Hole 1189C in the same vicinity was an uncored LWD hole drilled to 166.0 mbsf, also partly logged by wireline methods, a first for ODP.

The extent of alteration intersected beneath a thin cap of fresh lava at both Sites 1188 and 1189 was a major surprise. Prior to drilling, we expected to intersect only localized zones of alteration and mineralization within an overall relatively fresh volcanic sequence. Widespread disseminated pyrite was present in most of the altered rocks encountered, but a second major surprise was the very restricted development of subsurface massive and semimassive sulfides, both overall and especially below seafloor chimneys at Site 1189. Casing to 31 mbsf prevented this assessment in the topmost part of Hole 1189B. No buried deposits of Fe oxyhydroxide were encountered: minor intervals of bright red “jasperoid” at Site 1189 proved to be hematite-bearing quartz veins and matrixes of hydrothermal breccias (Binns, this volume).

Detailed lithologic and structural description of all cores recovered, supplemented by thin section petrology, X-ray diffraction (XRD), and chemical analyses of representative samples, constituted a major shipboard activity for the scientific party (see Binns, Barriga, Miller, et al., 2002) and formed a vital basis for subsequent onshore research. Results of downhole geophysical surveys, including resistivity images, were compiled on board, but there was insufficient time to integrate these with the core data. The highest borehole temperature recorded was 313°C at 360 mbsf in Hole 1188F, 8 days after completion of drilling. Early termination of the leg prevented comparable measurements in Hole 1189B. Attempts to collect subsurface hydrothermal fluids were frustrated by hole blockages and inadequate equipment (Binns et al., this volume). With protocols developed to minimize contamination, representative core samples were taken immediately after recovery for successful shipboard and onshore microbiological studies.

Cruises Subsequent to Leg 193

Four research expeditions and a commercial survey have been conducted at PACMANUS since the completion of Leg 193. During the BISMARCK-2002 cruise of the *Franklin* (Binns et al., 2002a) additional bottom sampling of chimneys and lavas was conducted, including small andesite cones along the crest of Pual Ridge and its adjacent flanks. A new hydrothermal field (North Pual) hosted by andesite at 1800 mbsl was discovered 8 km northeast of PACMANUS.

During the DaeYang02 cruise of the *Ommuri* (McConachy, 2002; Lee, 2003; Hong et al., 2003) reflection seismic and bottom-tow magnetic surveys were conducted in the Pual Ridge vicinity. Seismic evidence was obtained of a magma body under PACMANUS, ~2 km below the crest of Pual Ridge. Magnetic profiles indicated two intensity lows—centers of subsurface magnetite destruction—under Roman Ruins and from Snowcap to Satanic Mills, respectively (Lee, 2003; Hong et al., 2003), confirming similar indications from deep-tow magnetic surveys conducted during the earlier Binatang-2000 cruise of the *Franklin* (Binns et al., 2000; Cousens et al., 2003).

Shallow diamond drilling in 2002 from the *Sonne* (CONDRILL cruise: Herzig et al., 2003; Petersen et al., 2003, 2005) achieved 10 holes in close proximity to Hole 1189B at Roman Ruins, 4 of which penetrated to ~5 mbsf. The results partly fill the information gap to 31 mbsf arising from casing the top of Hole 1189B during Leg 193. Massive sulfides including chimney fragments and reworked sulfide sediments were recov-

ered, along with nodular sulfide breccias with anhydrite and altered wallrock fragments that are comparable with the first core sample in Hole 1189B. Two holes ended in weakly altered dacite.

A commercial survey of mineral deposits in the eastern Manus Basin conducted by a joint venture between Placer Dome Oceania Pty. Ltd. and Nautilus Minerals Inc. in January–March 2005 included deep-tow sidescan sonar, swath bathymetric, and magnetic coverage of Pual Ridge. The results are proprietary but reveal fault structures consistent with tilting of Pual Ridge, as was inferred by Shipboard Scientific Party (2002d) from an 8° difference from the present-day orientation in magnetic inclinations measured on unaltered rhyodacite cores at Site 1191.

In August 2006, during the MGLN06MV cruise of the *Melville*, the remotely operated vehicle *Jason-2* and autonomous underwater vehicle *ABE* were deployed at PACMANUS and other Manus Basin sites for geophysical surveys, mapping, and collection of vent fluids, rocks, and chimneys (Roman and Ferrini, 2006; Seewald et al., 2006; Tivey et al., 2006). An exceptional outcome was discovery and sampling of boiling vents (356°C) at a new site near the southern fringe of the Satanic Mills field.

VOLCANIC ARCHITECTURE OF PUAL RIDGE

Volcanic Facies and Geochemical Stratigraphy

Preservation of volcanic structures and textures in altered rocks recovered below Sites 1188 and 1189 allowed reconstruction of the architecture of the upper two-thirds of Pual Ridge under PACMANUS despite the lack of deep penetration at the planned “background” location (Site 1190). Recognizable relict structures and fabrics include flow banding, autoclastic breccias, former glassy rinds (perlite), conspicuous to sparse vesicularity, phenocrysts, and hyaline, microlitic, or spherulitic groundmasses. Apart from spherulitic structure, all these fabrics are represented in fresh lavas dredged from Pual Ridge, although flow banding is rarely obvious.

Identified paleoseafloor horizons include flow-top breccias and gravelly to sandy volcanoclastic sediments, some containing fragments with differing mineral assemblages and textures. Perlite horizons may also denote former seafloor. A significant feature, subject to the constraint of poor recovery, is the total absence in core of foraminiferal hemipelagic sediment layers between apparent flow units. This suggests very rapid construction of Pual Ridge in view of high hemipelagic sedimentation rates in the region (Barash and Kuptsov, 1997, cite a uniform rate of 15.5 cm/k.y. over the past 16,000 yr for the central Manus Basin; rates from ¹⁴C dating of foraminifers in shallow sediment cores at four sites in the eastern Manus Basin average 23 cm/k.y.; J.B. Keene and R.A. Binns, unpubl. data).

No plutonic or distinctly hypabyssal igneous rocks were encountered in any drill hole. In the Lower Sequence of Hole 1189B a homogeneous interval of altered dacite (128–147 mbsf) with subvertically stretched vesicles was considered on board to be a possible dike (Shipboard Scientific Party, 2002c). Interpretation of resistivity imagery confirmed the presence of a discordant body (123–145 mbsf) with contacts inclined 42°–66° from horizontal (Bartetzko et al., 2003). The geochemistry of this unit is consistent with a now-altered subvolcanic feeder for overlying lavas (Miller et al., this volume).

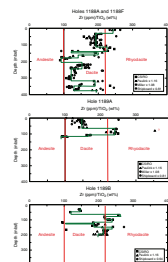
Paulick et al. (2004) delineate four main precursor volcanic facies in what were submarine, predominantly felsic eruptives below Snowcap and Roman Ruins, namely coherent lava, monomict breccia, polymict breccia, and volcanoclastic sediment. They interpret the coherent facies as the insulated central parts of individual flows and the autoclastic breccias and some volcanoclastic facies as the outer parts, and they suggest other volcanoclastic sediments were derived by gravity-driven mass transport. Noting greater abundance of coherent lavas at Site 1188 and of breccias at Site 1189, they propose that the former was close to an eruptive center whereas the latter was more distant. Assessments of geophysical logs and resistivity images of the borehole walls extend the volcanic facies analysis to intervals of zero or very poor core recovery and to uncored LWD Holes 1188B and 1189C (Bartetzko et al., 2003; Arnold et al., submitted [N1]). The results suggest small-scale lateral variability of structure within flow units below both sites. Throughout LWD Hole 1188B, for example, a higher proportion of brecciated lava is inferred than for the equivalent depth interval in cored Hole 1188A only ~5 m away at Snowcap. Interpreted facies units correlate poorly between Holes 1189A, 1189B, and 1189C at Roman Ruins despite their proximity (within 60 m).

Paulick et al. (2004) conclude that Pual Ridge was constructed from small-volume coherent and breccia flows, ranging from 5 to 40 m in thickness, with minor volcanoclastic horizons. Applying comparisons with exposed sections through shallow subaqueous rhyolitic lavas (Kano et al., 1991; McPhie et al., 1993), they propose inflationary growth as a common process, yielding domal topographies. This is not typical of dacite to rhyodacite eruptives at the PACMANUS seafloor, which range as thick as 30 m and several hundred meters in lateral extent, are highly fluid, and more closely resemble subaerial basaltic pahoehoe and aa flows in structure (Waters et al., 1996). The drilled volcanic sequence as at PACMANUS is attributed to three main phases of activity by Paulick et al. (2004), a conclusion greatly constrained by core recovery and restriction of observations to two sites not selected on volcanological grounds.

Fresh glassy lavas dredged along Pual Ridge and its flanks display a systematic increase in the ratio of Zr (in parts per million) to TiO_2 (in weight percent) with fractionation from basaltic andesite to rhyodacite (see Fig. AF1 in the "Appendix," p. 46). Zirconium and Ti are widely considered immobile elements during alteration and metamorphism, and this is supported for Leg 193 altered rocks by consistent Zr/ TiO_2 ratios in zoned samples with varying alteration assemblages. The ratio can be used to delineate precursor compositions for altered rocks (see Table AT1 in the "Appendix," p. 46).

On this basis, Figure F5 establishes a sequence of lavas below Sites 1188 and 1189 ranging from andesite through mafic and felsic dacite to rhyodacite, spanning most of the fractionation series represented by fresh seafloor lavas from Pual Ridge. Especially noteworthy are the closely comparable profiles in adjacent Holes 1189A and 1189B at Roman Ruins, with ~70 m of mafic dacite underlain by 40–50 m of rhyodacite, in turn underlain by a thin andesite, perhaps with a thin intermediate- SiO_2 dacite intervening between the latter two. There is no equivalent correlation between Sites 1188 and 1189, although altered andesites occur at about the same level under both sites, taking into account the ~45-m difference in collar elevation. An abrupt change in wallrock precursors within the Stockwork Zone of Hole 1189B occurs

F5. Zr/ TiO_2 in altered volcanic rocks, Sites 1188 and 1189, p. 54.



from mafic dacite to rhyodacite somewhere between 50 and 60 mbsf. This does not correspond to a facies change at 76 mbsf interpreted by Bartetzko et al. (2003).

A conservative interpretation of the immobile element geochemistry is that 12 compositional units (flows or flow sequences), averaging 31 m but ranging from a few meters to 60 m in thickness, are present between the seabed and 372 mbsf under Snowcap. At Roman Ruins, four units averaging ~30 m thick are indicated in Hole 1189A and six units averaging 28 m thick in Hole 1189B. Allowing for the many constraints, average flow thicknesses derived from facies analysis and geochemistry are comparable. The two approaches to understanding the volcanic architecture of Pual Ridge have not yet been integrated. Although Paulick et al. (2004) question application of the term “layer cake” to the sequence, it is clear that Pual Ridge is not constructed by inflation of only a few high-profile domes. Submersible observations and dredge samples suggest that individual flows may extend further than inferred in the models based on facies correlations between Site 1188 and Site 1189.

Cap of Unaltered Felsic Lavas

Fresh or relatively unaltered volcanic rocks, all coherent and significantly vesicular, were intersected immediately below the seafloor at the four Leg 193 drill sites. Their thickness exceeds penetration depth (17 and 20 m, respectively) at Sites 1190 and 1191. At Snowcap, changes in resistivity and gamma profiles at ~30 mbsf in LWD Hole 1188B (Bartetzko et al., 2003) define a fresh/altered boundary similar to that cored at ~35 mbsf in Hole 1188A. Below chimneys at Roman Ruins, Hole 1189A recovered ~0.2 m of fresh vesicular dacite samples before passing into altered rock. Casing obscured the immediate subseafloor in Hole 1189B, and LWD Hole 1189C appears entirely altered (Bartetzko et al., 2003).

The fresh lava caps at these sites range from mafic dacite to rhyodacite in composition and represent different lava flows. They display similar fractionation behaviors in major and trace elements (Miller et al., this volume) to seabed lavas dredged from Pual Ridge and vicinity (Binns et al., 2002b). The topmost fresh lavas intersected in cores compare closely with dredged seafloor exposures at Sites 1188, 1189, and 1191 (Fig. F3). Occasional rhyodacites dredged near Roman Ruins are absent from Hole 1189A and so must represent a younger flow or flow sequence relative to the dominant 64.9 wt% SiO₂ outcrops of that vicinity. The youngest “Tsukushi group” of glassy lavas (67.5 wt% SiO₂; open squares in Fig. F3) was not intersected in Hole 1188A, although it occurs overflowing altered outcrops in the vicinity.

Shipboard porosity measurements on samples from the fresh lava cap in Holes 1188A, 1190B, and 1191A range from 0.4% to 11.5%, less porous than underlying altered rocks. The measured core-scale permeabilities of samples from Hole 1188A and Hole 1191A (7.0×10^{-15} and 1.8×10^{-16} m², respectively), however, fall above or in the high range for altered rocks (Christiansen and Iturrino, this volume). Following X-ray computed tomography (CT) studies of the Hole 1188A specimen, Ketcham and Iturrino (2005) consider the core-scale permeability measurement unreliable because the sample was too small and state that whereas vesicles provide porosity they are disconnected and the rock is effectively impermeable. Formation Micro Scanner (FMS) resistivity imagery was not conducted for any intersection of fresh volcanic rocks; hence, any differences in fracture patterns or intensity compared to al-

tered rock intersections cannot be assessed. Whereas intuitively the fresh lavas directly below the seafloor appear to constitute an impervious cap to the hydrothermal system (otherwise venting would be far more widespread?), this remains unconfirmed by hard data.

An issue of importance to modeling the evolution of the PACMANUS hydrothermal system is whether the fresh lavas in Holes 1188A and 1189A pass abruptly or gradually into altered rocks below. Might they, for example, overlie the alteration system unconformably (as the "Tsukushi group" lavas do at Snowcap), or were they present prior to alteration to become preserved as relatively impervious caps to the system? If the fresh lavas were indeed erupted after formation of the drilled alteration system, the likelihood of repeated cycling between hydrothermal and volcanic events during the construction of Pual Ridge becomes enhanced and major uncertainties would be introduced regarding relationships between the present-day chimney-forming hydrothermal fluids at PACMANUS and those responsible for the underlying zone of extensive alteration and limited mineralization revealed by Leg 193 drilling.

Low core recoveries prevent a conclusive answer to the question. Based on changes in megascopic appearance and relative distribution of opaline silica and cristobalite, progressive downhole grading from largely unaltered lavas to pervasively altered rocks was inferred on board ship in both Hole 1188A (Shipboard Scientific Party, 2002b) and Hole 1189A (Shipboard Scientific Party, 2002c). Critical samples covering the transition, however, require detailed study to fully exclude any possibility, considered remote, of an "alteration unconformity." At both sites the transition evidently occurs within a few meters or less.

SUBSEAFLOOR HYDROTHERMAL ALTERATION AND MINERALIZATION

Key conclusions reached during Leg 193 regarding pervasively altered rocks underlying the thin cap of fresh lavas include the following (Binns, Barriga, Miller, et al., 2002):

1. Alteration is dominated by clay minerals, especially illite and chlorite, with less common pyrophyllite, mixed-layer clays, and smectite. Anhydrite is widespread but irregularly distributed.
2. The dominant silica phase at Site 1188 and in Hole 1189A changes from opal at the transition between fresh and altered rocks to cristobalite and then to quartz at depth. The boundary between cristobalite- and quartz-bearing domains is closer to the seafloor under Site 1189.
3. Cristobalite is not present in the upper Stockwork Zone of Hole 1189B at Roman Ruins (30 to ~100 mbsf). An abrupt change at ~118 mbsf, possibly a fault, divides this from a contrasted Lower Sequence characterized by interleaved cristobalite- and quartz-bearing assemblages, commonly retaining igneous plagioclase, and thereby tentatively considered less altered. Isolated samples (including possible "droppers" from higher levels) of similar rocks with cristobalite are also present within the deeper, quartz-dominated domain in Holes 1188A and 1188F.
4. The presence of K-feldspar below Roman Ruins (especially in Hole 1189B) is a conspicuous difference between the alteration

- assemblages beneath Sites 1188 and 1189 with their contrasted venting characteristics.
5. Three major pervasive alteration styles were defined and applied in logging: (a) soft, greenish colored silica-clay ("GSC"), (b) "bleaching" (pale silica clay usually with anhydrite and often pyrophyllite), and (c) pervasive "silicification," creating distinctly harder rocks.
 6. Superimposed alterations were inferred at Site 1188, especially pyrophyllite-bearing "bleached" zones and pale selvages adjacent to anhydrite veins, both considered to overprint darker chloritic "kernel" assemblages. Pervasive "silicification" was also interpreted as a later effect.

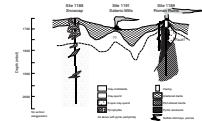
In the following sections we review shipboard results and new research relevant to genetic issues, including unpublished petrologic and geochemical interpretations (R.A. Binns) necessary to fill certain gaps. A highly simplified longitudinal section from Snowcap to Roman Ruins illustrating salient aspects of the alteration system (Fig. F6) is useful for the discussions. The diagram depicts alteration below Sites 1188 and 1189 as parts of one large hydrothermal system below a cap of unaltered lavas with varying thickness (as suggested by deep-tow magnetic surveys), but the hypothetical continuity implied at depth is untested.

Alteration Minerals

New clay mineral identifications in bulk rock samples measured by X-ray diffraction (XRD) and short-wave infrared spectrometry (SWIR) (Lackschewitz et al., this volume; Warden, this volume; Paulick and Bach, 2006) amplify shipboard data on the relative distribution of different clay mineral species below Sites 1188 and 1189. Specialized XRD investigations of clay mineral concentrates prepared from selected samples confirm the presence of occasional smectite accompanying chlorite between 34 and ~100 mbsf in Hole 1188A and clarify in particular the nature of varied mixed-layer phyllosilicates that may accompany illite and chlorite elsewhere (Lackschewitz et al., 2004). Although there are exceptions, mixed-layer clays appear more common in cristobalite-bearing assemblages and in rocks retaining relict plagioclase microlites.

Electron probe microanalyzer (EPMA) compositions of clay minerals are variously affected by fine grain size and intergrowths (Lackschewitz et al., 2004; Paulick and Bach, 2006; R.A. Binns, unpubl. data). Chlorites range from ripodolite to pycnochlorite ($Mg/[Mg+Fe] = 45\text{--}85$ mol%). EPMA data for illites demonstrate a wide compositional range from end-member illite (with 0.9 [K + Na] atoms per 11 oxygen anions, anhydrous, following Meunier and Velde, 2004) to lower-K variants containing substantial celadonite and pyrophyllite components. The ratio K/Na is variable, and some illites approach paragonitic compositions (Paulick and Bach, 2006, express uncertainty whether this represents solid solution or interlayering). Where measured, illites contain minor BaO (~0.2–0.4 wt%). A trend toward less sodic compositions with depth at Site 1188 occurs in EMPA and SWIR data (Warden, this volume; Paulick and Bach, 2006). This is the only systematic compositional trend with depth so far defined within the clay minerals. The illite crystallinity index measured following Kisch (1991) for clay fractions from 220 to 350 mbsf in Hole 1188F, and at 107 mbsf in Hole 1189A, range without a depth trend between 0.35° and $0.55^\circ 2\theta_{Cu}$ (R.A.

F6. Features of subseafloor hydrothermal alteration, p. 55.



Binns, unpubl. data), spanning the diagenesis and anchizone fields of Kübler (1964).

Chlorite and illite occasionally form thin seams in composite anhydrite veins and botryoidal growths or rosettes lining vesicles or irregular cavities, especially at Site 1188. Chlorite is absent from intervals of acid sulfate alteration and from pale selvages around fractures and anhydrite veins.

Comprehensive XRD and SWIR investigations (Lackschewitz et al., this volume; Warden, this volume) confirm two main pyrophyllite-bearing intervals below Snowcap, pervasive from 58 to 116 mbsf in Hole 1189A and more sporadic from 220 to 260 mbsf in Hole 1188F. The habit of pyrophyllite differs significantly between these intervals, as explained later. Pyrophyllite is unrecognized in Holes 1189A and 1189B under Roman Ruins.

Many samples from Site 1188 especially contain brownish patches and bands where clay minerals display distinctive waxy reflections in polished thin sections. The reason for this has not been established despite focused scanning electron microscope (SEM) studies, but the feature does not correlate with presence of pyrophyllite as suggested by Shipboard Scientific Party (2002b, 2002c). Distribution of the waxy brown patches commonly appears related to proximity of anhydrite veins or abundant disseminated anhydrite.

The relative distributions of different silica minerals in the subseafloor alteration system as established by shipboard XRD and optical microscopy have been confirmed by additional postleg identifications. Cristobalite and quartz are the main phases. Opal-A occurs within and immediately underlying the relatively unaltered volcanic cappings of Holes 1188A and 1189A, whereas rare XRD identifications of minor or trace tridymite in Hole 1188A are reported by Lackschewitz et al. (this volume).

Cristobalite tends to occur as tiny micrometer-scale particles and scattered rosettes intergrown with clays as alteration products of volcanic glass, and also as botryoidal linings to fractures and vesicles. It dominates assemblages in the domain above ~106 mbsf in Hole 1188A, whereas quartz dominates below ~106 mbsf and throughout Hole 1188F. The two species can occur in the same specimen throughout a transitional domain between 60 and 110 mbsf, which corresponds to the upper pyrophyllite interval of Hole 1188A. In Hole 1189A the transition from cristobalite to quartz is sharper and more shallow, at ~25 mbsf. Cristobalite also dominates approximately one-third of the lithologic units in the Lower Sequence (>118 mbsf) of Hole 1189B.

Quartz in altered wallrocks from the deeper domains of the alteration system is present as ragged anhedral grains 10–300 µm in diameter intergrown with clays (some resembling miniporphyroblasts), as euhedral crystals projecting into vesicles or filling amygdules, and as hairline veinlets. Continuous crystal growths or epitaxial overgrowths between these three habits imply close temporal relationship and at least local mobilization of SiO₂. Silica phases are subordinate or absent within altered wallrock fragments in hydrothermal breccias from the Stockwork Zone of Hole 1189B and from some breccias or net-veined intervals in other holes. The breccia matrixes and vein networks associated with such wallrocks, however, are dominated by quartz.

Typically, the same silica phase present in altered rock also forms the partial linings or complete fillings to fractures and vesicles. In the transition intervals between cristobalite- and quartz-dominated domains some samples contain both phases. In these, cristobalite almost invari-

ably occurs within the main rock body while the quartz occupies veinlets or fills former vesicles. From a variety of petrographic evidence such as pseudomorphous replacement textures it is clear that quartz generally formed later than cristobalite.

Igneous phenocrysts and microlites of calcic plagioclase are in places preserved within altered rocks from Sites 1188 and 1189 in association with either cristobalite or quartz. They are relatively common in the Lower Sequence of Hole 1189B. More generally they are altered to illitic clays.

Secondary sodic plagioclases are not commonly recognized outside the Lower Sequence of Hole 1189B (Paulick and Bach, 2006). Yeats et al. (2001) quote a compositional range from An₅ to An₁₅. Exceptional developments of granular secondary plagioclase are present in cavity-rich rocks from 175 to 185 mbsf toward the base of Hole 1188A, an interval where geochemistry denotes andesitic precursors and where some samples contain coexisting plagioclases close to pure albite and with An₂₅ compositions, respectively, bridging the “peristerite gap” in low-temperature plagioclase solid solutions.

The presence of secondary potassium feldspar at Site 1189 has been established as quite widespread by postleg XRD, SEM, and EPMA studies (Yeats et al., 2001; [Lackschewitz et al.](#), this volume; Paulick and Bach, 2006). Potassium feldspar is conspicuously absent from altered rocks below Site 1188. In some samples from the Lower Sequence of Hole 1189B, potassium feldspar has replaced former plagioclase microlites. Elsewhere, tiny irregular to blocky grains, intimately intergrown with flakes of illite without reaction relationships, are clearly hydrothermal in origin. From limited microprobe analyses, the potassium feldspars contain significant hyalophane component (1–2 wt% BaO). The structural type of the potassium feldspar has not been established.

Anhydrite is the common sulfate phase disseminated within altered wallrocks and as vesicle fillings at Site 1188 but is by comparison subordinate at Site 1189. Barite is present in the same settings but is scarce and sporadic. Rare wallrock gypsum probably represents a retrograde hydration product of anhydrite. In vesicles, cavities, and veinlets, anhydrite typically crystallized late, after quartz or cristobalite.

Pyrite is the predominant disseminated sulfide in all alteration lithologies. It varies greatly in grain size and habit, ranging from anhedral to euhedral. Paragenetic observations regarding pyrite and other sulfide minerals are presented in the site chapters of Binns, Barriga, Miller, et al. (2002), but many aspects and especially the relationships between sulfide and silicate parageneses remain unclear. Chalcopyrite and sphalerite accompany wallrock and vesicle pyrite in some samples, especially at Site 1189 ([Pinto et al.](#), this volume). Pyrrhotite is exceptionally rare, and arsenopyrite has nowhere been observed in Leg 193 cores.

Hematite is a rare wallrock phase. Secondary magnetite is a scarce accessory in two main intervals of altered rocks below Snowcap, from 135 to 197 mbsf in Hole 1188A and from 318 to total depth (386 mbsf) in Hole 1188F. In the upper interval, dominated by andesite and mafic dacite precursors, fine-grained magnetite intergrown with clays appears part of the hydrothermal assemblage. In the lower interval, similar magnetite is restricted to the borders of unusual fractures occupied by clay minerals. [Pinto et al.](#) (this volume) identify ilmenite and hercynite accompanying magnetite in this latter interval and a single example of pyrophanite (MnTiO₃). The lack of consistent compositional relation-

ships for these coexisting phases precludes estimations of temperature or oxygen fugacity during alteration.

Rutile, apatite, and submicrometer-sized zircon are ubiquitous accessories intergrown with clays in altered wallrocks. Anatase occasionally substitutes for rutile (Lackschewitz et al., this volume). Microprobe data indicate that wallrock apatites are chlorine bearing, in contrast to apatites from anhydrite veins, which have high fluorine contents (Yeats et al., 2001). Other trace minerals with development restricted to unusual alteration styles include kaolinite, diaspore, brucite, talc, and alunite. Apart from rare tentative optical identifications, amphibole, epidote, and zeolites are conspicuously lacking. Although CO₂ is a component of vent fluids at PACMANUS chimneys (20–40 mM in end-member hydrothermal fluid) (Ishibashi et al., 1996), calcite is known only as a trace mineral from 222 to 223 mbsf in Hole 1188F.

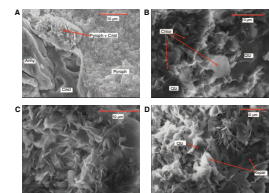
Alteration Petrology

At Site 1188 there is a broadly consistent difference in microfabric between clay-dominated assemblages of the upper alteration domain characterized by cristobalite and the lower quartz-bearing domain. Many samples of the former were described on board ship as devitrified glass with undulose, plumose, or mesh-textured anisotropism. Analytical SEM investigations reveal exceptionally fine grained aggregates (grain size = 0.1 μm or less) of hydrothermal pyrophyllite or illite flakes, imperfectly to moderately well aligned (Fig. F7A). By contrast, in samples from the lower quartz-bearing domain the clay mineral flakes are coarser and loosely packed in random orientation (Figs. F7B, F7C, F7D). The coarser microfabrics dominate Hole 1189A and wallrocks in the Stockwork Zone of Hole 1189B, whereas in the Lower Sequence of Hole 1189B the two styles are interleaved according to the distribution of cristobalite and quartz. The spaces between the clay flakes in both styles amount to a considerable proportion of the rock volume and clearly explain the surprisingly high porosity of altered cores recognized in shipboard physical property measurements. Void spaces up to 70% by volume are estimated from SEM images.

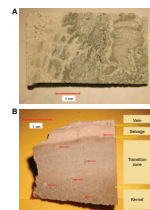
New observations raise uncertainties with the concept advanced in Binns, Barriga, Miller, et al. (2002) of an initial, pervasive, chlorite-bearing alteration which became modified by subsequent silicification, acid sulfate alteration (“bleaching”), and development of pale selvages around fractures generally occupied by anhydrite veins. Shipboard interpretations of superimposed pervasive silicification were quickly discounted by onshore geochemical studies showing little change in SiO₂ content relative to precursor lavas (see Fig. AF2 in the “Appendix,” p. 46). Localized silicification, however, occurs on a millimeter to centimeter scale within wallrocks adjacent to certain but by no means all quartz veins and quartz-rich breccia matrixes in Holes 1189A and 1189B.

Figure F8A exemplifies macroscopic features from the upper pyrophyllite-bearing interval of acid sulfate bleaching in Hole 1188A that led Binns, Barriga, Miller, et al. (2002) to deduce late-stage superimposition of this alteration style. It illustrates an altered perlitic glass in which bleaching appears at first sight to be advancing from left to right as a replacement front facilitated by fractures. The dark greenish “kernels” consist of patchy mixtures of just-resolvable illite, mixed-layer phyllosilicate, cristobalite, disseminated euhedral pyrite, and minor anhydrite. The white portion of the sample has scattered cristobalite

F7. Hydrothermal clay mineral assemblages, p. 56.



F8. Acid sulfate alteration; pale selvage structure, p. 57.



grains within optically irresolvable, pyrophyllite-dominated “glass” with undulose to mesh-textured anisotropism and is actually broken up by the anhydrite-cristobalite-pyrite-filled fractures rather than being developed as a reaction selvage around them. No replacement or pseudomorphous structures suggesting dissolution of kernel-style pyrite are present in the pale material. Since reversion of the apparently more crystallized clay assemblage of the dark kernels to an “anisotropic glass” appears most unlikely, the structure is more easily interpreted if the pyrophyllitic bleaching (acid sulfate alteration) were in fact the first phase of alteration or, alternatively, if the two alteration styles were essentially simultaneous.

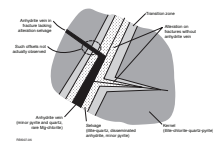
Samples from the lower pyrophyllite-bearing interval in Hole 1188F vary from uniformly pale in color to mottled, and many are not obviously associated with anhydrite veining. Analytical SEM studies reveal the mottling to reflect variations in the modal proportions of illite and relatively coarse (1–3 μm) pyrophyllite. Where both occur, adjacent flakes of illite and pyrophyllite coexist in apparent equilibrium. Pyrophyllite thus appears here to be more definitely part of a primary alteration assemblage.

Figure F8B illustrates a simple variant of pale selvage beside an anhydrite vein, the third kind of superimposed alteration considered by Binns, Barriga, Miller, et al. (2002) as a product of wallrock reaction between anhydrite vein-forming fluid and chloritic wallrock. Such selvages typically have a sharp border against a faintly layered “transition zone” that passes gradually into the inner, chloritic “kernel.” These structures are largely restricted to Site 1188 and are more common in the quartz-bearing domain, especially in Hole 1188F. More complex examples have multiple-layered selvages suggestive of repeated diffusion fronts. Not uncommonly, plagioclase microlites or phenocrysts are preserved in the kernel portions but are altered to clays in the selvage and transition zone, often abruptly, again apparently suggesting later development of the selvages. Greater abundance of disseminated anhydrite in the pale selvage zone supported a genetic relationship to the anhydrite vein.

Reexamination of many samples from Holes 1188A and 1188F reveals that there is not an exact correspondence between anhydrite veins and the pale selvages. Figure F9 schematically presents observations that collectively indicate the anhydrite veins were emplaced *after* formation of the pale selvages. Whereas the selvages clearly developed from fluids transported via preexisting fractures, the anhydrite veins fill openings caused by reactivation of the fractures and a jumbling or rotation of wallrock blocks between them.

Described as pyrophyllitic by Shipboard Scientific Party (2002b), most pale selvages in Holes 1188A and 1188F are in fact composed largely of illite intergrown with quartz (or cristobalite) and disseminated anhydrite (Fig. F7C). Pyrite is characteristically lacking or very scarce. In the greenish kernels illite is intergrown with chlorite or Mg-bearing mixed-layer clays (Fig. F7B), pyrite is common, but anhydrite is absent or subordinate. In the transition zones, chlorite generally becomes less abundant relative to kernels without evidence of replacement by illite, anhydrite may increase, and pyrite is usually less common but may be enriched in particular laminae. In the only known example of a selvage containing pyrophyllite, from the mottled lower pyrophyllitic interval of Hole 1188F, this mineral is also present (with smectite-illite mixed-layer phyllosilicate) in the kernel.

F9. Summary indicating anhydrite veins were emplaced after formation of pale selvages, p. 58.



Considering the exceptional porosity of clay mineral assemblages, the sharp outer borders of most selvages seem inconsistent with an origin by diffusive replacement of formerly chloritic assemblages, although the layering in transition zones certainly recalls double-diffusion processes. Where pyrite first appears abundantly in transition zones it shows no signs of corrosion or replacement. Pseudomorphous structures indicating former presence of kernel-type pyrite replaced by quartz or illite are altogether lacking in the selvages, and in some samples contrasted quartz microfabrics between selvages and kernels also appear inconsistent with replacive overprinting.

Although features such as the distribution of disseminated anhydrite remain to be explained (it would need to replace the clay minerals), the petrographic evidence again seems more consistent with simultaneous alteration of precursor volcanic wallrock in response to progressive composition changes in inwardly permeating fluids or, alternatively, that the selvages represent an *earlier* alteration phase with kernels altering later under changed fluid compositions.

Regardless of these genetic issues, petrologic studies permit a simplified classification of alteration types (Table T1), presented to facilitate the following discussion of alteration chemistry. It covers formerly coherent volcanic rocks. Rare or unusual alteration styles, as in some volcanoclastic horizons or flow-banded and spherulitic rocks, are not included.

Whole-Rock Geochemistry of Altered Rocks

Assuming immobility of Ti and Zr to assess precursor compositions, Lackschewitz et al. (2004) evaluate chemical changes in five altered samples from Holes 1188A and 1188F. Some but not all of the bulk elemental changes observed were explicable in terms of clay concentrate compositions. From a more extensive study of both Sites 1188 and 1189, Yeats (2003, 2004) notes that bulk Si is generally conserved, Mn is universally depleted, K is especially enriched at Site 1189 in rocks containing hydrothermal K-feldspar, and S is typically enriched by 2–3 orders of magnitude. A number of chalcophile elements (Zn, Pb, As, and Sb) display enrichment in the upper section of Hole 1188A but become progressively depleted at depth and in Hole 1188F; Zn returns to near-precursor levels at the base of Hole 1188F. Copper and Mo were considered to be enriched throughout Holes 1188A and 1188F, but Yeats (2004) cites “chaotic” behavior of chalcophile elements in Holes 1189A and 1189B.

These conclusions do not take account of significant differences in composition between adjacent samples with varied alteration style (Table T2), which could obscure genetically significant downhole or cross-site trends. In order to assess this, major and trace element data for the Commonwealth Scientific and Industrial Research Organisation (CSIRO) collection of Leg 193 samples have been examined in terms of the petrologic classification of Table T1. Procedures for calculating precursor rock compositions are outlined in the “Appendix,” p. 46. The principal uncertainty is with Cu, which exhibits significant variability and an abrupt change in fractionation behavior within Pual Ridge lavas (Sun et al., 2004). Salient outcomes of the study follow (see the “Appendix,” p. 46, for further details):

1. After accounting for alteration styles, the principal lateral geochemical differences between altered rocks below Snowcap

T1. Petrologic classification of subseafloor alteration styles, p. 62.

T2. Major elements in alteration categories at PACMANUS, p. 63.

- and Roman Ruins are the consistently higher enrichments (relative to precursor compositions) at the latter site in K and Ba (reflecting presence of potassium feldspar), and the contrast between U depletion at Site 1188 and U enrichment at Site 1189.
2. Silica is mostly conserved at precursor levels (including in intervals formerly described as “pervasively silicified”) but is highly depleted in Category Z wallrocks from the Stockwork Zone of Hole 1189B and from several veined or brecciated intervals in other holes. Silica is mildly enriched in a few samples showing petrologic evidence of localized replacive silicification or abundant quartz growth in secondary cavities (e.g., Category A).
 3. Taking into account modal abundances of microlites and phenocrysts and likely compositions of residual glasses in parent lavas, the contrasted behaviors in K, Mg, and Na at Site 1188 between kernel lithologies lacking or retaining relict plagioclase, respectively, lead to the conclusion that rocks retaining relict igneous microlites are not “less altered” in the sense originally supposed (Binns, Barriga, Miller, et al., 2002). Rather, they formed from reaction with hydrothermal fluids characterized by distinctly low potassium activity compared to other “kernel” material and with which calcic plagioclase is evidently stable. At Site 1189 this conclusion is less obvious, being obscured by factors governing potassium feldspar stability.
 4. For some elements the compositions of high-temperature fluids venting at Satanic Mills and Roman Ruins (Gamo et al., 1996; Douville, 1999), and also the computed hydrothermal components of borehole fluids (Binns et al., this volume), are consistent with potential leaching from the drilled volcanic sequence during hydrothermal alteration. For example, Li and Mn are consistently highly depleted (relative to precursors) in altered rocks and correspondingly enriched (relative to seawater) in the vent fluids. However, this does not apply to many other elements, notably potassium. High K/Ca ratios in vent fluids characterizing PACMANUS fluids in contrast to basalt-hosted sites elsewhere were ascribed by Gamo et al. (1996) to reaction with felsic rocks. However, K enrichment is typical of most alteration styles at Site 1188 and particularly Site 1189. Only the pyrophyllitic bleaching (Category XB) of Hole 1188A has the potential to release significant K, and this style of alteration is lacking below Roman Ruins.
 5. Leaching of Cu, Zn, and Pb during certain styles of hydrothermal alteration (as demonstrated, for example, by depletions in altered rocks from the quartz domain of Site 1188) represents a theoretically feasible source for base metal components of vent fluids and seabed chimneys. However, under the Roman Ruins chimney field (Site 1189) the altered sequence appears itself enriched overall in these elements, although there has been significant local remobilization as sulfides.
 6. Consistent downhole geochemical trends at Site 1188 for certain lithophile elements (Mg, K, Na, Rb, and Ba in plagioclase-free kernels) and chalcophile elements (Zn and Pb for most alteration styles) are imposed across the subseafloor sequence without disruption at assessed flow boundaries or paleoseafloor horizons.

Overall gains and losses during alteration, based on averages for all CSIRO samples irrespective of alteration style and possible nugget effects

are listed in Table T3 for major subdivisions at Sites 1188 and 1189. Although representivity is uncertain, the data emphasize, for example, the pronounced loss of SiO₂ from wallrocks in the Stockwork Zone of Hole 1189B and the marked differences in Mg, K, Ba, and U behavior between the two sites. High copper enrichments in a few samples at Site 1188 outweigh Cu depletions in others, leading to apparent overall gains within both cristobalite and quartz domains that may be statistically questionable. Overall Cu gains are more definite in Hole 1189A and the Lower Sequence of Hole 1189B. Zn appears lost overall from Site 1188 and from Category Z wallrock fragments in the Stockwork Zone of Hole 1189B, but it is gained overall in Hole 1189A and more so in the Lower Sequence of Hole 1189B. Upward transport of Pb is a possible explanation for the contrast between the enriched cristobalite domain and the depleted quartz domain at Site 1188, but at Site 1189 the wallrocks are again enriched overall in absolute terms. The behavior of gold has not yet been studied.

Volume Changes during Alteration

The elevated porosities of altered rocks measured on board ship have been confirmed on shore by Christiansen and Iturrino (this volume). They note that samples with >5% of plagioclase microlites from Site 1188 have relatively constant porosity (~15%–25%), but porosities of totally altered samples fall with increasing depth from ~30% below the fresh lava cap to ~15% at 336 mbsf. At Site 1189, Category Z wallrocks in the Stockwork Zone, lacking a silica phase, are exceptionally porous (45%–65%).

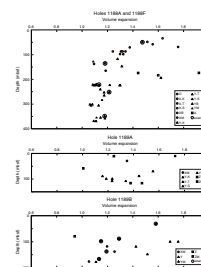
Sufficient chemically analyzed samples have measured bulk densities, or densities that can be reasonably inferred from equivalent neighbors, to allow assessment of volume changes during hydrothermal alteration of formerly hyaline lavas at PACMANUS (Fig. F10). Assumed immobility of Ti and Zr is used to determine precursor compositions (see the “Appendix,” p. 46) and thereby precursor densities from measurements on fresh Pual Ridge glasses and microlitic rocks.

Site 1188 shows a pronounced drop in volume expansion from ~60% directly below the fresh lava cap in Hole 1188A to ~20% at 150 mbsf, which continues as a more modest decline to ~15% at ~360 mbsf in Hole 1188F. The profile is interrupted by an interval of exceptionally high expansion (up to 92%) between ~170 and ~200 mbsf, the zone of cavity-rich altered andesites (Category A and a related Y-K). Apart from these there are no consistent differences in the depth relationships between the various alteration categories. Volume expansions in Holes 1189A and 1189B range from low values to 76%, with less systematic downhole trends.

Total volume change as plotted in Figure F10 represents an interplay between induced porosity (dilation arising from excess fluid pressure), volume changes governed by alteration reactions (cf. Tenthorey and Cox, 2003), and mass gains or losses. These factors may have additive or opposed influence. For example, the Category Z altered perlite at 30.12 mbsf in Hole 1189B is a case where there has been marked overall expansion during alteration (by 58%), yielding a rock with 67% porosity in which the solid constituents now have a bulk density of 3.26 g/cm³ and have shrunk to 54% of their original volume. From this and similar calculations for other samples it is evident that the induced porosity factor dominates.

T3. Mass transfers during hydrothermal alteration, p. 64.

F10. Volume expansion during hydrothermal alteration, Sites 1188 and 1189, p. 59.



Veins, Breccias, and Fractures

The mineralogy, geometry, abundance, and apparent timing relationships of veins from 1 mm to several centimeters wide at Sites 1188 and 1189 are extensively described by Shipboard Scientific Party (2002b, 2002c). The dominant vein assemblage at Site 1188 is anhydrite \pm (pyrite) \pm (cristobalite or quartz). An early generation of pyrite often forms marginal laminae at the wallrock contact. The mineralogy, structure, and paragenesis of this vein style are very similar to those of vesicle and amygdale fillings, and indeed there are examples of continuous development where veins cut into large vesicles. Observations presented above on the relative timing of illite selvages remove a main basis on which a sequence of veins at Site 1188 was deduced by Scientific Party (2002b).

At Site 1189, similar anhydrite veins are present but distinctly less frequent in Hole 1189A and in the Lower Sequence of Hole 1189B. Those in Hole 1189A typically contain more quartz than those at Site 1188 and may cut across an earlier generation of quartz veins, some with minor chalcopyrite and sphalerite (Shipboard Scientific Party, 2002c).

Hydrothermal breccias are also common, ranging from close-packed, jigsaw-fit structures to matrix-supported breccias with dispersed fragments of altered wallrock. The matrixes, variously dominated by anhydrite or quartz, generally with some pyrite, are essentially equivalent to vein fillings. In the Stockwork Zone of Hole 1189B the distinction between veins and breccias within the small samples recovered is essentially the proportion and relative dispersal of altered wallrock fragments. Prismatic quartz and euhedral pyrite favor margins against altered wallrock, whereas late-stage anhydrite may occupy the centers of veins or drusy pockets within breccia matrixes. Pyrite varies from a minor to a major constituent. In the matrixes of occasional hydrothermal breccias in Hole 1189A, anhydrite again typically has a late-stage paragenesis relative to quartz.

At the base of the Stockwork Zone (118.1 mbsf) a coarse monomineralic anhydrite vein cuts directly across a set of quartz-dominated veins containing pyrite, chalcopyrite, sphalerite, minor anhydrite, and the only recorded occurrence of gold (Pinto et al., 2003, 2005, this volume). Nearby, bladed anhydrite in the matrix of a rare second-generation breccia cuts earlier breccia fragments with quartz-pyrite matrixes.

A close relationship between Category Z wallrocks (depleted in SiO_2) and quartz-veined stockworks suggests that the source of SiO_2 in certain quartz veins and breccia matrixes may be relatively local. Wallrock fragments picked free of veins in a finely net-veined interval at 106.5 mbsf in Hole 1188A lost 260 g of SiO_2 per kg of precursor, but a bulk sample of the interval shows overall conservation of the precursor levels. In many samples from the quartz domain of Hole 1188F where bulk SiO_2 content was unchanged during alteration there is evidence of internal redistribution into abundant vesicle fillings, discontinuous veinlets, and large grains resembling porphyroblasts.

Barriga et al. (2001, 2004) ascribe formation of some breccias, particularly variants with stylolite-like residual enrichments in fine-grained rutile/anatase at the borders of atypically rounded fragments, to local corrosion or dissolution during hydrothermal alteration followed by collapse of remaining clasts. However, the determination that alteration predominantly involves volume expansion induced by overpressured fluids favors dilational hydrofracturing as the predominant process.

Semimassive Sulfide Mineralization

Few pieces of core recovered during Leg 193, all from Site 1189, contained sufficiently abundant sulfides to classify as massive (>75% sulfide) or semimassive (25%–75%) in ODP terminology. Nor were thick sulfide bodies detected by wireline or resistivity-at-the-bit logging at either Site 1188 or Site 1189 (Bartetzko et al., 2003). Small core fragments originally logged as massive sulfide from the Stockwork Zone of Hole 1189B represent portions of pyrite-quartz veins or breccia matrixes (Binns, this volume).

Two core samples of semimassive sulfide represent the only significant intersections recovered. An 8-cm piece of sulfide rock from 31.0 mbsf in Hole 1189B contains irregular massive aggregates or nodules of coarse pyrite with chalcopyrite overgrowths, set in a dark gray matrix of bladed to granular anhydrite (partly altered to gypsum) with disseminated pyrite and chalcopyrite. Amoeboid pods of pale gray, bladed anhydrite largely devoid of sulfides represent a final stage of deposition in what appears to have been a progressively dilated deposit characterized by open-space mineral growth. Barite is lacking, and quartz and sphalerite are rare. Fragments of altered dacite with disseminated sulfides are scattered throughout the sample, which thus appears a variant of breccia from the Stockwork Zone. Similar chalcopyrite-bearing “nodular breccias” were cored by CONDRILL shallow drilling (<5 mbsf) in the vicinity of Hole 1189B (Petersen et al., 2003, 2005; Binns, 2005). Although containing barite as well as later anhydrite, these samples also carry dispersed fragments of totally altered volcanic wallrock and they too have structures indicative of successive dilation and open space mineral growth. Together with the semimassive sulfide at 31.0 mbsf in Hole 1189B, these are interpreted as upper levels of the Stockwork Zone, underlying rather than merging above into the mound of collapsed chimneys at Roman Ruins.

The other large semimassive sulfide sample, at 107.7 mbsf in Hole 1189A, occurs within a layered volcanoclastic paleoseafloor horizon. In a band ~5 cm thick, abundant sulfides (predominantly pyrite with lesser chalcopyrite and sphalerite) together with quartz and minor anhydrite form a matrix to well-dispersed fragments of altered tube pumice and nonvesicular volcanic rock. In places the matrix invades altered volcanic clasts along fractures. Above and below the semimassive sulfide band are altered hyaloclastites with similar clasts, here closely packed and self-supported but containing only minor matrix sulfide. Both contacts of the ~5-cm layer are serrated as if the matrix of the sulfide layer was invading the bordering hyaloclastites.

Although contrary interpretations are offered by Shipboard Scientific Party (2002c) and Paulick et al. (2004), the semimassive sulfide in Hole 1189A is considered a mineralization variant formed during the same event that created stockwork veins and semimassive sulfide nearby in Hole 1189B. Preservation of angular outlines of the delicate tube pumice particles indicates that mineralization involved dilation of the deposit rather than widespread replacement. Equivalent seabed hyaloclastites with tube pumice particles, collected by dredge and submersible on Pual Ridge, are moderately well sorted and close-packed, as expected from submarine spallation of lava rinds (Waters et al., 1996; Waters and Binns, 1998).

Pinto et al. (this volume) provide electron probe microanalyses of pyrite, chalcopyrite, and sphalerite from the semimassive sulfides. Binns (this volume) presents bulk compositions and isotopic data for

five samples of massive and semimassive sulfide and for a hammer-drill sand (containing subequal proportions of altered wallrock and sulfide fragments) derived from the 0- to 30-mbsf cased portion of Hole 1189B. Maximum Cu and Zn concentrations are 5.0 and 1.6 wt%, respectively. Gold contents are moderate (0.9–2.0 ppm). The subseafloor semimassive sulfides are not as rich in base and precious metals as chimneys at Roman Ruins (average Cu = 7.0 wt%, Zn = 24 wt%, Au = 16 ppm, and Ag = 230 ppm) (Binns, 2004) but are richer in Co, Te, and Bi and are mildly enriched in Se. Isotopic ratios (Pb and S) of the subseafloor samples and seafloor chimneys are similar.

Temperatures of Hydrothermal Alteration and Vein Formation

Problems involved with estimating temperatures for hydrothermal and low-temperature metamorphic clay mineral assemblages arising from disequilibrium and sensitivity to fluid compositions (Árkai, 2002; Meunier and Velde, 2004) are compounded by the extrapolations involved in applying experimental data to the pressures of the subsurface PACMANUS hydrothermal system drilled during Leg 193 (0.16–0.20 kbar). The general presence of chlorite and illites with crystallinity indexes spanning the diagenesis and anchizone fields, plus comparisons with alteration in geothermal fields, suggests temperatures of 220° to 300°C, below those of the zeolite or greenschist facies of metamorphism (Browne, 1978; Srodon and Eberl, 1984; Árkai, 2002). Presence of pyrophyllite rather than kaolinite with silica minerals in alkali-poor assemblages at these relatively low pressures, by extrapolation from experiments of Chatterjee et al. (1984), favors the upper part of that temperature range.

Assuming equilibration with seawater-like hydrothermal fluid, calculated temperatures based on oxygen isotope ratios in near-monomineralic concentrates of illite and illite-dominated mixed-layer illite-smectite from 233 to 355 mbsf in Hole 1188F range from 250° to 300°C, increasing downhole (Lackschewitz et al., 2004). An illite at 40 mbsf in the Stockwork Zone of Hole 1189B has a calculated temperature of 305°C. Chlorites from illite-poor samples at 175 mbsf in Hole 1188A (225°C), 116 mbsf in Hole 1189A (250°C), and 118 and 197 mbsf in the Lower Sequence of Hole 1189B (235° and 220°C) yield temperatures lower than those for illites, whereas pyrophyllite concentrates between 50 and 117 mbsf in Hole 1188A yield elevated temperatures (260°–310°C).

No oxygen isotope temperature estimates have been made for pyrophyllite-free alteration in the cristobalite domain at Site 1188. Presence of smectite in some samples from this domain suggests alteration took place at least partly at temperatures lower than the 225°C calculated for chlorite at 175 mbsf.

Oxygen isotope ratios measured on quartz samples from veins, breccia matrixes, and vesicle linings in Holes 1189A and 1189B yield mostly higher temperature estimates, from 280° to 400°C (Lackschewitz et al., 2004; R.A. Binns and A.S. Andrew, unpubl. data). Because an empirical fractionation relationship extrapolated from low-temperature cherts (Knauth and Epstein, 1976) was used, it is not clear whether these apparently higher formation temperatures relative to those of alteration clay minerals are meaningful, but this is supported by the following fluid inclusion data.

Studies of fluid inclusions in vein anhydrite at Sites 1188 and 1189 unequivocally establish that phase separation occurred below the seafloor (Vanko et al., 2004; Vanko and Bach, 2005). Trapping temperatures range from 150° to 320°C at 48 mbsf. The range decreases progressively and temperatures increase at depth, to 270°–375°C below 200 mbsf. Knowing that anhydrite only forms in seawater above 150°C, the lower trapping temperatures correspond closely to the present-day thermal gradient interpolated from a borehole temperature measurement of 313°C at 360 mbsf (Shipboard Scientific Party, 2002b). The uppermost trapping temperatures mostly coincide with the two-phase boiling curve for seawater at the appropriate hydrostatic pressures (Bischoff and Pitzer, 1989). Most calculated salinities are close to seawater values, but some approach pure water and others are extremely saline (to 31 wt% NaCl equivalent). Trapping temperatures at Site 1189 are uniformly high (242°–368°C) and range as high as those of the seawater boiling curve. Salinities range from near pure water to ~7 wt% NaCl equivalent.

Preliminary studies of fluid inclusions in hydrothermal quartz from veins, breccia matrixes, and amygdules at Sites 1188 and 1189 yield results very similar to those in anhydrites, including evidence of phase separation (Vanko et al., 2006). At Snowcap, quartz trapping temperatures between 230 and 340 mbsf range from 300° to 400°C. Between 60 and 155 mbsf at Roman Ruins they range from 267° to 380°C. Although anhydrite tends consistently to be paragenetically later than quartz, the two minerals evidently formed at similar temperatures.

No temperature estimates based on isotope ratios or fluid inclusions are available for the two intersections of semimassive sulfide at Site 1189, nor have the illite selvages of Hole 1188F been compared with associated kernels in this respect.

One Hydrothermal Event or Many?

Glassy dacite lava belonging to a sequence that forms the substrate for active sulfide chimneys at Tsukushi has demonstrably flowed over seabed outcrops of altered rhyodacites at Snowcap and contains a xenolith of altered rock. This unequivocal evidence of overlap between hydrothermal activity and volcanic eruptions during the more recent history of Pual Ridge raises the question of whether cycles of volcanic eruption and hydrothermal activity were repeated many times during the construction of the Pual Ridge edifice.

Several observations at Site 1189 suggestive of repeated volcanic and hydrothermal events, initially recorded by Shipboard Scientific Party (2002c), are used by Paulick et al. (2004) in formulating their model of three phases of volcanism and hydrothermal activity. At ~186 mbsf in the Lower Sequence of Hole 1189B, chalcopyrite and sphalerite are present in an altered perlite clast within a polymict volcanoclastic horizon but are apparently absent from the matrix or other clasts, suggesting to Paulick et al. (2004) erosion of an outcrop mineralized during a hydrothermal event at the end of their Phase 1. Within their Phase 2, differently colored clasts with varying proportions of chlorite, illite, and quartz in another polymict volcanoclastic horizon at 117 mbsf in Hole 1189A are considered to be derived by erosion from previously altered outcrops with contrasted alteration styles. The overlying mineralized volcanoclastic horizon with tube pumice clasts (107.7 mbsf) is considered a possible fossil seafloor or immediately subseafloor hydrothermal deposit by Paulick et al. (2004). At Site 1188, noting that the upper pyrophyllite-bearing alteration interval in Hole 1189A could arise from

trapping of highly acid fluids below the impermeable cap of unaltered lava at Snowcap, Paulick and Bach (2006) suggest the lower pyrophyllitic unit in Hole 1188F might represent similar ponding beneath a former but no longer unaltered impervious cap present at the end of Phase 2 (225 mbsf, placed at a boundary between sparsely porphyritic and aphyric dacite by Paulick et al., 2004). These observations have other possible explanations and need further testing.

The arguments supporting the opposite hypothesis—that within the drilled section of Pual Ridge there has been only one overall hydrothermal and subsurface mineralization event—include

1. The comparatively regular zoned alteration profiles characterized successively by opal, cristobalite, and quartz at Site 1188 and in Hole 1189A;
2. Relatively systematic profiles in enrichment or depletion of certain lithophile and chalcophile elements within particular alteration styles, imposed across many lava flows with differing precursor compositions and without disruption at paleoseafloor horizons;
3. The downhole trend in paragonite component of illite in Hole 1188F; and
4. Distribution of features such as illitic selvages throughout Holes 1188A and 1188F and their scarcity at Site 1189.

Systematic downhole profiles for the ranges in fluid inclusion trapping temperatures for vein anhydrites and quartzes at Site 1188 imply one overall veining event throughout Holes 1188A and 1188F, imposed certainly after construction of most of the Pual Ridge edifice but not necessarily implying a single alteration event if that were earlier.

We consider that there is no convincing evidence of multiple alteration episodes in the cores at either Site 1188 or Site 1189, even though this is conceptually possible as shown by the “unconformable” Tsukushi-group flow at Snowcap. Clearly, however, within the alternative single event there have been complex variations in fluid compositions and perhaps physical conditions from place to place and over time. The pervasive alteration systems below both sites are large relative to the areal extent of seafloor hydrothermal activity. If they indeed link at relatively shallow depth as drawn in Figure F6, the subseafloor PACMANUS alteration system is an exceptional feature requiring copious fluid and heat flux. Abundance of unstable glass in the volcanic sequence may have reduced the energy requirements.

The Lower Sequence of Hole 1189B does not exhibit such regular alteration profiles. Its intercalated cristobalite-bearing and quartz-bearing assemblages might at face value suggest repeated alteration events, but from overview of cores with the benefit of reasonably good recovery Shipboard Scientific Party (2002c) inferred one event with varied alteration styles controlled by precursor lithology. Cristobalite-bearing rocks are dominated by coherent facies that were less permeable to hydrothermal fluid flow, whereas the quartz-bearing units were typically of brecciated and flow-banded facies.

Significance of the Cristobalite and Quartz Domains

Cristobalite is not a stable silica polymorph at hydrothermal alteration temperatures (Heaney, 1994). However, it commonly forms outside its stability conditions during burial diagenesis, in low-temperature

wallrock alteration at geothermal sites, and in acid sulfate alteration halos around some epithermal ore deposits. In active geothermal fields, Browne (1978) notes that cristobalite is generally restricted to temperatures below 100°–115°C, whereas quartz occurs at higher temperatures. He suggests that temperature is the dominant control, although differences in silica activity of geothermal fluids modify the relative distribution. Jones and Segnit (1972) proposed that if cristobalite nuclei are present (derived, for example, by high-temperature devitrification of volcanic glass), then epitaxial precipitation of cristobalite may be energetically more favorable in hydrothermal systems than deposition of quartz. Dissolution-precipitation experiments at 150°–300°C (Renders et al., 1995) confirm that cristobalite precipitates from hydrothermal solutions if $\text{Si}(\text{OH})_4$ concentrations exceed cristobalite saturation but are below quartz saturation and provided cristobalite nuclei are present. Except for the fact that the temperatures suggested by Browne appear unrealistically low for the entire cristobalite domain at Site 1188, the scenario is an attractive one for PACMANUS. Relict high-temperature cristobalite formed by devitrification is more likely to be present in felsic volcanic rocks than in basalts, and this could explain the contrast between PACMANUS and the Trans Atlantic Geotraverse (TAG, Mid-Atlantic Ridge) hydrothermal site, where chalcedony and quartz rather than cristobalite dominate seafloor altered assemblages (Hopkinson et al., 1999).

A variety of petrographic evidence in the broader transitional zone between the two domains at Site 1188 indicates that quartz generally formed later than cristobalite, locally replacing it. Hence, a time factor is also involved, in which respect the boundary between cristobalite and quartz domains (shown schematically on Fig. F6) is not the equivalent of a metamorphic “isograd” arising from a conductively imposed thermal gradient preceding or contemporary with alteration once fluid flow commenced. Instead, upwelling of progressively hotter hydrothermal fluids evidently converted earlier cristobalite-dominant assemblages to quartz-bearing assemblages at the sharp transition of Hole 1189A and across a broader domain in Hole 1188A. Advective heating by the fluids at Site 1188 and most of Site 1189 thereby established an overall but irregular upward thermal gradient, complicated by small-scale cells or eddies. Interleaving of cristobalite-bearing products of coherent-facies lavas and quartz-bearing brecciated facies in the Lower Sequence of Hole 1189B may arise from kinetic factors related to fluid/rock ratios together with or instead of temperature differences; lateral movement of quartz-forming fluid along permeable breccia horizons may outweigh effects of vertical upwelling.

Fluid Chemistry Controls on Alteration Styles

Accepting that the altered rocks drilled at Sites 1188 and 1189 represent a single overall event, many variations in fluid compositions and in the nature of fluid/rock interactions were involved, the relative timing of which remains subject to uncertainty and requires focused inquiry.

New observations suggest that the pale illite-rich selvages, formed at Site 1188 from exceptionally potassic fluids low in Mg and Fe, represent an early phase of alteration governed by preexisting fractures, perhaps primary igneous cooling features. Alteration then followed of remnant glassy “kernels” to more chloritic assemblages (with illite and pyrite) through reaction with relatively reduced Mg-rich fluids. Preservation of

igneous plagioclase reflects fluid composition rather than partial alteration; fluids associated with plagioclase-destructive alteration were relatively more enriched in potassium and reduced sulfur. Permeation of fluids from late-stage anhydrite veins into adjacent country rock appears to have had only limited effects, such as growth of disseminated anhydrite in porous illite selvages and development of a “waxy clay” phase on the surfaces of preexisting illites.

In the upper part of Hole 1188A, zones of pervasive pyrophyllite-bearing acid sulfate alteration (“bleaching”) represent reaction with particularly low pH fluid deficient in both Mg and K. The timing of this style of alteration relative to development of kernel-style chloritic assemblages is unclear. Microscopic characteristics suggest an early status for acid sulfate alteration, in conflict with macroscopic appearances. Alternatively, pervasive formation of pyrophyllitic bleached assemblages and associated chloritic kernel assemblages was contemporaneous and dictated by local variations in fluid chemistry. At deeper levels of Site 1188, pyrophyllite is texturally in equilibrium with illite, favoring the contemporaneous alteration alternative.

Limited quantitative modeling (Yeats et al., 2001; Paulick and Bach, 2006) indicates low-pH (<3), low-[K⁺]/[H⁺] fluids associated with pyrophyllitic acid sulfate alteration at Site 1188 vs. higher-pH (>5), high-[Mg²⁺]/[H⁺] fluids associated with chloritic kernel assemblages. Only extremely rarely was pH high enough to stabilize carbonate minerals. Chloritic assemblages containing hydrothermal potassium feldspar at Site 1189 reflect higher fluid [K⁺]/[H⁺] than in equivalents lacking this phase at Site 1188, rather than different temperatures. Rare alunite-bearing assemblages such as at 346 mbsf in Hole 1188F require exceptionally acid fluid (pH < 2).

Alteration temperatures estimated for the drilled portion of Pual Ridge are insufficient for phase separation, although in vein anhydrites and quartz there is clear evidence for this process quite close to the seafloor, possibly after most alteration had been effected. More deeply seated phase separation during the alteration event, however, provides a potential genetic link between low-pH and higher-pH alteration fluids plus a mechanism for widespread hydrofracturing and brecciation. Faster uprise of an aggressive vapor phase and condensed derivatives potentially explain the petrographic indications that development of pale selvages to fractures came first, preceding alteration of unaffected glass “kernels” to chloritic assemblages by reaction with higher-pH, Mg-bearing seawater or brine derivatives. Further support for such processes comes from laser ablation microanalyses of sulfur isotopes in pyrite, discussed later.

Relationships of Alteration to Mineralization

Given the paucity of massive and semimassive sulfide mineralization with elevated base and precious metal contents within the pervasively altered hydrothermal system drilled during Leg 193, scant direct evidence is available for assessing temporal and chemical relationships between hydrothermal alteration of the Pual Ridge volcanic sequence and the formation of sulfide chimneys at the seafloor. From geochemical reaction modeling, Yeats et al. (2001) and Paulick and Bach (2006) observe that hydrothermal end-members for vent fluids collected from Satanic Mills chimneys (Douville et al., 1999) are in equilibrium with pyrophyllite + quartz or kaolinite + cristobalite. End-member compositions and pH of vent fluids collected at 180°C from Roman Ruins (e.g.,

molar K/Ca = 7.8) are similar to those of fluids collected at higher temperatures (250° and 268°C) from Satanic Mills (molar K/Ca = 5.0) (Gamo et al., 1996; T. Gamo, pers. comm., 1996). It is accordingly perplexing that no equivalent pyrophyllite- or kaolinite-bearing alteration occurs in either Holes 1189A or 1189B, both of which were collared beside chimneys. Instead, the common presence of K-feldspar and chlorite (together with illite) in alteration assemblages at Site 1189 indicates alteration fluids with substantially different chemical properties from those forming the chimneys. Together with the disparity between K enrichment of altered rocks as well as of vent fluids at Site 1189, this suggests that the exact conduits for present-day chimney-forming fluids at Roman Ruins were either not intersected or not recovered during Leg 193, for at least some diagnostic acid alteration would be expected in their vicinity.

The relatively few samples recovered in the Stockwork Zone of Hole 1189B, combined with those of CONDRILL shallow drilling, show a vertically upward change from quartz veins to quartz-anhydrite veins and breccia matrixes to nodular semimassive sulfides into a fallen chimney mound then the active chimney field. Pyrite dominates the sulfide assemblages except in the chimneys, whereas chalcopyrite then sphalerite become increasingly abundant in semimassive sulfides then dominate the chimneys. Drawing comparisons with fossil volcanogenic massive sulfide systems, this sequence certainly suggests a genetic relationship between sulfides in the Stockwork Zone and the seafloor chimneys. However, altered wallrocks (Category Z) from the Stockwork Zone are conspicuously potassic and denote equilibration with near-neutral fluids rather than those currently venting at seafloor chimneys. The same difficulties apply to rare quartz veins, carrying minor chalcopyrite, sphalerite, and even gold, that are cut by the more common style of quartz-anhydrite vein at Site 1189.

Overall, much of the extensive subseafloor alteration evident at PACMANUS may have been completed prior to uprise of high-temperature acid fluids in constrained (but as yet undiscovered) conduits feeding the chimneys.

Importance of Dilation within the PACMANUS Hydrothermal System

One of the more striking outcomes of research on Leg 193 cores has been evidence of dilational processes during formation of the subseafloor hydrothermal system at PACMANUS. Preservation of open or partly filled vesicles and cavities in altered volcanic rocks, many of which lie buried beneath considerable overburden, is a remarkable feature of the drilled sequence. Geochemical modeling and density measurements indicate substantial volume expansion of the volcanic sequence during hydrothermal alteration, especially in the upper cristobalite domain. The dominant factor in this expansion is an imposed dilation arising from elevated pore fluid pressures (greater than lithostatic), creating the high porosity between loosely packed clay mineral particles. This creates a most fertile environment for diffusion and mineral deposition, something that would not be recognized in metamorphosed ore environments where the physical evidence will not survive.

Dilational fracturing and infill of created spaces with hydrothermal minerals (quartz, anhydrite, and pyrite) are characteristic of hydrothermal breccias and most veins at Sites 1188 and 1189. The hydrofractur-

ing process again requires excess fluid pressure. Dilation is also ascribed importance for formation of the two semimassive sulfide intersections below Roman Ruins and in shallow CONDRILL equivalents. Subsurface sulfide deposition in open spaces created by such dilation is a process deserving consideration for so-called “subhalative” or “subseafloor exhalative” massive sulfide deposits in ancient sequences where the textural evidence may be destroyed by metamorphism or incorrectly interpreted as replacement wallrock silicate minerals.

One process that could cause repeated dilation is subsurface phase separation or boiling of hydrothermal fluids. If transported rapidly enough in freshly created fractures to avoid cooling by conduction, batches of fluid close to their boiling point at depth would flash on rising adiabatically to a lower-pressure environment resulting in explosive fragmentation followed by mineral deposition. It is unlikely that boiling occurred during pervasive alteration of the drilled volcanic sequence because estimated alteration temperatures are well below the boiling curve of seawater at 1600–2000 mbsl. However, the evidence for boiling fluids in vein anhydrites and quartz is unequivocal (Vanko et al., 2004). Excess fluid pressures during alteration could be a consequence of boiling at deeper levels, transmitted hydraulically through pores and fractures. Because of latent heat effects, flashing of uprising fluid batches will be short lived. Displacements on tectonic fractures could cause more dramatic but perhaps less frequent flashing and dilational effects.

A possible large-scale effect of expansion of the hydrothermal alteration system could be fracturing and breaching of the carapace or cap of relatively impermeable, unaltered lava, thereby enabling escape and venting of fluids at the seafloor (e.g., at Roman Ruins). In this respect, the overall PACMANUS system might be visualized as a geological “pressure cooker.”

On a smaller scale, excessive dilation of delicately cohesive clay aggregates might lead to fluidization, an alternative to the process of hydrothermal corrosion and collapse proposed by Barriga et al. (2001, 2004) as a causal mechanism for some breccia structures and for generation of incoherent domains in the Stockwork Zone of Hole 1189B that might in future become the locus of a large subhalative sulfide ore body.

FLUID SOURCES AND SUBSEAFLOOR HYDROTHERMAL FLUID FLOW

From only two deeply drilled sites, it is clearly not possible to develop conclusive three-dimensional hydrologic models for the subseafloor PACMANUS hydrothermal system, yet valuable constraints have been gained from new measurements of physical properties and a variety of postleg isotopic research enabling assessment of fluid sources and mixing behaviors. In addition, aspects of research on precursor volcanic facies, alteration chemistry, and borehole imagery also relate to understanding fluid pathways.

Porosity, Permeability, Fracturing, and Fluid Flow

From measurements of porosity and intrinsic permeability on representative minicore samples from Sites 1188 and 1189, [Christiansen](#)

and Iturrino (this volume) find porosity and permeability of totally altered rocks to be well correlated, both decreasing with depth from ~30% and $\sim 10^{-16}$ m², respectively, near the seafloor to ~15% and $\sim 10^{-18}$ m² below 300 mbsf. Although ranges overlap, the average permeability of PACMANUS samples is two to four orders of magnitude higher than other seafloor sites where this has been measured, most of which, however, are in basaltic crust with less pronounced alteration.

From X-ray CT studies, Iturrino et al. (this volume) and Ketcham and Iturrino (2005) examine processes associated with porosity and permeability development during alteration, noting that alteration may itself generate microfracturing and thereby increase fluid flow. These studies create new understandings of fluid behavior during hydrothermal alteration that could not be gained from investigating metamorphosed hydrothermal settings in ancient sequences. However, the similarity of ranges in core-scale permeability measured at Sites 1188 and 1189 indicate that other factors govern the contrast between low-temperature diffuse venting at Snowcap and high-temperature focused venting at Roman Ruins. Applying properties of seawater, a thermal gradient corresponding to borehole temperature measurements, and a permeability of 10^{-16} m² in a simple linear model, Christiansen and Iturrino (this volume) calculate a diffusive fluid flow velocity through coherent rocks of <2 cm/yr. This is grossly deficient for explaining observed vent rates at Roman Ruins and most probably at Snowcap as well, so they conclude that focused fluid flow within open fractures is the predominant mechanism at both sites.

Bartetzko et al. (2006) provide electrical conductivity measurements on seawater-saturated minicores from a range of altered lithologies at Sites 1188 and 1189, concluding that porosity and pore space structure (tortuosity) are the main controls on conductivity, with connectivity of sulfide minerals important in some cases. Significantly, they observed that downhole geophysical logging during Leg 193 indicates substantially higher conductivities than those measured on the minicore samples. The logging profiles integrate much larger volumes and thus reinforce the importance of fractures dominating fluid flow regimes. From resistivity imagery of borehole walls, Iturrino and Bartetzko (2002) describe a predominance of subvertical fractures striking north-northeast, suggesting a possible tectonic control on fluid pathways.

Variations in the parental fabrics and precursor compositions of the altered sequence below Pual Ridge are unlikely to have a major influence on fluid flow patterns, except at the very early stages of hydrothermal alteration. Paulick and Herzig (2003) suggest that higher primary porosity and permeability of volcanoclastic horizons would focus fluid flow and facilitate higher fluid/rock ratios during alteration. Reflecting this, they measured significant silica loss from altered dacite clasts in volcanoclastic units, balanced by gains in the matrix, recalling Category Z alteration in the Stockwork Zone of Hole 1189B.

Strontium and Sulfur Isotope Ratios in Anhydrite

The use of strontium isotope ratios in sulfate minerals is a well-established tool for fingerprinting fluid sources and mixing in active seafloor hydrothermal systems (Tivey et al., 1995; Teagle et al., 1998). Analyses of ⁸⁷Sr/⁸⁶Sr in anhydrites filling veins, breccia matrixes, and vesicles from Sites 1188 and 1189 are presented by Roberts et al. (2003) and Bach et al. (this volume). Interpretations rely on knowing the ⁸⁷Sr/⁸⁶Sr ratios of seawater (0.7092), of fresh Pual Ridge lavas (0.7036 throughout

the fractionation series), and of high-temperature end-member vent fluid at PACMANUS (0.7050, extrapolated from Douville et al., 1999).

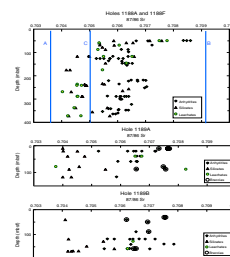
Vein anhydrites to 70 mbsf in the upper cristobalite domain of Hole 1188A have distinctly radiogenic $^{87}\text{Sr}/^{86}\text{Sr}$ (0.7067–0.7086). Below 87 mbsf in the cristobalite domain and continuing through the underlying quartz domain to 364 mbsf, $^{87}\text{Sr}/^{86}\text{Sr}$ varies between 0.7050 and 0.7070 with no clear downhole trend (Fig. F11). In Hole 1189A there is a possibly coincidental difference between veins and breccias: anhydrites from veins span a similar range of bulk $^{87}\text{Sr}/^{86}\text{Sr}$ ratios (0.7052–0.7072) to the 87- to 364-mbsf section at Site 1188, whereas all but one of those from breccias are more radiogenic ($^{87}\text{Sr}/^{86}\text{Sr} = 0.7073$ –0.7077) whether from the cristobalite or the quartz domains (Fig. F11). In the Stockwork Zone of Hole 1189B, however, breccia and vein anhydrites have overlapping $^{87}\text{Sr}/^{86}\text{Sr}$ ratios ranging from 0.7062 to 0.7076. In the Lower Sequence, anhydrite veins in cristobalite-bearing samples have $^{87}\text{Sr}/^{86}\text{Sr}$ ratios from 0.7069 to 0.7079, more radiogenic mostly than equivalents from quartz-bearing samples (0.7055–0.7071).

Roberts et al. (2003) and Bach et al. (this volume) ascribe the $^{87}\text{Sr}/^{86}\text{Sr}$ data to variable mixing between seawater and a high-temperature hydrothermal end-member ($^{87}\text{Sr}/^{86}\text{Sr} = 0.7050$) in the fluids that deposited the anhydrites. They calculate proportions of admixed seawater varying from 89% for the uppermost anhydrites (cristobalite domain) to an average of ~30–40 wt% in the quartz domains. Significant fluctuations around these values at both sites, however, imply a very heterogeneous mixing system, a conclusion supported by ion microprobe evidence of considerable $^{87}\text{Sr}/^{86}\text{Sr}$ variability in individual anhydrite veins (Craddock and Bach, 2004). Where evidence exists for timing (e.g., multiple vein fillings) the evolutionary trend is generally toward higher indicated seawater proportions. In the Lower Sequence of Hole 1189B, veins in cristobalite-bearing alteration assemblages formed from fluids with a higher proportion of admixed seawater than those from quartz-bearing intervals.

Paulick et al. (this volume) provide $^{87}\text{Sr}/^{86}\text{Sr}$ analyses of disseminated and veinlet anhydrite leached from a range of altered rocks at Sites 1188 and 1189, together with analyses of the corresponding bulk rocks from which anhydrite was removed. At both sites the majority of anhydrite-free altered rocks (“silicate” fractions in Fig. F11) have $^{87}\text{Sr}/^{86}\text{Sr}$ ratios (0.704–0.706) that span the inferred end-member vent fluid ratio and are more radiogenic than those of glassy Pual Ridge lavas, comparing closely with altered volcanic outcrops at the Snowcap seafloor (0.7044–0.7052; CSIRO data). The silicate fraction of altered rocks in the cristobalite domain of Hole 1188A, and a few at deeper levels, have even more radiogenic Sr ($^{87}\text{Sr}/^{86}\text{Sr}$ as high as 0.7076). Variable degrees of exchange between igneous, hydrothermal, and seawater strontium have clearly occurred within the altered rocks, mostly with a net loss of total Sr (see Table T3). Disseminated anhydrites (the “leachates” of Fig. F11) at Site 1188 have $^{87}\text{Sr}/^{86}\text{Sr}$ ratios that correspond closely to those of silicate components of their host altered rocks, rather than to nearby vein or breccia anhydrites. At Site 1189 the reverse is the case (Fig. F11). If disseminated anhydrites at Site 1188 reflect permeation of the same fluids that deposited anhydrite veins, then there has been considerable exchange with the host rocks, but at Site 1189 they appear more directly cogenetic with vein or breccia anhydrites.

Barites and rare early formed anhydrites in PACMANUS chimneys have a limited range of $^{87}\text{Sr}/^{86}\text{Sr}$ from 0.7046 to 0.7054. Anhydrite more

F11. Strontium isotope ratios, Sites 1188 and 1189, p. 60.



often occurs as a late-stage chimney mineral in transgressive veinlets or cavity fillings where $^{87}\text{Sr}/^{86}\text{Sr}$ varies from 0.7069 to 0.7090 (Binns et al., 2002b; R. A. Binns et al., unpubl. data; Kim et al., 2004). In shallow CONDRILL semimassive sulfides (<2 mbsf), early formed barites ($^{87}\text{Sr}/^{86}\text{Sr} = 0.7046\text{--}0.7059$), mid-stage anhydrite ($^{87}\text{Sr}/^{86}\text{Sr} = 0.7076$), and late-stage anhydrites ($^{87}\text{Sr}/^{86}\text{Sr} = 0.7068\text{--}0.7080$) define progressive dilution of hydrothermal fluids by seawater during continuing dilation and mineral deposition. Pulses of fluid with higher "hydrothermal" component followed by progressive dilution with seawater appear a common aspect of the PACMANUS system generally.

Sulfur isotope characteristics of anhydrite differ between Snowcap and Roman Ruins (Roberts et al., 2003). Apart from two veins in the uppermost cristobalite domain (+21.6‰ and +21.7‰), anhydrite $\delta^{34}\text{S}$ values at Site 1188 range from +18.1‰ to +21.1‰, below that of seawater (21.0‰; Rees et al., 1978). Anhydrite $\delta^{34}\text{S}$ at Site 1189 mostly ranges from +20‰ to +22.3‰ with the majority above the seawater value. Roberts et al. (2003) ascribe the contrast to disproportionation of a magmatic SO_2 component at Snowcap and partial reduction of seawater sulfate by wallrock ferrous iron at Roman Ruins.

Sulfur Isotope Ratios in Pyrite

Conventional sulfur isotope analyses of hand-picked grains (Roberts et al., 2001; R.A. Binns and A.S. Andrew, unpubl. data) and laser ablation microanalyses of ultra-thin sections (R.A. Binns and J.B. Gemmell, unpubl. data) yield comparable results for coarser pyrites from veins, vesicles, breccia matrixes, and semimassive sulfides from both Site 1188 and Site 1189. The overall range in $\delta^{34}\text{S}$, from -0.7‰ to $+5.2\text{‰}$ (mostly $+2\text{‰}$ to $+4\text{‰}$), overlaps that of sulfides from PACMANUS chimneys (-2.1‰ to $+7.5\text{‰}$; average at Snowcap = $+0.3\text{‰}$, Satanic Mills = $+0.4\text{‰}$, and Roman Ruins = $+3.0\text{‰}$; Gemmell et al., 1996; Binns et al., 2002b).

By contrast, finely disseminated pyrites in altered volcanic rocks at Site 1188 (kernels and transitional zones) range to higher values of $\delta^{34}\text{S}$ ($+1.0\text{‰}$ to $+13.7\text{‰}$). Those in altered wallrock clasts within breccias from the Stockwork Zone of Hole 1189B range from $+0.3\text{‰}$ to $+10.9\text{‰}$. The more elevated $\delta^{34}\text{S}$ values suggest substantial contributions from seawater sulfate reduced by ferrous iron contained within altered or altering volcanic rocks.

Fluid Flow Models

Adopting the concept of single hydrothermal events at each site, Roberts et al. (2003) use strontium and sulfur isotope data for vein, breccia, and vesicle anhydrites to propose separate upwelling zones below each drilled vent field and describe contrasted fluid evolutions at Snowcap and Roman Ruins involving sulfate-rich low-pH and sulfate-poor high-pH fluids, respectively. At each site they envisage introduction of seawater from local shallow circulation systems, whereas a deeper circulation and mixing system surrounds the entire PACMANUS site. A genetic connection between anhydrite veins and wallrock alteration is assumed, and to account for the presence of pyrophyllite at Snowcap only, they introduce to this system a component of magmatic volatiles from depth from which SO_2 disproportionation causes acid sulfate conditions.

Lackschewitz et al. (2004) develop a different model to explain their oxygen isotope temperature profiles for clay minerals and quartz, particularly the apparently higher temperatures evident in the upper pyrophyllite interval of Hole 1188A and also in the Stockwork Zone of Hole 1189B. This model involves advective heating of the Pual Ridge sequence and progressive cooling through admixture of seawater within separate high-temperature fluid upwelling zones located to the sides of each of Sites 1188 and 1189. The upwelling zones spread laterally on encountering the fresh lava cappings in each case. At both sites drill holes penetrated the fringes of the ponded fluid bodies, but at Snowcap Hole 1188F continued to drill through a small-scale descending eddy beside the main upwelling zone.

Paulick and Bach (2006) suggest that abundance of fragmental volcanic facies below Roman Ruins favors development of secondary circulation cells dominated by seawater to the sides of a constrained conduit with focused flow of high-temperature vent fluid. For Snowcap they propose that the predominant coherent lava flows hinder drawdown of seawater in secondary cells and that relatively less modified hydrothermal fluids flowing in a nonfocused manner become ponded directly below the unaltered and impermeable dacite cap, causing pyrophyllite-bearing acid sulfate alteration. In a different explanation for opposed venting characteristics between the two sites, Vanko et al. (2004) suggest that an anhydrite-cemented shell surrounding the Roman Ruins upflow zone isolated it from seawater ingress.

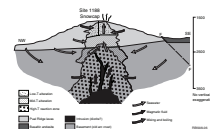
Looking at finer details, Roberts et al. (2003) and Vanko et al. (2004) draw attention to discrepancies between temperatures indicated by fluid inclusion studies and those calculated for isenthalpic mixing of cold seawater and a hypothetical 250°C hydrothermal fluid in ratios indicated by the Sr isotope data. Various scenarios of conductive heating of seawater or conductive cooling of the ascending high-temperature hydrothermal fluid prior to their mixing, advanced to explain relationships at the respective sites, may need reassessment following recent measurements of much higher temperatures at PACMANUS vents (as high as 356°C; Seewald et al., 2006; Tivey et al., 2006).

Such models rely on selective data sets and would likely change if many more holes were to be drilled at PACMANUS. They overlook the issue of phase separation and uncertainties in the relative timing of different alteration styles or between alteration, veining, and mineralization. Nevertheless, the models clearly demonstrate considerable complexity of fluid pathways within the subseafloor hydrothermal system at PACMANUS, and processes such as heating by advective fluid circulation. They point the way toward new approaches to interpreting ancient massive sulfide ore bodies and their environments.

Source of Chimney Metals: The Role of Magmatic Volatiles

Figure F12 is a cartoon originally drawn to illustrate the conceptual background and objectives of Leg 193 in its pre-cruise *Scientific Prospectus* (www-odp.tamu.edu/publications/prosp/193_prs/193toc.html). In a broad sense it still illustrates the general fluid flow pattern believed to occur below Snowcap, ignoring the numerous complexities in detail arising as described above from the drilling and subsequent research, such as advective thermal and chemical changes associated with small-scale fluid cells. Excess fluid pressures indicated by volume expansion during pervasive alteration, evidence for phase separation or boiling at

F12. “PACMANUS pressure cooker” model, p. 61.



least within vein systems, and presence of an almost continuous impervious capping of unaltered lava below the seabed constitute unforeseen outcomes of the leg that collectively form the basis of a “PACMANUS pressure cooker” model in which episodic breaching of the cap leads to development of individual chimney fields at the seafloor. In the pre-cruise hypothesis, magma-derived metal-rich fluids rising from a subjacent intrusion have become increasingly mixed at all levels with circulating seawater. That mixing happens in the higher drilled part of Pual Ridge is unequivocally established by results presented above. That it also happens at deeper levels than explored by drilling is required by the more radiogenic nature of the modeled high-temperature end-member fluid of the upper system ($^{87}\text{Sr}/^{86}\text{Sr} = 0.7050$) relative to the highly constrained Sr isotope ratio of Pual Ridge glassy lavas ($^{87}\text{Sr}/^{86}\text{Sr} = 0.7036$), provided the intrusion and lavas are cogenetic ($^{87}\text{Sr}/^{86}\text{Sr}$ varies little across the various neovolcanic edifices of the eastern Manus Basin) and, of course, depending on the confidence assigned to the magmatic fluid concept itself. It is therefore appropriate to conclude the geological part of this synthesis with a review of the evidence favoring that concept and its implied importance in governing the high Cu, Zn, Ag, and Au tenors of PACMANUS chimneys.

Fluid bubbles in melt inclusions within phenocrysts from lavas at various eastern Manus Basin volcanic edifices including Pual Ridge contain high levels (weight percent range) of Cu and Zn (Yang and Scott, 1996). Treating these bubbles as a proxy for the behavior of large magma bodies, Yang and Scott (1996, 2002, 2005) extensively investigate degassing of lavas or devolatilization of subjacent magma bodies as feasible mechanisms for introducing magma-derived metals into seawater-dominated hydrothermal fluids. In a separate study, abrupt decreases in Cu and Au contents at the basaltic andesite stage of fractionation in east Manus lavas recorded by Sun et al. (2004) are attributed to their removal into exsolved fluids as a consequence of redox effects associated with initiation of magnetite precipitation. The process is more likely to apply in water-rich, relatively oxidized island arc magmas as distinct from those associated with mid-ocean or backarc spreading. Only small volumes of exsolved magmatic fluids need adding to dominant seawater-derived hydrothermal fluids in order to sufficiently enrich the overall mixture in the metals that ultimately deposit in seafloor chimneys.

Adding to earlier geochemical and isotopic interpretations for PACMANUS chimneys and vent fluids (see “**Geological Setting,**” p. 4, above), Leg 193 has contributed further indirect evidence for involvement of magmatic fluids in the hydrothermal system. At Snowcap, sulfur isotope ratios in vein and breccia anhydrites and the presence of pyrophyllite-bearing intervals of hydrothermal alteration are interpreted as consequences of SO_2 disproportionation and thus of magmatic volatiles in the hydrothermal fluid (Roberts et al., 2003). Relatively light sulfur isotope ratios in pyrites from veins and semimassive sulfides bear the same connotation, although relative to other sites (e.g., Lau Basin; Herzig et al., 1998) there may be a higher proportion of reduced seawater sulfate at PACMANUS. The nature of rare earth element (REE) patterns in anhydrites from Snowcap implies input of magmatic hydrofluoric acid as well as SO_2 (Bach et al., 2003).

The alternative to a magmatic source for base and precious metals is leaching during alteration of subseafloor sequences traversed by seawater-dominated hydrothermal fluids. Below Snowcap, some altered

volcanic rocks are depleted in Cu, Zn, and Pb relative to their precursors, so this is also a feasible process. However, except for Zn and Cd, the overall abundances of chalcophile elements (including “magmatophile” trace elements) in altered wallrocks, particularly at Roman Ruins, discount significant contribution of these elements to chimney-forming hydrothermal fluids during alteration of the volcanic sequence drilled during Leg 193. Barium—by far the dominant gangue element of chimneys at Roman Ruins—is also conspicuously enriched in underlying altered rocks at Site 1189. Derivation of Cu and associated elements by alteration at deeper levels including basement can not be discounted, but for As and Sb in particular the enrichments in both chimneys and overall in the drilled subseafloor sequence appear difficult to explain in this way. Slight differences in Pb isotope ratios of glassy Pual Ridge lavas and subseafloor or chimney sulfides at Roman Ruins suggest that Pb in the latter is derived in part from deep-seated reaction of hydrothermal fluids with radiogenic basement (Binns, this volume).

Had we drilled deeper, or if, as initially expected, the vertical sequence from intrusion to high-temperature reaction zone to upper crustal hydrothermal system were more condensed than proved the case, more conclusive evidence for the magmatic component might have been gained. Among the initial objectives of Leg 193 we also hoped to find explanations for the particularly high Cu, Zn, Ag, and Au contents of PACMANUS chimneys. In the event, scarcity of subsurface mineralization in the cores recovered has prevented assessment of potential processes such as phase separation or “zone refining.” Subseafloor precipitation, predominantly of pyrite in altered rocks, veins, and breccias, may have depleted the hydrothermal fluids in Fe. In the semimassive sulfide at 31 mbsf in Hole 1189B and similar material from shallow CONDRILL cores, pyrite is the first-formed sulfide and is followed by chalcopyrite then sphalerite, suggesting the possibility of a “fluid fractionation” process leading to Cu and Zn enrichment (Binns, 2005). Such a process is an alternative to “zone refining” that involves dissolution, upward transport, and reprecipitation of elements like Cu, but it is unlikely to be uniquely operative at PACMANUS.

DEEP BIOSPHERE AND BIOMINERALIZATION

A major success of Leg 193 was confirmation that microbes including actinomycetes (filamentous or dendritic bacteria), cocci, and bacilli flourish in the shallow subsurface portion of the PACMANUS hydrothermal system. Bacteria were found by direct counting of total cells in core samples from depths to ~70 mbsf in Hole 1188A and ~80 mbsf in Holes 1189A and 1189B (Kimura et al., 2003). Adenosine triphosphate (ATP) analysis detected live cells in cores recovered to ~50 mbsf under Site 1188 and ~40 mbsf under the high-temperature chimney field at Site 1189. Cell counts fell progressively with depth at both sites.

Growth occurred of colonial and dispersed individual bacteria in anaerobic cultivation experiments at 60°C in samples from 60 to 88 mbsf at Site 1188 and from 50 to 99 mbsf at Site 1189 (Kimura et al., 2003). In experiments at 90°C, growth occurred in samples from 69 to 107 mbsf at Site 1188 and from 68 to 129 mbsf at Site 1189. This extends the range of microbial habitats relative to those detected by the ATP analysis. In neither experiment set was growth observed in shallower or deeper samples than the ranges cited. Higher cultivation temperatures favor microbes from deeper core samples. Using 16S

ribosomal deoxyribonucleic acid (rDNA) analysis, Kimura et al. (2003) identified bacteria from the 60° and 90°C cultures as new subspecies of *Geobacillus* sp. and *Deinococcus* sp., respectively, the latter being previously regarded as a more typically aerobic strain.

Within the PACMANUS hydrothermal alteration system Asada et al. (2003) found clay minerals to be the preferred microbial habitat, suggesting these may act as a buffer against hydrothermal fluids and as a source of K⁺ and H₂O nutrients via bacterial dissolution. In the unaltered volcanic caprock, glass is the preferred microbe habitat. Chemical analyses of microbial samples revealed relatively low carbon contents (150–1270 ppm; mean = 320 ppm), whereas nitrogen was not detected. Paucity in C and N, or limited flux of nutrient-bearing hydrothermal fluids, may restrict microbe abundances.

Transmission electron microscope evidence for biomineralization found within cores from 87.9 and 106.8 mbsf in Hole 1188A includes clay flakes covering the outer cell walls and mineralized cell interiors of two bacteria and a thick gridlike cell wall covered by excretal exopolymers in a third (Asada et al., 2003).

Below 129 mbsf the PACMANUS hydrothermal system is evidently sterile. Unfortunately, temperature logging was inadequate for translating this into a maximum temperature limit for microbial life.

SUMMARY

Despite the technical challenges presented during the drilling program and the overall poor core recovery, multidisciplinary research on board ship and subsequently at many laboratories around the world has successfully achieved most major objectives of Leg 193. We now know that Pual Ridge was constructed by many lava flows ranging from andesite to rhyodacite, displaying coherent and brecciated facies and with some volcanoclastic horizons. Several paleoseafloor horizons have been identified, but there are no accumulations of hemipelagic sediment at these to indicate major hiatuses in volcanic activity, nor is there unequivocal evidence of fossil chimneys or other hydrothermal deposits at paleoseafloor positions. No plutonic rocks were encountered by drilling, so we have no further insights into the inferred intrusive or magma chamber that represents the heat engine to drive the hydrothermal system and a possible source of fluids and metals.

Detailed pictures of subsurface alteration phenomena and processes have emerged. The evidence favors one major alteration event pervasively imposed on all but the youngest lavas at the crest of Pual Ridge. It is unclear how the alteration systems link at depth between Snowcap (1635–1645 mbsl), where diffuse low-temperature venting occurs at seabed outcrops of altered volcanic rock, and Roman Ruins (1680–1690 mbsl, 1.0 km away), where focused high-temperature venting occurs at sulfide chimneys. Both sites display a change downhole from cristobalite-bearing assemblages to quartz-bearing alteration assemblages, but this occurs at a shallower level below Site 1189. Clay mineral assemblages dominate both sites but show no pronounced vertical change in character, reflecting advective heating by hydrothermal fluid cells rather than a conductive thermal gradient. Isotopic estimates of alteration temperatures in the quartz domains are in the range 220°–300°C; those in the cristobalite domain are not yet delineated. The presence of hydrothermal K feldspar and enrichments in K, Ba, and U at Roman Ru-

ins constitute the principal lateral differences between alteration assemblages at Sites 1188 and 1189, respectively.

Two intervals of semimassive sulfide were cored. Semimassive sulfide near the base of Hole 1189A involved dilation and dispersal of clasts within a volcanoclastic horizon, with precipitation of quartz and sulfides in newly created matrix space. The other, in a Stockwork Zone directly below the cased top of Hole 1189B, was formed by extreme and repetitive dilation and mineral deposition in altered volcanic rock. Its paragenetic sequence from early sulfides to late anhydrite reflects progressive dilution by seawater of a high-temperature hydrothermal fluid sourced from deeper in the system. By preferentially removing Fe from hydrothermal fluids, seafloor deposition of pyrite in the Stockwork Zone underlying Roman Ruins may contribute to chimney enrichments in base and precious metals.

Strontium isotopic evidence indicates mixing between seawater and a high-temperature hydrothermal fluid that itself has a component of seawater intermixed with fluids derived from igneous or magmatic sources at deeper levels than those explored by drilling. Fluid inclusions in anhydrites establish that phase separation or boiling has occurred in fractures that became veins and breccia matrixes within the pervasively altered volcanic sequence, and possibly at deeper levels than those drilled during alteration itself.

The presence of pyrophyllite-bearing acid sulfate alteration indicating former presence of SO₂ represents the main new evidence, not unequivocal, for magmatic fluid components. Curiously, this acid sulfate style of alteration has limited occurrence at Site 1188 and is absent from Site 1189 where subsurface mineralization and seafloor chimneys are more prominent. The sulfur isotope characteristics of some pyrites and anhydrites also indicate a magmatic component mixed with variable proportions of seawater-derived sulfur. REE distribution patterns in anhydrites are considered to imply transport by fluorine complexes and thus a magmatic ligand source.

Geochemical assessments reveal extensive mass transfer during alteration but establish that Cu and trace chalcophile metals were not significantly leached from the drilled volcanic sequence and did not thereby contribute to the metal contents of seabed chimneys. Likewise, the gangue barite of chimneys does not derive from leached wallrock barium. While leaching at unexplored deeper levels is not ruled out, the concept of a magmatic origin for enriched base and precious metals in PACMANUS chimneys remains attractive.

Elevated porosity and permeability of the altered volcanic rocks facilitated diffusion during alteration processes, but fracturing is the more important control on fluid flow. Restriction of physical property and isotopic data to essentially two vertical drill profiles with uncertain hydrologic connectivity does not allow construction of definitive fluid flow models for the overall hydrothermal system. High porosity and consequent volume expansions appear imposed by excess fluid pressures during alteration, possibly related to phase separation at deeper levels in the system. Volume expansion provides an alternative mechanism to tectonic fracturing for breaches of the impervious capping of unaltered volcanic rock that, perhaps temporarily, become sites of chimney formation.

The presence has been established of a microbial biosphere within the active hydrothermal system, extending to ~130 mbsf, below which the system is sterile. The maximum temperature for microbial life here has not been quantified as a consequence of insufficient meaningful

borehole temperature measurements. Indications of mineralized microbes were found, but biomineralization does not appear to be a significant process below the seabed as compared to some chimneys.

From the discussions in this Synthesis chapter there are clearly many issues of detail in the PACMANUS hydrothermal system that remain unresolved or uncertain. Definite scope remains for further research on cores and logging data from Leg 193, particularly for integrated studies directed at samples and correlated resistivity images that have been specifically selected to address those issues.

For the longer term, PACMANUS is now established as a most appropriate site for continued drilling investigations. We have so far explored only the upper levels of this modern analog of ancient ore-forming systems. The next steps required to further advance our understanding are (1) to drill even deeper toward the inferred intrusive body and its surrounding high-temperature reaction zone, (2) to attempt deeper penetration below the Satanic Mills site for comparison of hydrothermal products and processes with Roman Ruins, and (3) to drill sufficiently deep holes between these sites to establish continuity or otherwise of alteration and mineralization patterns between them and to investigate their relationships with thickness variations of the unaltered volcanic capping. Leg 193 has demonstrated that these requirements are technically feasible under the Integrated Ocean Drilling Program (IODP), although coring methods that increase recovery rates will be highly desirable.

ACKNOWLEDGMENTS

This research used samples provided by the Ocean Drilling Program (ODP). ODP is sponsored by the U.S. National Science Foundation (NSF) and participating countries under management of Joint Oceanographic Institutions (JOI), Inc. R.A. Binns acknowledges funding provided by CSIRO and the P2+ consortium of Australian mineral companies and assistance from colleagues at CSIRO and staff at the Electron Microscopy Unit and the Department of Earth and Marine Sciences at the Australian National University. F.J.A.S. Barriga acknowledges Fundação para a Ciência e Tecnologia and GRICES for support through travel grants and projects Seahma (POCTI/MAR/15281/1999) and Archimedes (FCT/SAPIENS 2001/41393) and various forms of support and help from colleagues and staff at the University of Lisbon. D.J. Miller was funded by the JOI/U.S. Science Advisory Committee and ODP/IODP. Collectively, we acknowledge the hard work and stimulating discussions of the Shipboard Scientific Party, both during and after Leg 193. Randolph Koski and Jose Honnorez are thanked for their comprehensive reviews, which greatly improved this chapter.

REFERENCES

- Arkai, P., 2002. Phyllosilicates in very low-grade metamorphism: transformation to micas. In Mottana, A., Sassi, F.P., Thompson, J.B., Jr., and Guggenheim, S. (Eds.), *Micas: Crystal Chemistry and Metamorphic Petrology*. Rev. Mineral. Geochem., 46:463–478.
- Asada, R., Tazaki, K., Kimura, H., Masta, A., and Barriga, F.J.A.S., 2003. Transmission electron microscopic observation and drilling microbiological core samples from a deep seafloor at hydrothermal vent field. In Tazaki, K. (Ed.), *Water and Soil Environments: Biological and Geological Perspectives: Biological and Geological Perspectives*. Proc. Int. Symp. Kanazawa Univ. 21st Century COE Program, 294–299.
- Bach, W., Roberts, S., Vanko, D.A., Binns, R.A., Yeats, C.J., Craddock, P.R., and Humphris, S.E., 2003. Controls of fluid chemistry and complexation on rare earth element contents of anhydrite from the PACMANUS seafloor hydrothermal system, Manus Basin, Papua New Guinea. *Miner. Deposita*, 38(8):916–935.
- Barash, M.S., and Kuptsov, V.M., 1997. Late Quaternary palaeoceanography of the western Woodlark Basin (Solomon Sea) and Manus Basin (Bismarck Sea), Papua New Guinea, from planktic foraminifera and radiocarbon dating. *Mar. Geol.*, 142(1–4):171–187. doi:10.1016/S0025-3227(97)00049-2
- Bartetzko, A., Klitzch, N., Iturrino, G., Kaufhold, S., and Arnold, J., 2006. Electrical properties of hydrothermally altered dacite from the PACMANUS hydrothermal field (ODP Leg 193). *J. Volcanol. Geotherm. Res.*, 152(1–2):109–120. doi:10.1016/j.jvolgeores.2005.10.002
- Bartetzko, A., Paulick, H., Iturrino, G., and Arnold, J., 2003. Facies reconstruction of a hydrothermally altered dacite extrusive sequence: evidence from geophysical downhole logging data (ODP Leg 193). *Geochem., Geophys., Geosyst.*, 4(10):1087. doi:10.1029/2003GC000575
- Barriga, F.J., Binns, R.A., and Miller, D.J., 2001. Hydrothermal corrosion: a major pre-ore forming process documented by ODP Leg 193 (PACMANUS, Manus Basin, Papua New Guinea). *Eos., Trans. Am. Geophys. Union*, 82(47)(Suppl.):OS11A-0339. (Abstract)
- Barriga, F.J.A.S., Binns, R.A., and Miller, D.J., 2004. Leg 193: the third dimension of a felsic-hosted, massive sulphide hydrothermal system in a back-arc basin (Pac-manus, Papua New Guinea). *Proc. Int. Geol. Congr.*, 32(2):1425. (Abstract)
- Binns, R.A., 2004. Eastern Manus Basin, Papua New Guinea: guides for volcanogenic massive sulphide exploration from a modern seafloor analogue. In McConachy, T.F., and McInnes, B.I.A. (Eds.), *Copper-Zinc Massive Sulphide Deposits in Western Australia*. CSIRO Explores, 2:59–80.
- Binns, R.A., 2005. Strontium and sulfur isotopes in anhydrite and barite from CONDRILL cores at PACMANUS, eastern Manus Basin, Papua New Guinea. In Herzig, P.M., and Petersen, S. (Eds.), *Detailuntersuchung der Magmatisch-Hydrothermalen Goldvererzung des Conical Seamount (Papua-Neuguinea) mit Flachbohrungen*. BMBF Proj. 03G0166 Final Rep., TU Freiberg: 30–44.
- Binns, R.A., Barriga, F.J.A.S., Miller, D.J., et al., 2002. *Proc. ODP, Init. Repts.*, 193: College Station, TX (Ocean Drilling Program). doi:10.2973/odp.proc.ir.193.2002
- Binns, R.A., Brodie, P., Fulton, R., Mapham, B., Park, S.H., Parr, J.M., Pinto, A., Rees, C., Subandrio, A., Thomas, S., Wama, J., and Whiting, R., 2002a. Submarine hydrothermal and volcanic activity in the western Bismarck island arc, Papua New Guinea. *CSIRO Explor. Min. Rep.*, 939C.
- Binns, R., Dekker, D., and Franzmann, P., 2000. Cruise summary, R/V *Franklin* FR03/00, Binatang-2000 cruise. *CSIRO Explor. Min. Rep.*, P2005/227.
- Binns, R.A., McConachy, T.F., Parr, J.M., and Yeats, C.J., 2002b. The PACMANUS Memoir (P2+). *CSIRO Explor. Min. Rep.*, 1032C [CD-ROM]. Available from: CSIRO Exploration and Mining, PO Box 883, Kenmore QLD 4069, Australia.
- Binns, R.A., Parr, J.M., Scott, S.D., Gemmell, J.B., and Herzig, P.M., 1995. PACMANUS: an active seafloor hydrothermal field on siliceous volcanic rocks in the eastern

- Manus Basin, Papua New Guinea. In Mauk, J.L., and St. George, J.D. (Eds.), *Proc. 1995 Pac. Rim Congress*. AusIMM Bull., 49–54.
- Binns, R.A., and Scott, S.D., 1993. Actively forming polymetallic sulfide deposits associated with felsic volcanic rocks in the eastern Manus back-arc basin, Papua New Guinea. *Econ. Geol.*, 88:2226–2236.
- Binns, R.A., Waters, J.C., Carr, G.R., and Whitford, D.J., 1996. A submarine andesite-rhyodacite lineage of arc affinity, Pual Ridge, eastern Manus back-arc basin, Papua New Guinea. *Eos, Trans. Am. Geophys. Union*, 77:119–120.
- Bischoff, J.L., and Pitzer, K.S., 1989. Liquid-vapor relations for the system NaCl-H₂O: summary of the P-T-x surface from 300° to 500°C. *Am. J. Sci.*, 289:217–248.
- Browne, P.R.L., 1978. Hydrothermal alteration in active geothermal fields. *Annu. Rev. Earth Planet. Sci.*, 6:229–248. doi:10.1146/annurev.ea.06.050178.001305
- Chatterjee, N.D., Johannes, W., and Leistner, H., 1984. The system CaO-Al₂O₃-SiO₂-H₂O: new phase equilibria data, some calculated phase relations, and their petrological applications. *Contrib. Mineral. Petrol.*, 88(1–2):1–13. doi:10.1007/BF00371407
- Corliss, J.B., Dymond, J., Gordon, L.I., Edmond, J.M., von Herzen, R.P., Ballard, R.D., Green, K., Williams, D., Bainbridge, A., Crane, K., and van Andel, T.H., 1979. Submarine thermal springs on the Galápagos rift. *Science*, 203(4385):1073–1083. doi:10.1126/science.203.4385.1073
- Cousens, D.R., Ralston, J.A., Hainsworth, D., Matejowsky, E., and Flynn, D., 2003. Magnetic and resistivity measurements on hydrothermal vents. In Yeats, C.J. (Ed.), *Seabed Hydrothermal Systems of the Western Pacific: Current Research and New Directions*. CSIRO Explor. Min. Rep., 1112F:75–76.
- Craddock, P.R., and Bach, W., 2004. Microbeam analyses of rare-earth element (REE) and Sr isotopes of anhydrite veins from the PACMANUS hydrothermal system. *Eos, Trans. Am. Geophys. Union*, 85(47)(Suppl.):V54A-05. (Abstract)
- Douville, E. 1999. Les fluides hydrothermaux océaniques comportement géochimique des éléments traces et des terres rares: processus associés et modélisation thermodynamique [Ph.D. thesis]. Univ. Brest, France.
- Douville, E., Bienvenu, P., Charlou, J.L., Donval, J.P., Fouquet, Y., Appriou, P., and Gamo, T., 1999. Yttrium and rare earth elements in fluids from various deep-sea hydrothermal systems. *Geochim. Cosmochim. Acta*, 63(5):627–643. doi:10.1016/S0016-7037(99)00024-1
- Francheteau, J., Needham, H.D., Choukroune, P., Juteau, T., Séguret, M., Ballard, R.D., Fox, P.J., Normark, W., Carranza, A., Cordoba, D., Guerrero, J., Rangin, C., Bougault, H., Cambon, P., and Hekinian, R., 1979. Massive deep-sea sulfide ore deposits discovered on the East Pacific Rise. *Nature (London, U. K.)*, 277(5697):523–528. doi:10.1038/277523a0
- Gamo, T., Okamura, K., Kodama, Y., Charlou, J.-L., Urabe, T., Auzende, J.-M., Shipboard Scientific Party of the ManusFlux Cruise, and Ishibashi, J., 1996. Chemical characteristics of hydrothermal fluids from the Manus back-arc basin, Papua New Guinea, I. Major chemical components. *Eos, Trans. Am. Geophys. Union*, 77(22):W116. (Abstract)
- Gemmell, J.B., Binns, R.A., and Parr, J.M., 1996. Comparison of sulfur isotope values between modern back-arc and mid-ocean ridge seafloor hydrothermal systems. *Eos, Trans. Am. Geophys. Union*, 77(22):W117. (Abstract)
- Gennerich, H.-H., 2001. Der Tabar-Feni-Inselbogen und sein Plattentektonisches Regime [Ph.D. dissert.]. Universität Bremen.
- Giorgetti, G., Monecke, T., Kleeburg, R., and Hannington, M.D., 2006. Low-temperature hydrothermal alteration of silicic glass at the PACMANUS hydrothermal vent field, Manus Basin: an XRD, SEM and AEM-TEM study. *Clays Clay Miner.*, 54(2):240–251. doi:10.1346/CCMN.2006.0540209
- Heaney, P.J., 1994. Structure and chemistry of the low-pressure silica polymorphs. In Heaney, P.J., Prewitt, C.T., and Gibbs, G.V. (Eds.), *Silica: Physical Behavior, Geochemistry and Materials Applications*. Rev. Mineral., 29:1–40.

- Heath, S., Yeats, C.J., and Binns, R.A., 2000. Fe-Mn-Si oxides of the PACMANUS sea-floor massive sulfide field, eastern Manus Basin, Papua New Guinea. *Geol. Soc. Aust. Abstr.*, 59:217.
- Herzig, P.M., Hannington, M.D., and Arribas, A., Jr., 1998. Sulfur isotopic composition of hydrothermal precipitates from the Lau back arc: implications for magmatic contributions to sea-floor hydrothermal systems. *Miner. Deposita*, 33(3):226–237. doi:10.1007/s001260050143
- Herzig, P.M., Humphris, S.E., Miller, D.J., and Zierenberg, R.A. (Eds.), 1998. *Proc. ODP, Sci. Results*, 158: College Station, TX (Ocean Drilling Program). doi:10.2973/odp.proc.sr.158.1998
- Herzig, P.M., Petersen, S., Kuhn, T., Hannington, M.D., Gemmell, J.B., and Skinner, A.C., 2003. Shallow drilling of seafloor hydrothermal systems: the missing link. In Eliopoulos, D.G., et al. (Eds.), *Mineral Exploration and Sustainable Development: Rotterdam* (Millpress), 103–105.
- Hong, J.K., Lee, S.-M., and McConachy, T., 2003. Reflection studies on the plate boundaries in the Bismarck microplate and deep tow magnetics on PACMANUS. In Yeats, C.J. (Ed.), *Seabed Hydrothermal Systems of the Western Pacific: Current Research and New Directions*. CSIRO Explor. Min. Rep., 1112F:77.
- Hopkinson, L., Roberts, S., Herrington, R., and Wilkinson, J., 1999. The nature of crystalline silica from the TAG submarine hydrothermal mound, 26°N Mid-Atlantic Ridge. *Contrib. Mineral. Petrol.*, 137(4):342–350. doi:10.1007/s004100050554
- Ishibashi, J., Wakita, H., Okamura, K., Gamo, T., Shitashima, K., Charlou, J.L., Jean-Baptiste, P., and Shipboard Party, 1996. Chemical characteristics of hydrothermal fluids from the Manus back-arc basin, Papua New Guinea, II. Gas components. *Eos, Trans. Am. Geophys. Union*, 77:W116. (Abstract)
- Iturrino, G.J., and Bartetzko, A., 2002. Subsurface fracture patterns in the PACMANUS hydrothermal system identified from downhole measurements and their potential implications for fluid circulation. *Eos, Trans. Am. Geophys. Union*, 83(47)(Suppl.):T11B-1253. (Abstract)
- Jones, J.B., and Segnit, E.R., 1972. Genesis of cristobalite and tridymite at low temperatures. *J. Geol. Soc. Aust.*, 18:419–422.
- Kamenetsky, V.S., Binns, R.A., Gemmell, J.B., Crawford, A.J., Mernagh, T.P., Maas, R., and Steele, D., 2001. Parental basaltic melts and fluids in eastern Manus backarc basin: implications for hydrothermal mineralization. *Earth Planet. Sci. Lett.*, 184(3–4):685–702. doi:10.1016/S0012-821X(00)00352-6
- Kano, K., Takeuchi, K., Yamamoto, T., and Hoshizumi, H., 1991. Subaqueous rhyolite block lavas in the Miocene Ushikiri formation, Shimane Peninsula, SW Japan. *J. Volcanol. Geotherm. Res.*, 46(3–4):241–253. doi:10.1016/0377-0273(91)90086-F
- Ketcham, R.A., and Iturrino, G.J., 2005. Nondestructive high-resolution visualization and measurement of anisotropic effective porosity in complex lithologies using high-resolution X-ray computed tomography. *J. Hydrol. (Amsterdam, Neth.)*, 302(1–4):92–106. doi:10.1016/j.jhydrol.2004.06.037
- Kim, J., Lee, I., and Lee, K.-Y., 2004. S, Sr, and Pb isotopic systematics of hydrothermal chimney precipitates from the eastern Manus Basin, western Pacific: evaluation of magmatic contribution to hydrothermal system. *J. Geophys. Res.*, 109(B12):B12210. doi:10.1029/2003JB002912
- Kimura, H., Asada, R., Masta, A., and Naganuma, T., 2003. Distribution of microorganisms in the subsurface of the Manus Basin hydrothermal vent field in Papua New Guinea. *Appl. Environ. Microbiol.*, 69(1):644–648. doi:10.1128/AEM.69.1.644-648.2003
- Kisch, H.J., 1991. Illite crystallinity: recommendations on sample preparation, X-ray diffraction settings, and interlaboratory samples. *J. Metamorph. Geol.*, 9:665–670.
- Knauth, L.P., and Epstein, S., 1976. Hydrogen and oxygen isotope ratios in nodular and bedded cherts. *Geochim. Cosmochim. Acta*, 40(9):1095–1108. doi:10.1016/0016-7037(76)90051-X

- Kübler, B., 1964. Les argiles, indicateurs de métamorphisme. *Rev. Inst. Fr. Pet.*, 19:1093–1112.
- Lackschewitz, K.S., Devey, C.W., Stoffers, P., Botz, R., Eisenhauer, A., Kummetz, M., Schmidt, M., and Singer, A., 2004. Mineralogical, geochemical and isotopic characteristics of hydrothermal alteration processes in the active, submarine, felsic-hosted PACMANUS field, Manus Basin, Papua New Guinea. *Geochim. Cosmochim. Acta*, 68(21):4405–4427. doi:10.1016/j.gca.2004.04.016
- Lee, S.-M. (Ed.), 2003. Multidisciplinary investigation of the western Pacific I (2000–2001). *Ocean Polar Res.*, 24(3).
- Macpherson, C.G., Hilton, D.R., Matthey, D.P., and Sinton, J.M., 2000. Evidence for an ^{18}O -depleted mantle plume from contrasting $^{18}\text{O}/^{16}\text{O}$ ratios of back-arc lavas from the Manus Basin and Mariana Trough. *Earth Planet. Sci. Lett.*, 176(2):171–183. doi:10.1016/S0012-821X(00)00002-9
- Macpherson, C.G., Hilton, D.R., Sinton, J.M., Poreda, R.J., and Craig, H., 1998. High $^3\text{He}/^4\text{He}$ ratios in the Manus backarc basin: implications for mantle mixing and the origin of plumes in the western Pacific Ocean. *Geology*, 26(11):1007–1010. doi:10.1130/0091-7613(1998)026<1007:HHHRIT>2.3.CO;2
- Malahoff, A., Embley, R., Cronan, D.S., and Skirrow, R., 1983. The geological setting and chemistry of hydrothermal sulfides and associated deposits from the Galapagos rift at 86°W. *Mar. Min.*, 4:123–137.
- Martinez, F., and Taylor, B., 1996. Backarc spreading, rifting, and microplate rotation, between transform faults in the Manus Basin. *Mar. Geophys. Res.*, 18(2–4):203–224. doi:10.1007/BF00286078
- McConachy, T.F., 2002. Preliminary cruise report DaeYang02, RV *Onnuri*, Lihir-Bismarck Sea, Papua New Guinea. *CSIRO Explor. Min. Rep.*, 1009C.
- McPhie, J., Doyle, M., and Allen, R., 1993. *Volcanic Textures: A Guide to the Interpretation of Textures in Volcanic Rocks*: Hobart (Tasmanian Govt. Printing Office).
- Meunier, A., and Velde, B., 2004. *Illite—Origins, Evolution and Metamorphism*: Heidelberg (Springer-Verlag).
- Moss, R., and Scott, S.D., 2001. Geochemistry and mineralogy of gold-rich hydrothermal precipitates from the eastern Manus Basin, Papua New Guinea. *Can. Mineral.*, 39:957–978.
- Mottl, M.J., Davis, E.E., Fisher, A.T., and Slack, J.F. (Eds.), 1994. *Proc. ODP, Sci. Results*, 139: College Station, TX (Ocean Drilling Program). doi:10.2973/odp.proc.sr.139.1994
- Parr, J., Yeats, C., and Binns, R., 2003. Petrology, trace element geochemistry and isotope geochemistry of sulfides and oxides from the PACMANUS hydrothermal field, eastern Manus Basin, Papua New Guinea. In Yeats, C. (Ed.), *Seabed Hydrothermal Systems of the Western Pacific: Current Research and New Directions*. CSIRO Explor. Min. Rep., 1112F:58–64.
- Parr, J.M., Murao, S., and Binns, R.A., 1995. A comparison of massive sulfide deposits forming at the PACMANUS (Manus Basin, PNG) and JADE (Okinawa Trough, South China Sea) seafloor hydrothermal fields. *AusIMM Proc.*, 9/95:453–458.
- Paulick, H., and Bach, W., 2006. Phyllosilicate alteration mineral assemblages in the active subsea-floor Pacmanus hydrothermal system, Papua New Guinea, ODP Leg 193. *Econ. Geol.*, 101(3):633–650. doi:10.2113/gsecongeo.101.3.633
- Paulick, H., and Herzig, P., 2003. Volcanic facies controls on mass transfer at the active, dacite-hosted PACMANUS hydrothermal system, Manus Basin, Papua New Guinea (Ocean Drilling Program Leg 193). In Eliopoulos, D.G., et al. (Eds.), *Mineral Exploration and Sustainable Development*: Rotterdam (Millpress), 167–170.
- Paulick, H., Vanko, D.A., and Yeats, C.J., 2004. Drill core-based facies reconstruction of a deep-marine felsic volcano hosting an active hydrothermal system (Pual Ridge, Papua New Guinea, ODP Leg 193). *J. Volcanol. Geotherm. Res.*, 130(1–2):31–50. doi:10.1016/S0377-0273(03)00275-0
- Petersen, S., Herzig, P.M., Hannington, M.D., and Gemmell, J.B., 2003. Gold-rich massive sulfides from the interior of the felsic-hosted PACMANUS massive sulfide

- deposit, eastern Manus Basin (PNG). In Eliopoulos, D.G. et al. (Eds.), *Mineral Exploration and Sustainable Development*: Rotterdam (Millpress), 171–174.
- Petersen, S., Herzig, P.M., Kuhn, T., Franz, L., Hannington, M.D., Monecke, T., and Gemmell, J.B., 2005. Shallow drilling of seafloor hydrothermal systems using the BGS rockdrill: Conical Seamount (New Ireland fore-arc) and PACMANUS (eastern Manus Basin), Papua New Guinea. *Mar. Georesour. Geotechnol.*, 23(3):175–193. doi:10.1080/10641190500192185
- Pinto, A.M.M., Barriga, F.J.A.S., Scott, S.D., and Roberts, S., 2003. PACMANUS: the subsurface sulfide/oxide/gold mineralization. In Eliopoulos, D.G. et al. (Eds.), *Mineral Exploration and Sustainable Development*: Rotterdam (Millpress), 175–178.
- Pinto A.M.M., Relvas, J.M.R.S., Barriga, F.J.A.S., Munhá, J., Pacheco, N., and Scott, S.D., 2005. Gold mineralization in recent and ancient volcanic-hosted massive sulphides: the PACMANUS field and the Neves Corvo deposit. In Mao, J., and Bierlein, F. (Eds.), *Mineral Deposits Research: Meeting the Global Challenge*, Vol. 1: Beijing (Springer Verlag), 683–686.
- Rees, C.E., Jenkins, W.J., and Monster, J., 1978. The sulphur isotopic composition of ocean water sulphate. *Geochim. Cosmochim. Acta*, 42(4):377–381. doi:10.1016/0016-7037(78)90268-5
- Renders, P.J.N., Gammons, C.H., and Barnes, H.L., 1995. Precipitation and dissolution rate constants for cristobalite from 150 to 300°C. *Geochim. Cosmochim. Acta*, 59(1):77–85. doi:10.1016/0016-7037(94)00232-B
- Roberts, S., Bach, W., Binns, R.A., Vanko, D.A., Yeats, C.J., Teagle, D.A.H., Blacklock, K., Blusztajn, J.S., Boyce, A.J., Cooper, M.J., Holland, N., and McDonald, B., 2003. Contrasting evolution of hydrothermal fluids in the PACMANUS system, Manus Basin; the Sr and S isotope evidence. *Geology*, 31(9):805–808. doi:10.1130/G19716.1
- Roberts, S., Teagle, D.A., Bach, W., Binns, R.A., Boyce, A., Holland, N., and Vanko, D.A., 2001. Sr and stable isotope (S,O) chemistry of anhydrite and sulphide phases from the PACMANUS hydrothermal system, Site 1188, ODP Leg 193. *Eos, Trans. Am. Geophys. Union*, 82(47)(Suppl.):OS11A-0348. (Abstract).
- Roman, C.N., and Ferrini, V.L., 2006. High-resolution mapping in Manus Basin. *Eos, Trans. Am. Geophys. Union*, 87(52)(Suppl.):OS33A-1680. (Abstract)
- Scott, S.D., and Binns, R.A., 1995. Hydrothermal processes and contrasting styles of mineralization in the western Woodlark and eastern Manus Basins of the western Pacific. In Parson, L.M., Walker, C.L., and Dixon, D. (Eds.), *Hydrothermal Vents and Processes*. Geol. Soc. Spec. Publ., 87:191–205.
- Seewald, J., Reeves, E., Saccocia, P., Rouxel, O., Walsh, E., Price, R., Tivey, M., Bach, W., and Tivey, M., 2006. Water-rock reaction, substrate composition, magmatic degassing, and mixing as major factors controlling vent fluid compositions in Manus Basin hydrothermal systems. *Eos, Trans. Am. Geophys. Union*, 87(52)(Suppl.):B34A-02. (Abstract)
- Shipboard Scientific Party, 2002a. Leg 193 summary. In Binns, R.A., Barriga, F.J.A.S., Miller, D.J., et al., *Proc. ODP, Init. Repts.*, 193: College Station, TX (Ocean Drilling Program), 1–84. doi:10.2973/odp.proc.ir.193.101.2002
- Shipboard Scientific Party, 2002b. Site 1188. In Binns, R.A., Barriga, F.J.A.S., Miller, D.J., et al., *Proc. ODP, Init. Repts.*, 193: College Station, TX (Ocean Drilling Program), 1–305. doi:10.2973/odp.proc.ir.193.103.2002
- Shipboard Scientific Party, 2002c. Site 1189. In Binns, R.A., Barriga, F.J.A.S., Miller, D.J., et al., *Proc. ODP, Init. Repts.*, 193: College Station, TX (Ocean Drilling Program), 1–259. doi:10.2973/odp.proc.ir.193.104.2002
- Shipboard Scientific Party, 2002d. Site 1191. In Binns, R.A., Barriga, F.J.A.S., Miller, D.J., et al., *Proc. ODP, Init. Repts.*, 193: College Station, TX (Ocean Drilling Program), 1–46. doi:10.2973/odp.proc.ir.193.106.2002
- Spieß, F.N., MacDonald, K.C., Atwater, T., Ballard, R., Carranza, A., Cordoba, D., Cox, C., Diaz Garcia, V.M., Francheteau, J., Guerro, J., Hawkins, J., Haymon, R., Hessler, R., Juteau, T., Kastner, M., Larson, R., Luyendyk, B., Macdougall, J.D., Miller, S.,

- Normak, W., Orcutt, J., and Rangin, C., 1980. East Pacific Rise: hot springs and geophysical experiments. *Science*, 207(4438):1421–1433. doi:10.1126/science.207.4438.1421
- Srodon, J., and Eberl, D.D., 1984. Illite. In Bailey, S.W. (Ed.), *Micas*. Rev. Mineral., 13:495–544.
- Sun, W., Arculus, R.J., Kamenestky, V.S., and Binns, R.A., 2004. Release of gold-bearing fluids in convergent margin magmas prompted by magnetite crystallization. *Nature (London, U. K.)*, 431(7011):975–978. doi:10.1038/nature02972
- Teagle, D.A.H., Alt, J.C., Chiba, H., Humphris, S.E., and Halliday, A.N., 1998. Strontium and oxygen isotopic constraints on fluid mixing, alteration and mineralization in the TAG hydrothermal deposit. *Chem. Geol.*, 149(1–2):1–24. doi:10.1016/S0009-2541(98)00030-8
- Tenthorey, E., and Cox, S.F., 2003. Reaction-enhanced permeability during serpentine dehydration. *Geology*, 31(10):921–924. doi:10.1130/G19724.1
- Tivey, M., Bach, W., Tivey, M., Sewald, J., Craddock, P., Rouxel, O., Yoerger, D., Yeats, C., McConachy, T., Quigley, M., and Vanko, D., 2006. Investigating the influence of magmatic volatile input and seawater entrainment on vent deposit morphology and composition in Manus Basin (back-arc) hydrothermal systems. *Eos, Trans. Am. Geophys. Union*, 87(52)(Suppl.):B34A-01. (Abstract)
- Tivey, M.K., Humphris, S.E., Thompson, G., Hannington, M.D., and Rona, P.A., 1995. Deducing patterns of fluid flow and mixing within the TAG active hydrothermal mound using mineralogical and geochemical data. *J. Geophys. Res.*, 100(B7):12527–12556. doi:10.1029/95JB00610
- Vanko, D.A., and Bach, W., 2005. Heating and freezing experiments on aqueous fluid inclusions in anhydrite: recognition and effects of stretching and the low-temperature formation of gypsum. *Chem. Geol.*, 223(1–3):35–45. doi:10.1016/j.chemgeo.2004.11.021
- Vanko, D.A., Bach, W., Roberts, S., Yeats, C.J., and Scott, S.D., 2004. Fluid inclusion evidence for subsurface phase separation and variable fluid mixing regimes beneath the deep-sea PACMANUS hydrothermal field, Manus Basin back-arc rift, Papua New Guinea. *J. Geophys. Res.*, 109(B3):B03201. doi:10.1029/2003JB002579
- Vanko, D.A., Wicker, S.G., and Binns, R.A., 2006. Conditions of formation of secondary quartz in hydrothermally altered, subsurface dacite beneath the deep-sea PACMANUS hydrothermal field, Manus Basin, Papua New Guinea. *Eos, Trans. Am. Geophys. Union*, 87(36)(Suppl.):U41A-02. (Abstract)
- Waters, J.C., and Binns, R.A., 1998. Contrasting styles of felsic submarine volcanism, eastern Manus Basin, Papua New Guinea. *Geol. Soc. Aust. Abstr.*, 49:459. (Abstract)
- Waters, J.C., Binns, R.A., and Naka, J., 1996. Morphology of submarine felsic volcanic rocks on Pual Ridge, eastern Manus Basin, Papua New Guinea. *Eos, Trans. Am. Geophys. Union*, 77:W120. (Abstract)
- Woodhead, J.D., and Johnson, R.W., 1993. Isotopic and trace-element profiles across the New Britain island arc, Papua New Guinea. *Contrib. Mineral. Petrol.*, 113(4):479–491. doi:10.1007/BF00698317
- Yang, K., and Scott, S.D., 1996. Possible contribution of a metal-rich magmatic fluid to a sea-floor hydrothermal system. *Nature (London, U. K.)*, 383(6599):420–423. doi:10.1038/383420a0
- Yang, K., and Scott, S.D., 2002. Magmatic degassing of volatiles and ore minerals into a hydrothermal system on the modern sea floor of the eastern Manus back-arc basin, western Pacific. *Econ. Geol.*, 97(5):1079–1100. doi:10.2113/97.5.1079
- Yang, K., and Scott, S.D., 2005. Vigorous exsolution of volatiles in the magma chamber beneath a hydrothermal system on the modern sea floor of the eastern Manus back-arc basin, western Pacific: evidence from melt inclusions. *Econ. Geol.*, 100(6):1085–1096. doi:10.2113/100.6.1085
- Yeats, C.J., 2003. Mineralogy and geochemistry of alteration at the PACMANUS hydrothermal field, eastern Manus Basin, Papua New Guinea: vertical and lateral variation at low- and high-temperature vent sites. In Yeats, C.J. (Ed.), *Seabed Hydro-*

- thermal Systems of the Western Pacific: Current Research and New Directions*. CSIRO Explor. Min. Rep., 1112F:53–57.
- Yeats, C.J., 2004. Mineralogy and geochemistry of alteration at the PACMANUS hydrothermal field, eastern Manus Basin, Papua New Guinea. In Muhling, J., Goldfarb, R.J., Vielreicher, N., Bierlein, F.P., Stumpfl, E.F., Groves, D.I., Kenworthy, S., and Knox-Robinson, C.M. (Eds.), *SEG 2004: Predictive Mineral Discovery Under Cover—SEG Conference and Exhibition: Extended Abstracts*. Publ.—Cent. Global Metall., Univ. West. Aust., 33:224–227.
- Yeats, C.J., Bach, W., Vanko, D.A., Roberts, S., Lackschewitz, K., and Paulick, H., 2001. Fluid-dacite interaction in the PACMANUS subseafloor hydrothermal system—preliminary results from secondary mineral chemistry and geochemical modeling. *Eos, Trans. Am. Geophys. Union*, 82(47)(Suppl.):OS11A-0346. (Abstract)
- Yeats, C.J., Binns, R.A., and Parr, J.M., 2000. Advanced argillic alteration associated with actively forming, submarine polymetallic sulfide mineralization in the eastern Manus Basin, Papua New Guinea. *Geol. Soc. Aust. Abstr.*, 59:555. (Abstract)
- Zierenberg, R.A., Fouquet, Y., Miller, D.J., and Normark, W.R. (Eds.), 2000. *Proc. ODP, Sci. Results*, 169: College Station, TX (Ocean Drilling Program). [doi:10.2973/odp.proc.sr.169.2000](https://doi.org/10.2973/odp.proc.sr.169.2000)

APPENDIX

Alteration Geochemistry: Methods and Results

Assessing the Parentage of Altered Rocks

Aphyric and sparsely porphyritic glassy lavas from Pual Ridge ranging from basaltic andesite to rhyodacite display highly constrained geochemical fractionation trends for most major and trace elements (Binns et al., 2002b). Systematic increase in Zr content and decrease of TiO_2 content plotted, for example, against SiO_2 in Harker-type diagrams make the Zr/TiO_2 ratio a sensitive measure of fractionation status. These elements are widely considered immobile during hydrothermal alteration. In Leg 193 altered cores the concept of Ti and Zr immobility is supported by their presence in resistate minerals rutile and zircon, respectively, and by consistency in Zr/TiO_2 ratios across zoned samples with varying alteration assemblages (see Table T2).

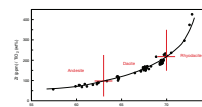
Algorithms for calculating precursor compositions, assuming consanguinity of seabed and subseafloor lavas at Pual Ridge, are listed in Table AT1. These have been derived from the glassy lava database (~70 samples, recalculated to 100% anhydrous totals) by plotting each element against Zr/TiO_2 and selecting the better of logarithmic or exponential functions calculated to illustrate the trend. Zirconium is expressed in parts per million and TiO_2 in weight percent. Resultant precursor compositions are also in 100% anhydrous format.

Relative precision of the algorithms for different elements is indicated by cited variances in the ratio of calculated to actual element abundances obtained by reapplying the algorithms to the fresh lava database itself. Algorithms for Cr, Ni, S, and certain other low-abundance elements (e.g., Te) that display scatter in fresh lavas are useful only to assess gross changes in composition and should be applied with due consideration of potential errors. For Cu, the algorithm is derived using only fresh lavas with >60 wt% SiO_2 to avoid the abrupt change in fractionation behavior displayed by this element in more mafic rocks (Sun et al., 2004), but even so scatter remains in Cu contents, leading to an elevated variance. Of the major elements, only Mg shows significant variance, but this is caused by a small number of anomalous samples in the fresh lava database and the algorithm is considered valid overall.

In comparing altered rock compositions with their (anhydrous) precursors it is necessary to take account of water contents of the (clay dominated) former. Structurally combined water has not been separately analyzed for CSIRO samples from Leg 193, and "loss on ignition" determinations for sulfide-bearing samples are an unreliable measure of water. To remove the effects of hydration in comparative plots (e.g., Figure AF1) a factor, calculated from the average for Zr and TiO_2 , respectively, of the ratios between *actual* and *algorithm-derived precursor* contents of these two constituents, must be applied. Thereby we are comparing a fixed weight of precursor rock with whatever its weight has become after alteration. On diagrams like Figure AF1, Ti and Zr will plot exactly at the unity ratio as required by the immobility concept, except for any minor analytical errors in either element. By restricting the study of alteration geochemistry to CSIRO samples analyzed by the same methods as used for glassy lavas, we avoid interlaboratory variability.

AT1. Algorithms for estimating precursor compositions of altered rock, p. 70.

AF1. Zr/TiO_2 and anhydrous SiO_2 , p. 65.



To assess mass changes on a volume basis, it is necessary to use measured or estimated SGs of altered rocks, and precursor SGs (at calculated precursor compositions) derived from measurements on Pual Ridge glasses. This was necessary, for example, in assessing volume changes during alteration (see Fig. F10).

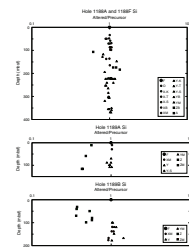
Summary of Results

Abbreviations used below for alteration categories are set out in Table T1 of the main chapter.

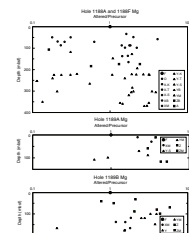
Lithophile Elements

- Si is preserved at precursor levels irrespective of alteration style, except for moderate to severe depletion in Category Z samples (e.g., from the Stockwork Zone of Site 1189) and for mild enrichments in a few samples that show petrologic indications of silicification or extensive quartz growth in cavities (Fig. AF2).
- Al behaves overall in an immobile fashion.
- Total Fe is severely depleted in pyrite-poor selvages (Subcategory S) from Site 1188, but is highly enriched (along with S) in most Category Z wallrocks from the Stockwork Zone of Hole 1189B, where much pyrite has deposited in vesicles and microcavities. Elsewhere Fe varies between moderate enrichment and depletion in a manner suggesting overall sulfidation of precursor Fe but with local redistribution of resultant pyrite.
- Mn is everywhere depleted except in the Lower Sequence of Hole 1189B.
- Mg and K show the greatest diversity in behavior across different alteration styles, reflecting respective clay mineralogies (Figs. AF3, AF4).
- Selvages and most pyrophyllite-bearing rocks at Site 1188 are extremely depleted in Mg. At both Site 1188 and 1189 kernel lithologies are moderately to significantly enriched, but this is less pronounced for samples with relict plagioclase (Fig. AF2). Kernels lacking plagioclase below ~190 mbsf at Site 1188 show a slight downhole increase in Mg enrichment. Transitional samples (Subcategory T) vary considerably from depletion to low-level enrichment in Mg.
- Plagioclase-free kernel lithologies at Site 1188 are only slightly enriched in K relative to precursors, the levels increasing slightly downhole. Their equivalents retaining plagioclase are highly K-depleted in the cristobalite domain and less depleted in the quartz domain (Fig. AF3). Bleached samples from the upper pyrophyllitic interval in Hole 1188A are severely depleted in K, whereas those from the lower interval of Hole 1188F are only mildly depleted by comparison. Most selvages and transitional samples are more enriched in K than associated kernels.
- Higher levels of K enrichment typify all alteration categories at Site 1189, reflecting presence of hydrothermal K feldspar. In the Lower Sequence of Hole 1189B, cristobalite-bearing samples are less enriched than those containing quartz.
- Rb closely follows the behavior of K. So does Cs, except its downhole profiles are displaced to lower altered/precursor ratios. Lithium is universally depleted.
- At Site 1188, Ba displays a similar behavior pattern to K across differing alteration styles. At Site 1189, however, Ba departs from conformity with K, varying from slightly to extremely enriched. Except in the most extremely enriched samples where barite is probably present,

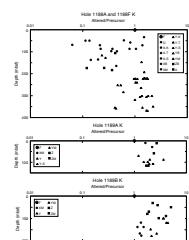
AF2. Ratio of Si in altered volcanic samples to that in their precursors, p. 66.



AF3. Ratio of Mg in altered volcanic samples to that in their precursors, p. 67.



AF4. Ratio of K in altered volcanic samples to that in their precursors, p. 68.



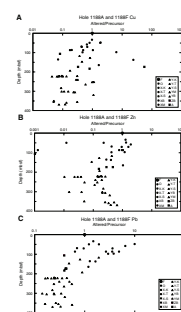
bulk Ba contents are explicable by levels present in illite and potassium feldspar.

- Ca and Sr behave similarly but vary considerably across alteration styles depending on relative abundances of anhydrite and relict plagioclase. Kernel lithologies lacking plagioclase are slightly depleted in the cristobalite domain at Site 1188, highly depleted in the quartz domain, and highly to extremely depleted at Site 1189.
- Contrary to reported immobile behaviors in many ancient metamorphic and hydrothermal environments, rare earth elements (REEs) are variably depleted within the PACMANUS hydrothermal system, the effect being least for plagioclase-bearing material and increasing from La to Yb across the REE series. Typically the light REEs (LREEs; La-Sm) are approximately conserved or mildly depleted, while from Gd onward to Yb the heavy REEs (HREEs) become progressively depleted (to ~0.1 for Yb). Illite selvages (Subcategory S) and transitional alteration styles (Subcategory T) tend to overlap kernels in behavior, whereas pyrophyllite-bearing bleached rocks (Subcategory B) are even more highly depleted.
- At Site 1188 Eu/Eu* anomalies range from mildly negative in most kernels to positive in anhydrite-bearing alteration styles such as illitic selvages. In wallrocks from Site 1189, where anhydrite is subordinate, the Eu/Eu* anomalies are almost exclusively negative.
- Scandium and Y display depletion levels and relationships with alteration style similar to those of the LREEs. Thorium behaves in a very similar fashion to the HREEs.
- Uranium ranges from precursor levels to highly depleted at Site 1188 and from precursor levels to very highly enriched at Site 1189. Below ~150 mbsf at Site 1188 U becomes increasingly depleted with depth. Except that in most plagioclase-bearing samples the levels of depletion or enrichment, respectively, are subdued, there is no clear relationship to alteration styles. This contrasted behavior of U between Sites 1188 and 1189 was observed also in downhole gamma ray logging (Shipboard Scientific Party, 2002b, 200c) and constitutes one of the most prominent lateral geochemical differences between Snowcap and Roman Ruins. A major uranium anomaly (Shipboard Scientific Party, 2002b) in downhole spectral gamma at 197–209 mbsf in Hole 1188F (an uncored interval) remains unexplained.

Chalcophile Elements

- Chalcophile metals show less tendency than lithophiles to vary with alteration style (Fig. AF5), except they are particularly depleted in illitic selvages (Subcategory S) compared to associated kernels (Subcategory K) and transition zones (Subcategory T).
- Sulfur (total) is consistently enriched by two to three orders of magnitude for most alteration styles at Sites 1188 and 1189. Some category Z wallrocks in the Stockwork Zone of Hole 1189B are even more enriched relative to precursors, by 4 orders or more: parallel Fe enrichments indicate mineralization by pyrite. In the Lower Sequence of Hole 1189B, many samples with plagioclase are enriched in S by only 1 to 2 orders of magnitude.
- Tellurium is less dramatically and less systematically enriched than S.
- The behavior of copper is obscured by occasional samples with extreme “nugget effect” enrichments. If the extreme values are disregarded, then at Site 1188 Cu is generally depleted, increasingly so at depth. Most samples in Hole 1189A are mildly depleted. Wallrocks from the upper Stockwork Zone in Hole 1189B vary widely from de-

AF5. Ratios of Cu, Zn, and Pb in altered volcanic samples to those in their precursors, p. 69.



pletion to enrichment in Cu, whereas in the Lower Sequence it is essentially conserved in category X rocks but enriched in most category Y samples.

- Zinc displays a more coherent downhole profile at Site 1188. It falls progressively from precursor levels at ~50 mbsf to significant depletion at ~250 mbsf, then the profile reverses back toward precursor levels at ~370 mbsf. In Hole 1189A Zn varies from moderate depletion to enrichment in a nonsystematic manner. In Hole 1189B, Zn is mildly to moderately depleted in wallrocks from the Stockwork Zone, whereas in the Lower Sequence it varies from very depleted to highly enriched, the latter being possibly another nugget effect reflecting sphalerite presence. Cadmium closely reflects the behavior of Zn at Site 1189, but at Site 1188 it becomes increasingly depleted at depth without the reversal shown by Zn.
- Lead at Site 1188 exhibits a marked downhole trend from distinct enrichment in the upper cristobalite zone to progressively increasing depletion below ~150 mbsf in quartz-bearing lithologies. In Hole 1189A, Pb is enriched in all but a few samples. In Hole 1189B, Pb spans precursor levels in wallrocks from the Stockwork Zone and varies from slightly depleted to distinctly enriched in the Lower Sequence.
- At Site 1188, both arsenic and antimony show progressive downhole change from enrichment just below the capping of fresh lava to depletion at depths below 120–150 mbsf. This behavior closely follows that of Pb, suggesting that Pb in the altered rocks (as in PACMANUS chimneys) is associated mainly with traces of disseminated sulfosalts. In Holes 1189A and 1189B these elements vary from moderate enrichment to moderate depletion, but only Sb appears closely related to Pb.
- Bismuth is highly enriched at Site 1189 and in the cristobalite domain of Site 1188. Indium is depleted at Site 1188 but mostly enriched at Site 1189. Thallium shows variable behavior at Site 1188 but is slightly enriched at Site 1189.
- Cobalt, a trace element typically hosted in pyrite, behaves similarly to Fe at Site 1188. At Site 1189 it is mostly enriched in Hole 1189A, distinctly enriched in wallrocks from the Stockwork Zone of Hole 1189B, and essentially conserved relative to precursors in the Lower Sequence.

Figure F1. Tectonic setting (inset) and regional seafloor geology (main diagram) of the eastern Manus Basin, site of Leg 193. Distributed extension between the Djaul and Weitin transform faults, accommodated by northeast-trending normal faults (thin lines) in the eastern Manus Basin rift zone, matches focused extension associated with backarc spreading zones (thick lines of inset) farther west. An east-west series of neovolcanic edifices links the seismically active ends of the Djaul and Weitin faults. The PACMANUS hydrothermal field lies at the crest of a linear edifice dominated by dacite. NB = New Britain (adapted from Binns et al., 1995).

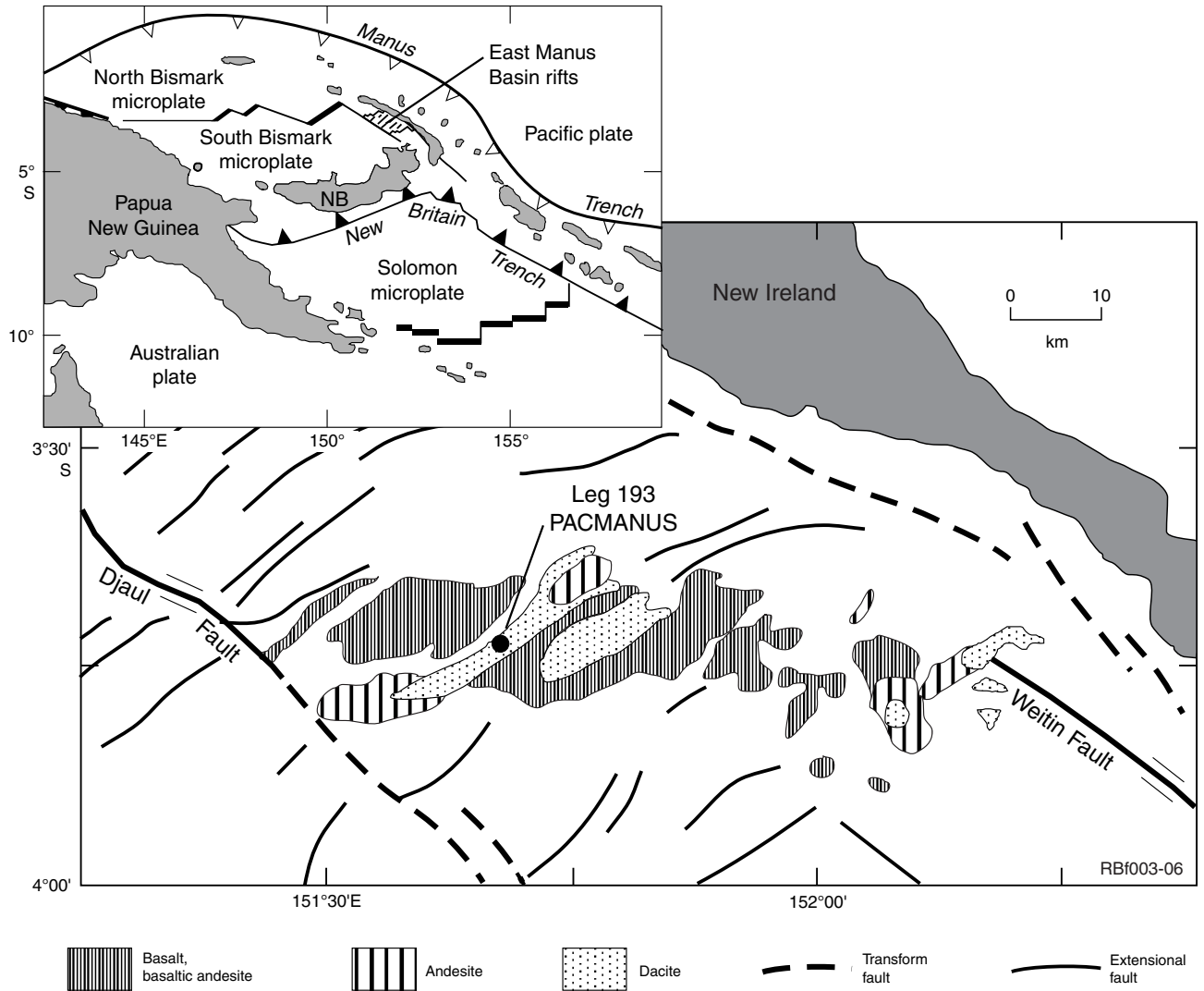


Figure F2. Bathymetric setting of Leg 193 drill sites on Pual Ridge, eastern Manus Basin, Papua New Guinea. Pual Ridge is a predominantly felsic neovolcanic edifice with local cones and flows of andesite, standing 500–600 m above valleys floored by sediments to the west and basaltic andesites to the east. Its southeastern flank is a major extensional fault. Volcanic cones northwest from Pual Ridge (Marmin Knolls) are picritic basalt. Bathymetry from an IFREMER database, processed by J.R. Waters at CSIRO. Isobaths are in meters below sea level.

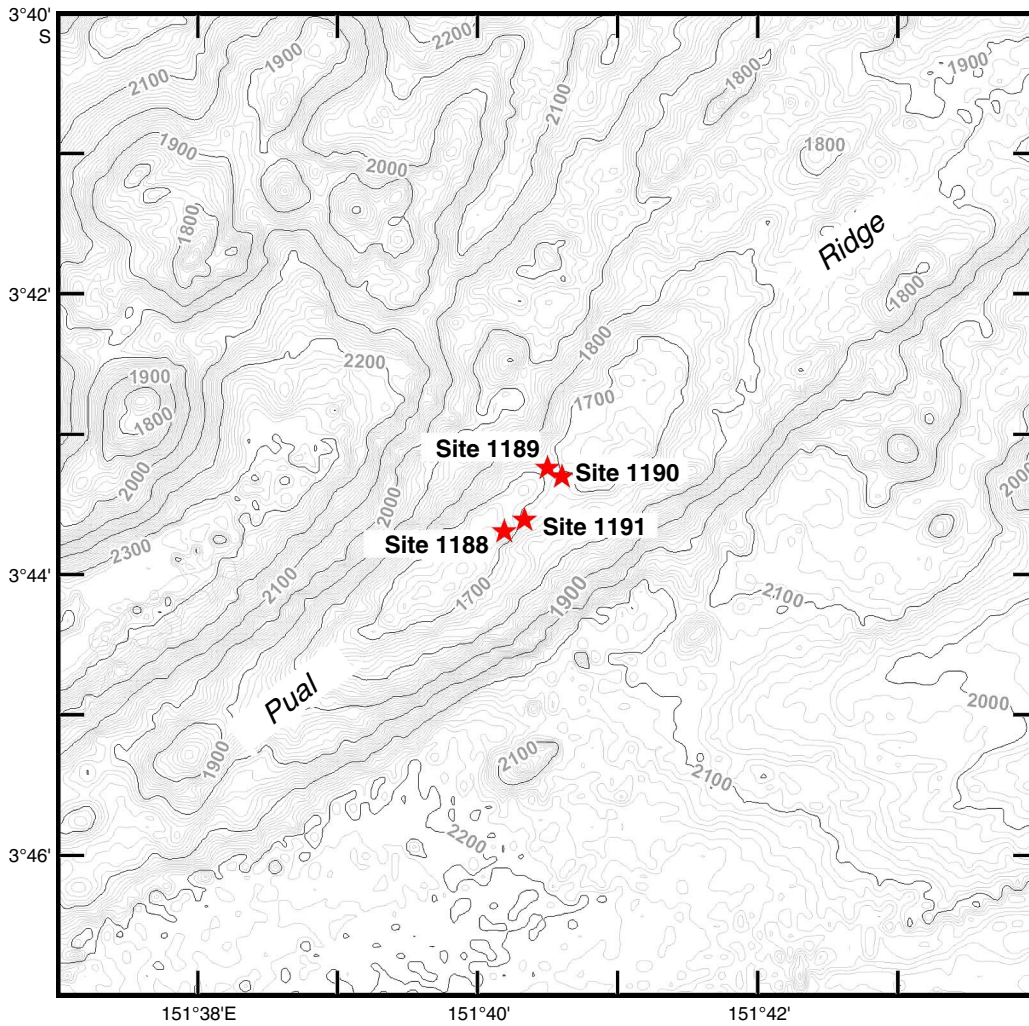


Figure F3. Distribution of lava groups sampled by dredge, grab, and submersible in the PACMANUS vicinity (unpublished CSIRO data). Relatively few exposures do not fall into one of three comparatively invariant compositional groups. Typically lobate exposures of a glassy dacite averaging 67.5 wt% SiO_2 extend from southwest of the Tsukushi hydrothermal site (T) to Snowcap (Site 1188), where bottom-tow photographs and submersible observations show lava fronts extruded over altered rock outcrops. Block lavas with compositions spanning the dacite/rhyodacite border ($\text{SiO}_2 = 69.0\text{--}70.5$ wt%) dominate at Snowcap and Satanic Mills (Site 1191) and continue to the northeast of the latter toward Site 1190. Low-silica lavas (average $\text{SiO}_2 = 64.9$ wt%) typify the Roman Ruins (Site 1189) and Rogers Ruins (200 m north of Site 1189) hydrothermal sites. Boxes indicate wt% SiO_2 of lavas cored in the uppermost intervals of Holes 1188A, 1189A, and 1191A; their compositions conform to the dominant outcrops at those sites. The younger ~ 67.5 wt% SiO_2 lava sequence extending from Tsukushi to Snowcap was not drilled. Penetrations at the reference Site 1190 may belong to the same high-silica lava group exposed at Snowcap and Satanic Mills. All SiO_2 values cited refer to anhydrous compositions. Most sampling operations used in this diagram were deployed or navigated with high precision and hauled only short distances, but uncertainties in positioning of samples (~ 50 m) may be responsible for some of the scattered anomalies. Isobaths are in meters below sea level.

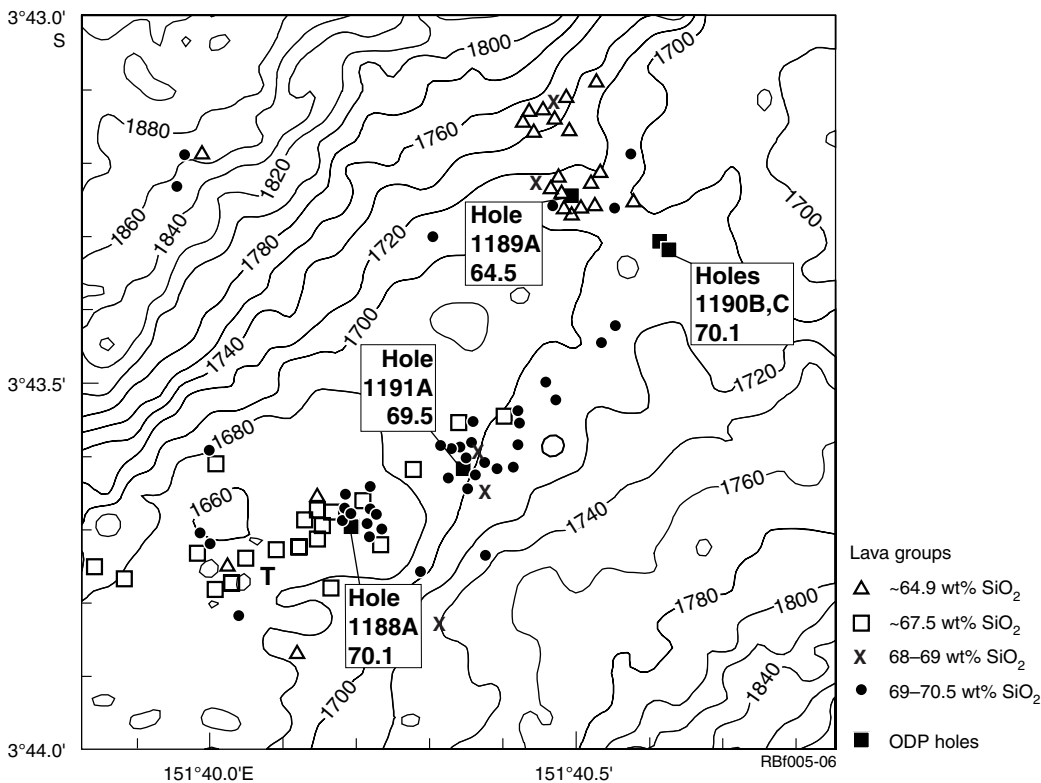


Figure F4. Hydrothermal sites and distribution of hydrothermal deposit types at the PACMANUS field on the crest of Pual Ridge, showing the position of ODP Sites 1188, 1189, 1190, and 1191. Roman Ruins, Satanian Mills, Tsukushi, and Rogers Ruins (the small field north from Roman Ruins) are sites of high-temperature focused venting with sulfide chimneys. Snowcap is a field of exposed altered rocks with diffuse low-temperature venting. Numerous small fields of Fe-Mn oxides scattered along the ridge (overlying dacite-rhyodacite lavas in blank areas) are not shown. Isobaths are in meters below sea level.

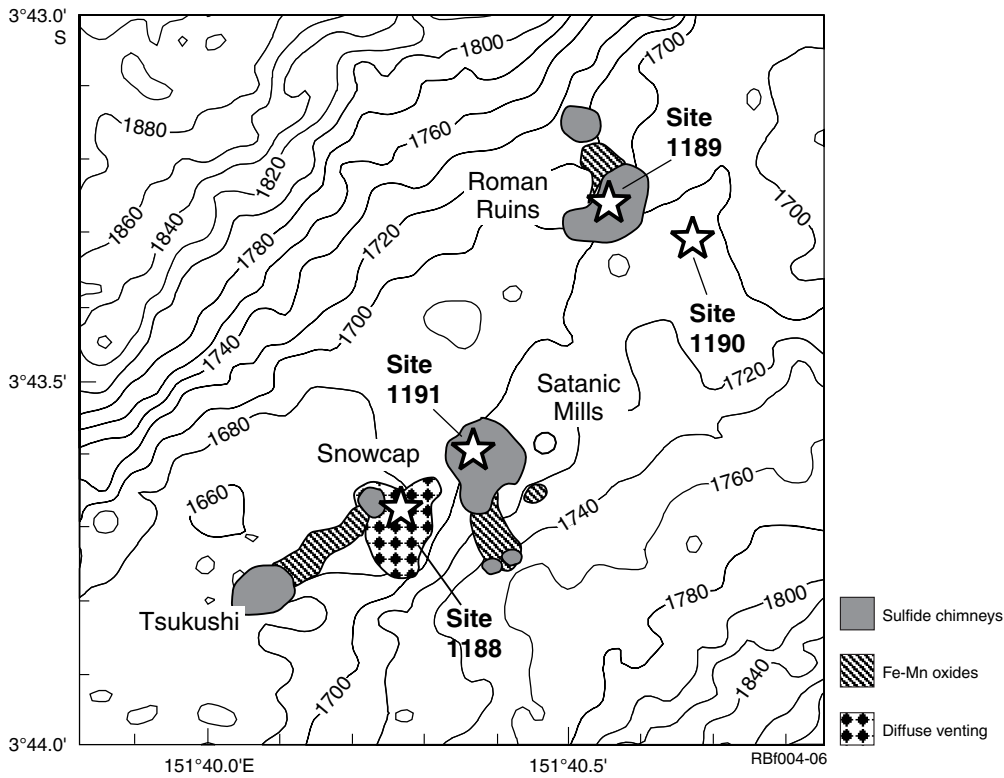


Figure F5. Profiles of Zr/TiO₂ ratios in altered volcanic rocks from Sites 1188 and 1189 at PACMANUS, plus unaltered caprocks at the tops of Holes 1188A and 1189A. Boundaries between andesite, dacite, and rhyodacite (red vertical lines) derive from Figure AF1, p. 65. Plot lines (green) represent a conservative interpretation of the data in terms of a sequence of lavas with differing composition. Original data from Paulick et al. (this volume), Miller et al. (this volume), and shipboard analyses (Binns, Barriga, Miller, et al., 2002) plot as parallel, very similar profiles displaced laterally relative to unpublished CSIRO ratios (analyzed by the same methods as for Fig. AF1, p. 65). Here they are adjusted for interlaboratory calibration differences as indicated; factors were calculated from duplicated analyses of individual or nearby similar samples (both altered and fresh), plus comparative data for two Leg 193 reference standards (Miller et al., this volume). For the shipboard analyses it was necessary to assume a “batch difference” for the Zr analyses from Hole 1189B, and thus a different adjustment factor relative to shipboard analyses from other holes.

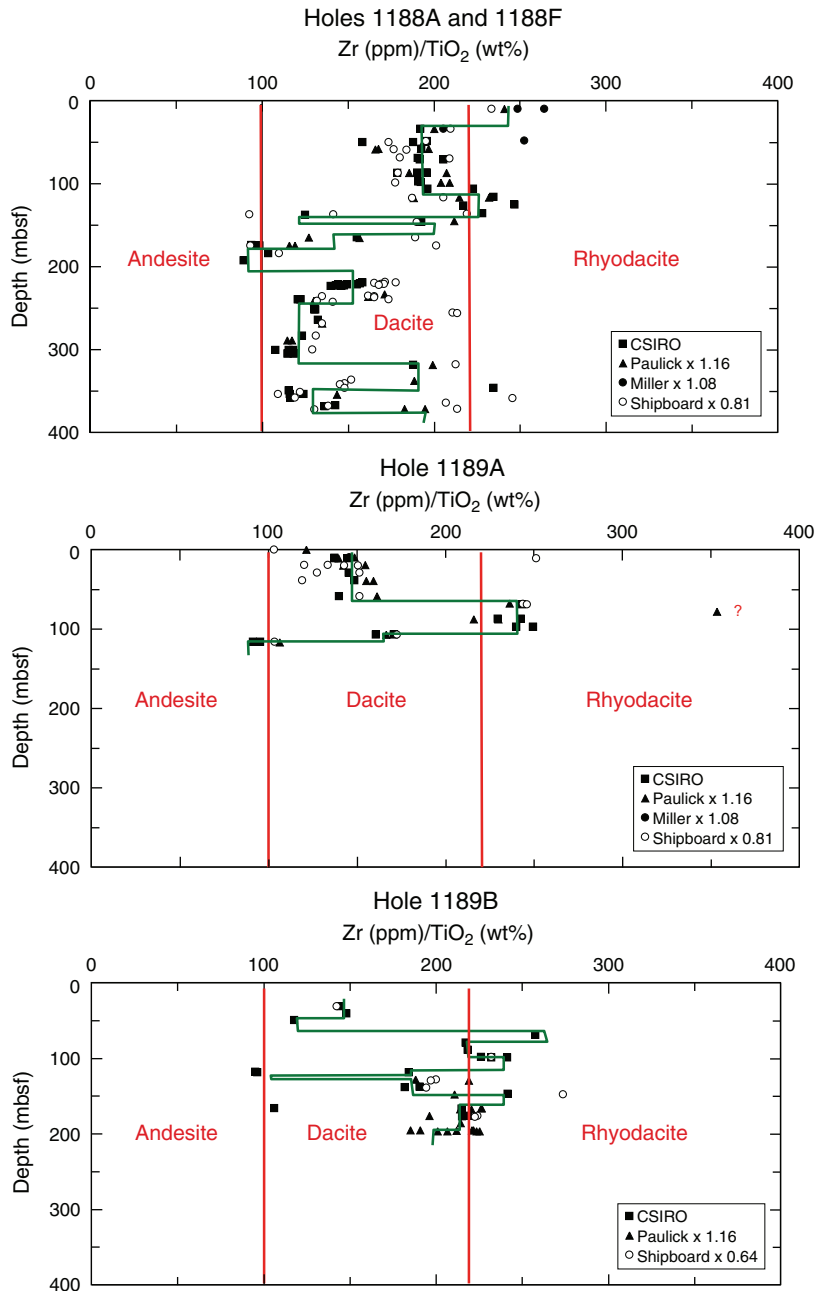


Figure F6. Simplified longitudinal section along the crest of Pual Ridge, illustrating salient features of the subseafloor hydrothermal alteration at PACMANUS as an aid to discussions in the text. Since Hole 1191A at Satanic Mills did not penetrate beyond largely unaltered lava, the lower boundary of the unaltered volcanic cap as drawn between Snowcap and Roman Ruins is hypothetical and there is no certainty that the alteration systems below Snowcap and Roman Ruins are linked at relatively shallow depth as depicted. The boundaries of pyrophyllite-bearing acid sulfate alteration zones below Snowcap are diagrammatic, and a transition zone between cristobalite-bearing and quartz-bearing domains at Site 1188 is not shown. As argued in the text, “part-altered” may be a misnomer for the Lower Sequence of Hole 1189B and for isolated intervals below Snowcap containing relict plagioclase. The fault shown between the Stockwork Zone and Lower Sequence of Hole 1189B corresponds to a marked change in fracture pattern revealed by borehole logging and core recovery, but no displacement has been proven.

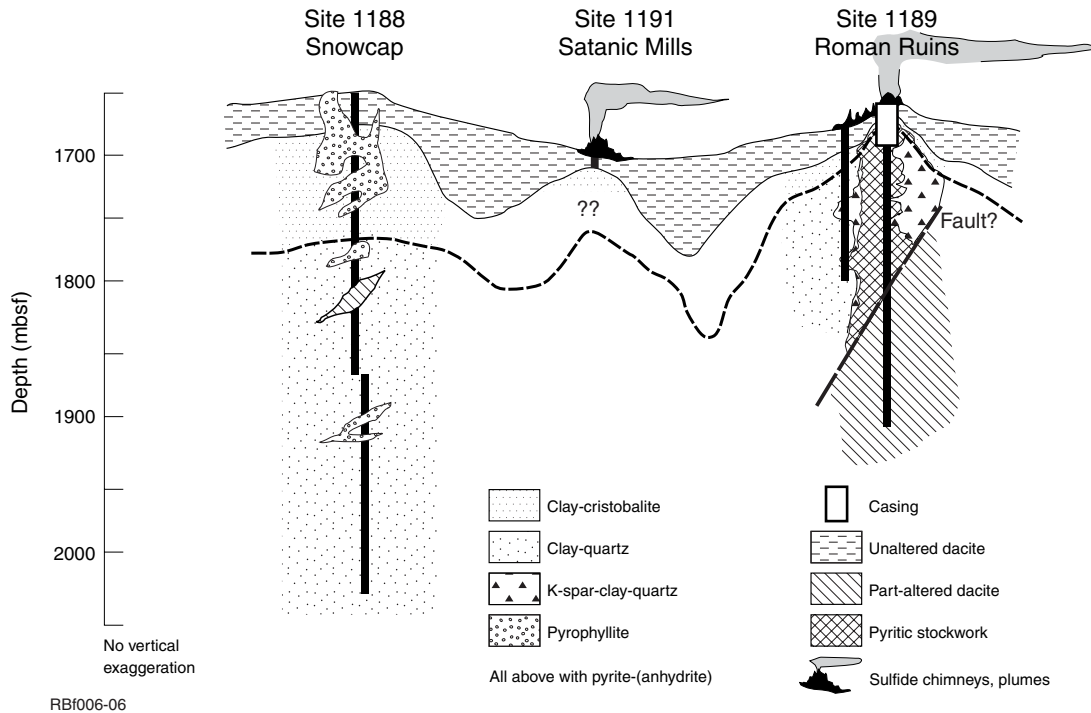


Figure F7. SEM images of hydrothermal clay mineral assemblages (freshly broken surfaces). **A.** Altered glass (showing undulose anisotropism in thin section) from the upper cristobalite zone of Hole 1188A, composed chiefly of very fine grained pyrophyllite (Pyroph) with a crystal of disseminated anhydrite (Anhy), a mass of cristobalite (Crist), and a patch of coarser pyrophyllite flakes intergrown with cristobalite (Sample 193-1188A-9R-2 [Piece 1, 0–5 cm]; 69.10 mbsf; CSIRO 142653). **B, C.** Sample 193-1188F-26Z-1 (Piece 4, 62–64 cm); 300.72 mbsf; CSIRO 142684; (B) typical illite-chlorite quartz kernel assemblage from the quartz domain of Hole 1188F. Quartz (Qtz) grains and chlorite (Chlor) flakes are labeled; most other flakes are illite. Pyrite occurs elsewhere; (C) pale selvage composed principally of illite; quartz and anhydrite occur outside the field of view. **D.** Hydrothermal potassium feldspar (Kspar) intergrown with flakes of illite (majority of view) and grains of quartz. Pyrite and chlorite occur nearby (Sample 193-1189B-8R-1 [Piece 9, 33–36 cm]; 98.73 mbsf; CSIRO 142709).

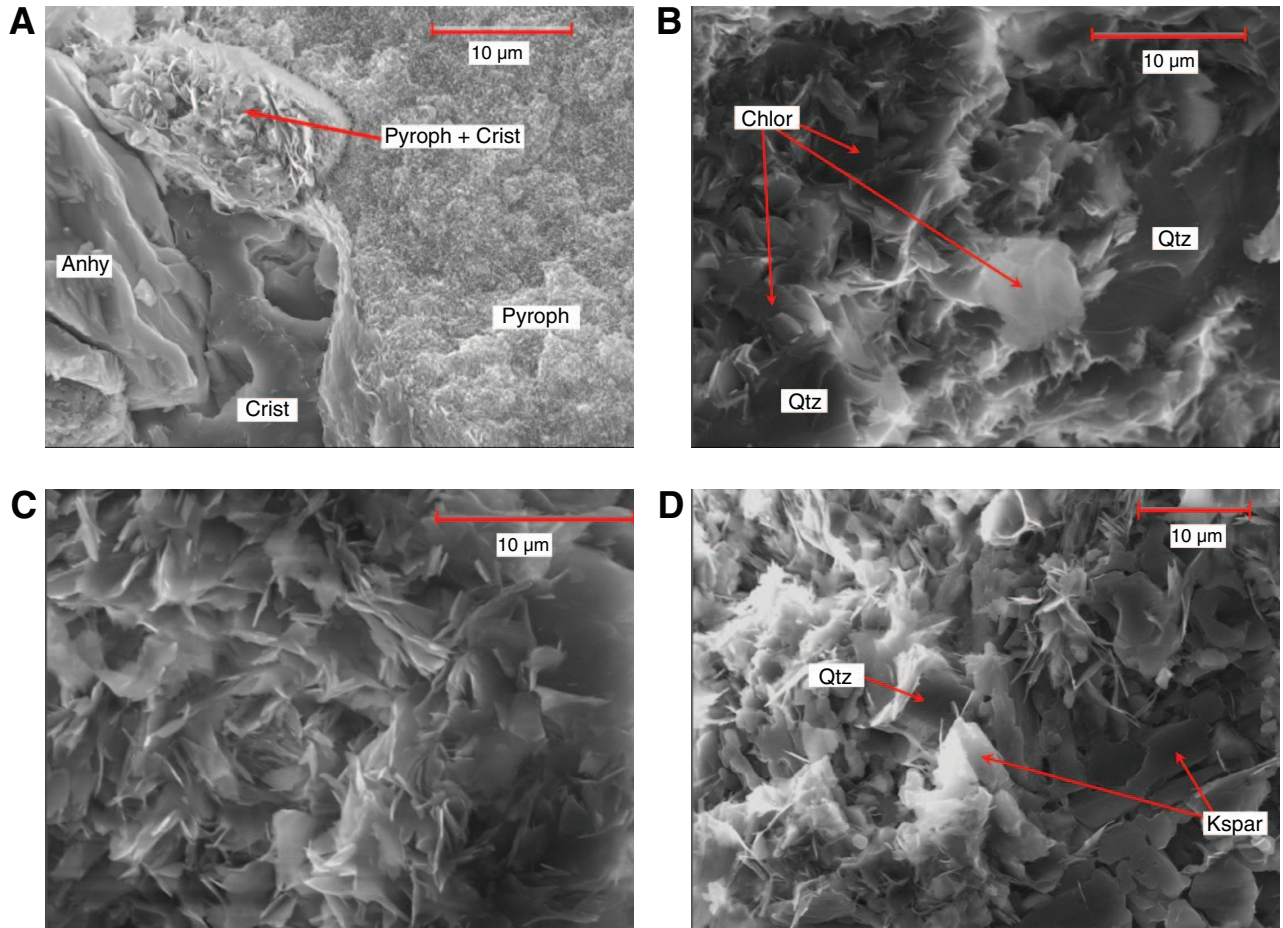


Figure F8. A. Pyrophyllite-dominated acid sulfate alteration (very pale grey) on the left appears at first sight to be superimposed via a fracture set on earlier greenish illite-chlorite alteration (with patchy coloration arising from perlitic structure). Petrographic evidence cited in the text, however, suggests instead that the two alteration styles are contemporary or that the acid sulfate alteration was the earlier (Sample 193-1188A-9R-3 [Piece 2, 22–26 cm]; 70.73 mbsf; CSIRO 142654). B. A relatively simple example of pale selvage structure adjacent to an anhydrite vein cutting altered mafic dacite. The illite-quartz-anhydrite selvage (see Fig. F7C, p. 56) contains no chlorite and little pyrite. A laminated transition zone with pyrite and subdued chlorite has a sharp border against the selvage and grades into the illite-chlorite-quartz-pyrite kernel (see Fig. F7B, p. 56). The brown zone at the lower border of the selvage arises from presence of “waxy illite” (see text). Plagioclase phenocrysts (arrows) are fresh or partly altered in the kernel zone but totally altered to illite in the transition zone and selvage, their outlines becoming increasingly indistinct. Despite first appearances of overprinting, it is argued that the selvage alteration preceded kernel alteration (see text) (Sample 193-1188F-26Z-1 [Piece 4, 62–64 cm]; 300.72 mbsf; CSIRO 142684).

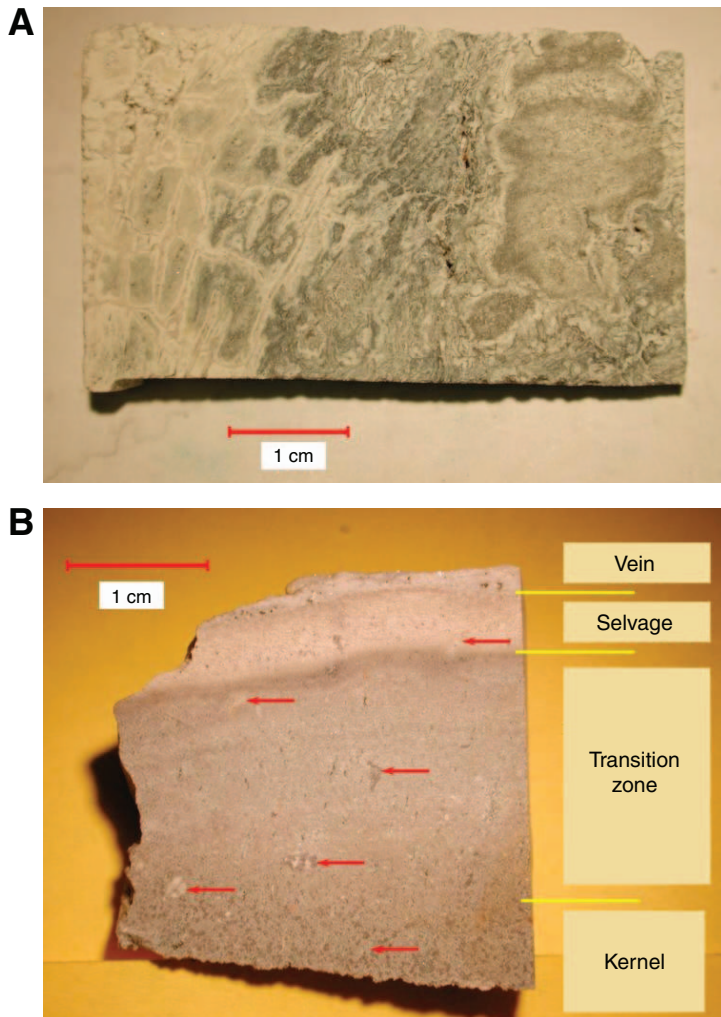
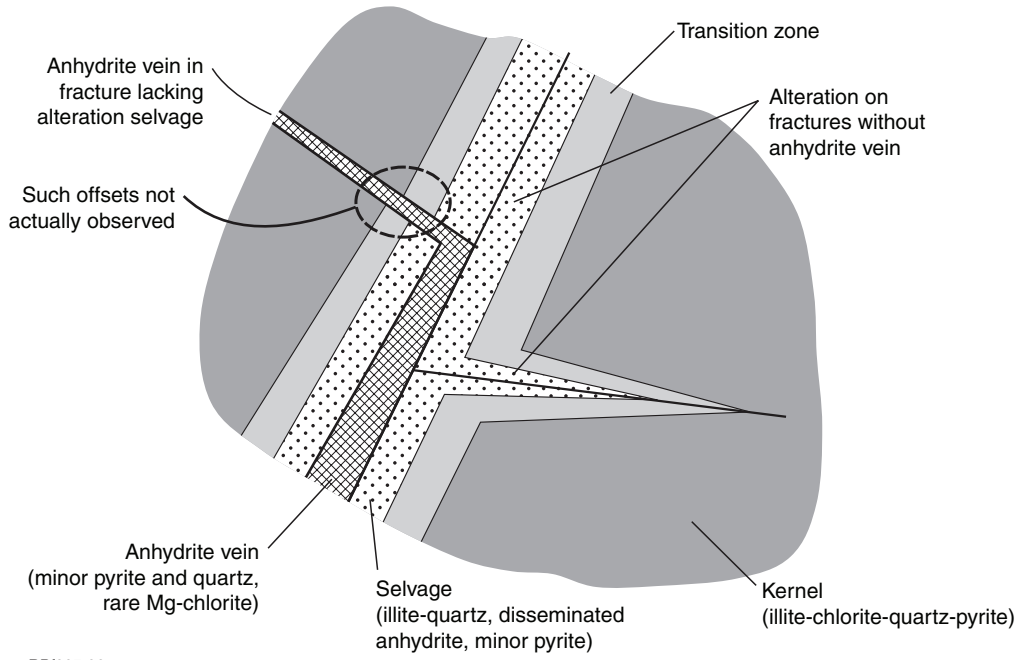


Figure F9. Schematic diagram summarizing observations on many samples from Holes 1188A and 1188F, collectively indicating that anhydrite veins were emplaced after formation of the pale selvages. Whereas the selvages clearly developed from fluids transported via preexisting fractures, the anhydrite veins fill jogs and openings caused by reactivation of the fractures and a jumbling or rotation of wallrock blocks between them. The circled offset relationship would represent unequivocal evidence but has not been convincingly observed.



RBf007-06

Figure F10. Downhole profiles of volume expansion during hydrothermal alteration for Sites 1188 and 1189. Symbols denote the petrographic categories set out in Table T1, p. 62. Circled symbols (“exact”) denote altered samples with measured specific gravity (SG) (from Binns, Barriga, Miller, et al., 2002); for others the SGs of nearby analogous samples were used in calculations. Volume expansion = $SG_{parent}/SG_{sample}/X$, where X = ratio of immobile element content in the altered sample to that of its presumed parent (averaged for Zr and Ti). The plots do not account for precursor vesicularity. Vuggy altered andesites (Category A and one Y-K) and a vuggy bleached dacite (69.1 mbsf) in Hole 1188A show exceptional expansion, reflecting high fluid pressures during alteration. Precursor SGs obtained by reference to measurements on Pual Ridge glasses and microlitic glasses (unpublished CSIRO data), using Zr/TiO₂ to compute precursor composition.

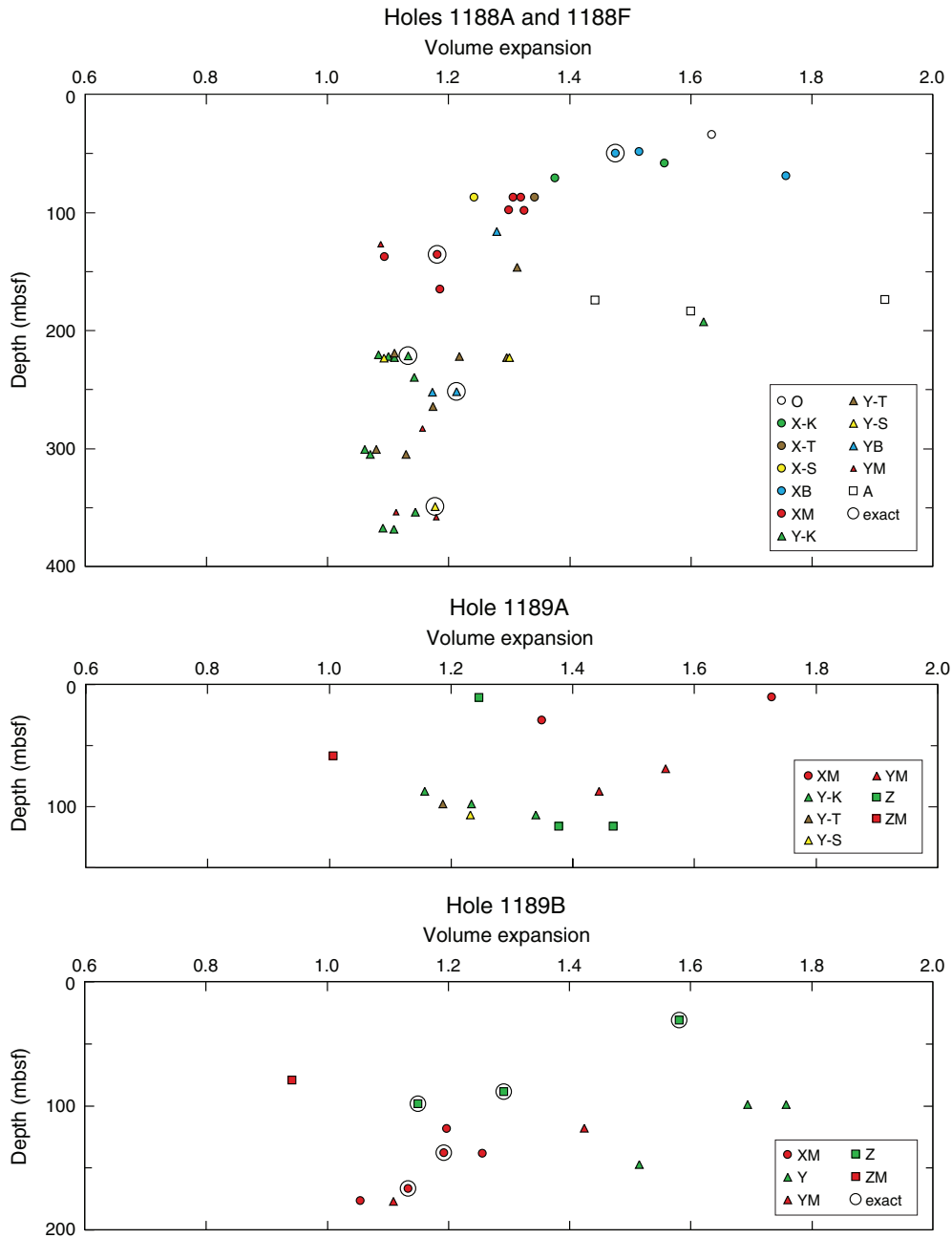


Figure F11. Profiles of strontium isotope ratios for Sites 1188 and 1189. “Anhydrites” are hand-picked from veins, breccia matrixes, and vesicle linings (data from Roberts et al., 2003; [Bach et al.](#), this volume). “Silicates” refer to altered rocks from which anhydrite was removed ([Paulick et al.](#), this volume) and elutriated clay fractions (Lackschewitz et al., 2004). “Leachates” refer to disseminated anhydrites leached from altered rocks ([Paulick et al.](#), this volume). Lines on the Site 1188 plot represent (A) the isotopic composition of fresh glassy lavas from Pual Ridge (CSIRO data), (B) seawater, and (C) end-member hydrothermal fluid as defined by PACMANUS vent fluids (Douville et al., 1999) and chimney barites (CSIRO data). Circled symbols denote anhydrite from breccia matrixes at Site 1189.

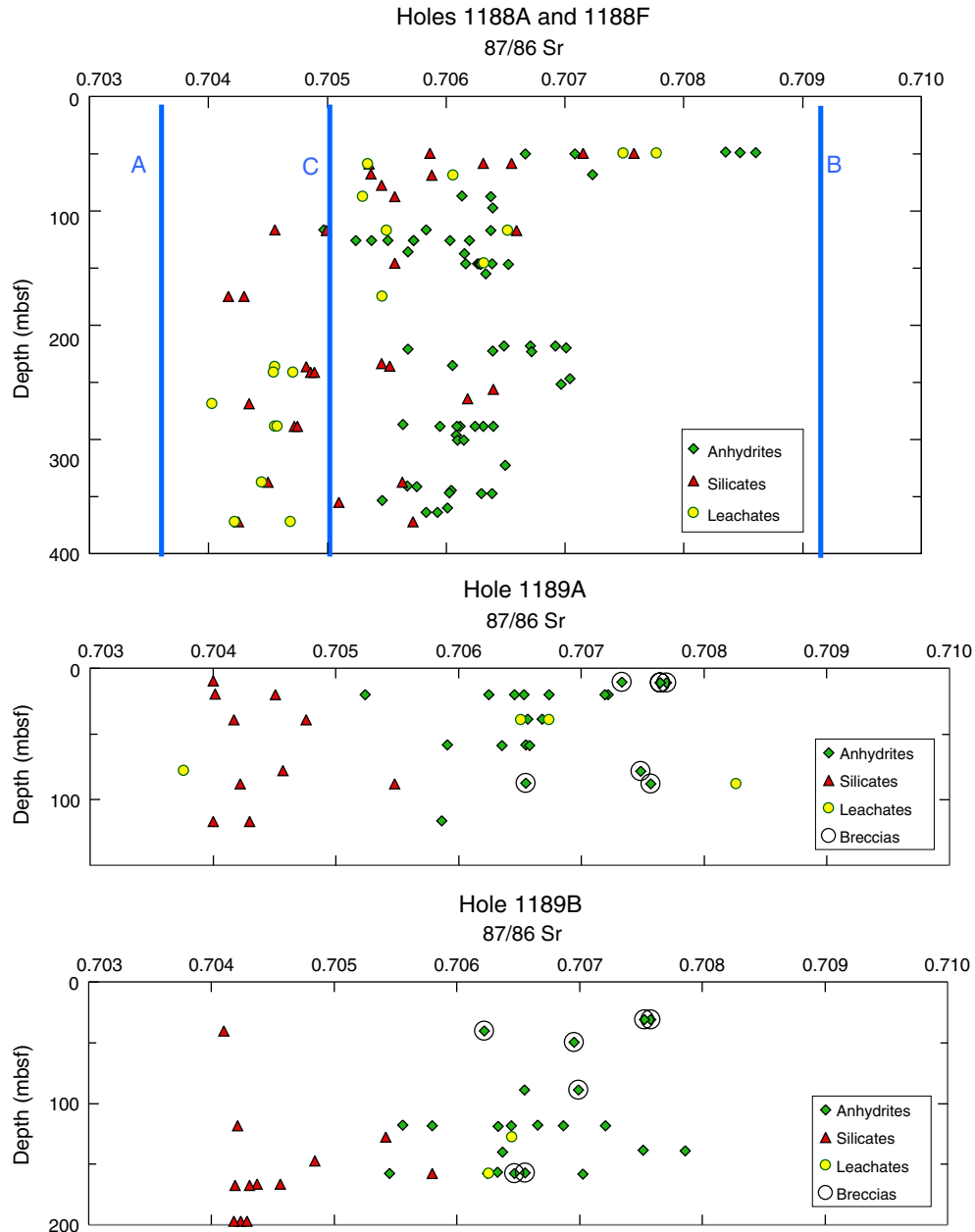


Figure F12. Conceptual cross section through the Snowcap site of the PACMANUS hydrothermal system, illustrating salient features of a “PACMANUS pressure cooker” model. Drilling to 387 mbsf at Site 1188 penetrated more than halfway into the Pual Ridge volcanic edifice but remained within the relatively low temperature, clay-dominated crest of the subseafloor alteration system. Magmatic fluids emanating from a sub-jacent intrusion (acting also as the heat source driving fluid circulation) have progressively mixed with seawater drawn in at all levels, commencing in the high-temperature reaction zone (probably within basement) directly above the intrusion. Fluid flow was predominantly via fractures (not illustrated). Volume expansion induced by high fluid pressures during alteration of the volcanic sequence and fluid expansion caused by phase separation contributed to breaching of an impervious cap of unaltered lavas, enabling venting at the seafloor. In reality the patterns of alteration and fluid flow are far more complex than illustrated (see text). The diagram does not show presence of a younger lava flow and chimney field at Tsukushi, just south of the section line, nor does it attempt to portray other temporal complexities such as relationships between phases of alteration and mineralization.

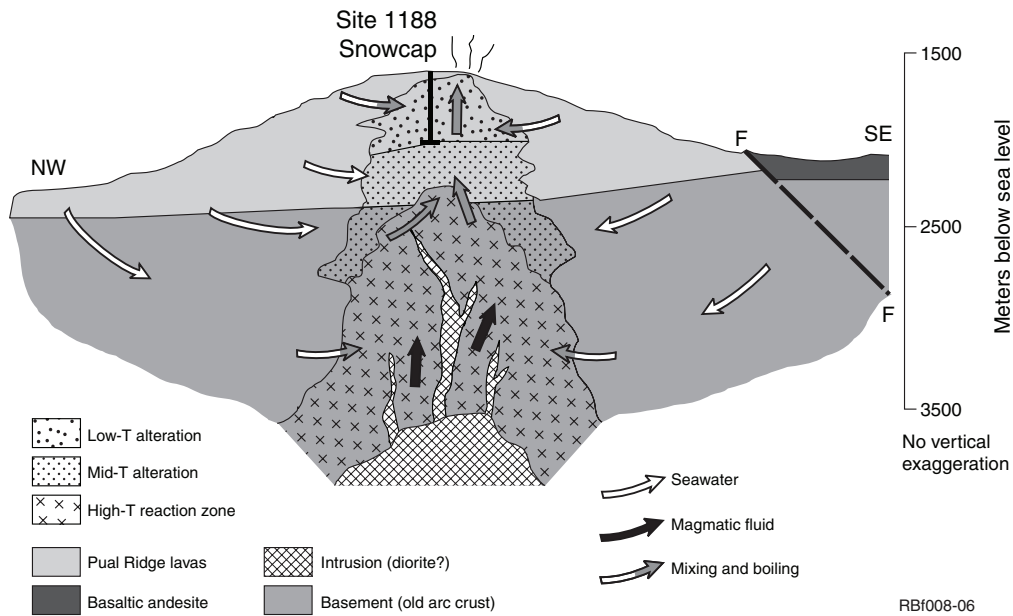


Table T1. A simplified petrologic classification of subseafloor alteration styles at PACMANUS, with abbreviations used in the text and figures.

First-order categories:

F	Fresh lavas near seafloor
O	Opal-bearing altered rocks
X	Cristobalite-bearing altered rocks
Y	Quartz-bearing altered rocks
Z	Altered rocks lacking silica phases, generally occurring as fragments in hydrothermal breccias or between stockwork quartz veins
A	Albite-rich altered rocks (andesite precursors)
U	Unclassified

Second-order categories:

M	Plagioclase (mostly microlites) retained
B	Pyrophyllite-bearing "bleached" rocks

Third-order categories:

-K	Kernels in samples with fracture-controlled pale selvages
-T	Transition zones between kernels and selvages
-S	Pale selvages

Table T2. Major element constitution of samples representing main alteration categories at PACMANUS.

Core, section:	1188A-9R-3	1188A-9R-3	1188F-15Z-1	1188F-26Z-1	1188F-26Z-1	1188F-26Z-1	1189A-1R-1
Piece, interval (cm):	2, 22–26	2, 22–26	16, 139–146	4, 62–64	4, 62–64	4, 62–64	2, 10–14
Depth (mbsf):	70.73	70.73	251.79	300.72	300.72	300.72	31.20
CSIRO:	142654a	142654b	142676	142684a	142684b	142684d	142806
Description:	White, bleached rock with pyrophyllite	Greenish gray kernel (Fig. F8B)	Mottled rock with pyrophyllite	Kernel	Transition zone	Pale selvage (Fig. F8A)	Pale gray altered perlite from Stockwork Zone
Alteration category:	XB	X-K	YB	Y-K	Y-T	Y-S	Z
Major element (wt%):							
SiO ₂	63.2	61.2	57.5	62.2	60.7	55.9	36.0
TiO ₂	0.56	0.54	0.75	0.80	0.78	0.77	1.06
Al ₂ O ₃	13.7	12.8	14.0	13.8	13.8	13.7	20.8
FeO (total)	1.11	4.6	6.3	4.6	5.0	0.67	13.6
MnO	0.01	0.02	0.01	0.05	0.02	0.01	0.0
MgO	0.24	0.55	0.17	5.9	3.3	0.35	4.2
CaO	5.7	2.9	3.6	1.2	2.1	8.5	0.4
Na ₂ O	0.64	0.77	0.44	0.43	0.43	0.53	0.8
K ₂ O	0.34	2.29	0.65	1.80	2.4	2.5	5.0
P ₂ O ₅	0.12	0.14	0.22	0.30	0.35	0.22	0.3
S (total)	4.4	5.6	8.0	2.0	4.1	5.2	11.0
LOI	10.5	8.5	10.7	6.7	7.7	10.0	14.0
Total*	100.5	99.9	102.4	99.8	100.6	98.3	107.0
Zr/TiO ₂	192	205	130	115	118	108	145

Notes: See Table T1, p. 62, for alteration categories. LOI = loss on drying (105°C) + loss on ignition (1050°C). * = uncorrected for oxygen in sulfides allocated to FeO(t) or not allocated to S(t) for sulfates.

Table T3. Overall mass transfers during hydrothermal alteration within major subdivisions of the seafloor PACMANUS system, relative to 1 kg of precursor rock (Ti and Zr assumed immobile).

	1188A	1188A + 1188F	1189A	1189B	1189B
Location:	Cristobalite domain	Quartz domain		Stockwork Zone	Lower Sequence
Depth (mbsf):	49–165	106–368	10–116	31–98	99–176
N:	17	36	13	7	12
Major elements (g/kg):					
SiO ₂	-0	1	-111	-360	47
Al ₂ O ₃	4	-1	0	12	-0
FeO (total)	-2	-10	5	43	14
MnO	-1.0	-1.2	-1.0	-1.1	-0.4
MgO	4	8	29	16	13
CaO	-2	-10	-23	-29	-14
Na ₂ O	-25	-34	-36	-42	-22
K ₂ O	-9	2	17	32	23
P ₂ O ₅	0.1	0.2	0.8	-0.6	0.4
S (total)	39	37	28	62	25
Minor elements (mg/kg):					
Li	-11	-9	-9	-12	-9
Be	-0.1	-0.3	-0.4	-0.5	-0.2
Sc	-5	-5	-1	0	-1
V	5	-1	-2	2	8
Cr	7	9	19	6	11
Co	-0.6	0.1	12	16	11
Ni	-0.3	3	4	-1	5
Cu	42	29	770	13	286
Zn	-17	-67	17	-31	300
Ga	4	-0	3	7	1
Ge	-5	-7	-5	-3	-4
As	11	3	6	10	46
Rb	-13	-7	15	39	17
Sr	-25	-99	-199	-246	-80
Y	-6	-6	-5	-10	-2
Mo	0.6	4.3	1.5	-0.0	1.2
Ba	-10	305	2,500	2,400	2,600
La	-3.4	-2.8	-1.4	-2.2	-1.1
Ce	-7.2	-5.8	-2.9	-4.3	-2.1
Pr	-1.0	-0.9	-0.5	-0.7	-0.3
Nd	-3.9	-3.3	-1.7	-2.8	-0.7
Sm	-1.0	-1.1	-0.7	-1.5	-0.4
Eu	-0.4	-0.4	-0.7	-0.8	-0.3
Gd	-1.5	-1.7	-1.2	-2.2	-0.6
Tb	-0.4	-0.4	-0.3	-0.5	-0.2
Dy	-2.4	-2.9	-2.0	-3.3	-1.1
Ho	-0.6	-0.7	-0.5	-0.8	-0.3
Er	-1.9	-2.3	-1.6	-2.2	-0.9
Tm	-0.3	-0.4	-0.3	-0.4	-0.2
Yb	-2.1	-2.6	-1.8	-2.3	-1.0
Lu	-0.4	-0.5	-0.4	-0.4	-0.2
Pb	11	-3	5	3	15
Trace elements (µg/kg):					
Cd	-196	-296	-155	-218	750
In	-8	-44	20	66	93
Sb	316	9,600	395	130	51,500*
Te	716	175	1,434	1,533	390
Cs	-553	-535	-592	-567	-615
Tl	142	-2	1,057	730	1,050
Bi	160	103	565	1,375	430
Th	-515	-664	-365	-534	-144
U	-226	-314	1,940	1,155	1,060
Total gain/loss (g/kg) (excluding H ₂ O)	8	-8	-87	-265	89

Notes: N = number of samples. * = extreme nugget effect.

Figure AF1. The systematic relationship between the ratio of Zr to TiO_2 and anhydrous SiO_2 content for Pual Ridge glassy lavas (unpublished CSIRO data) enables assessment of the parentage for altered rocks cored at PACMANUS during Leg 193, on the assumption that Zr and Ti behave in immobile fashion during hydrothermal alteration. Plot uses XRF data only.

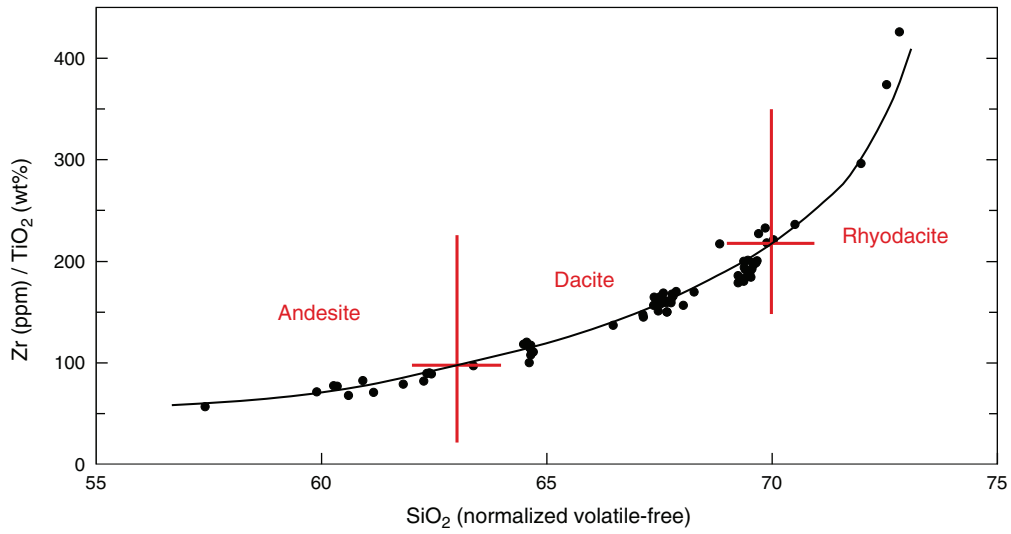


Figure AF2. Downhole profiles at Sites 1188 and 1189 for the ratio of Si content in altered volcanic samples to that in their precursors (plotted logarithmically and computed as described in the “Appendix,” p. 46). Symbols denote petrographic categories set out in Table T1, p. 62, (assessed from macroscopic, XRD, and petrographic examination). Only relatively homogeneous subsamples analyzed at CSIRO are plotted. The “fresh” symbol is plotted at unity ratio and zero depth for added clarity.

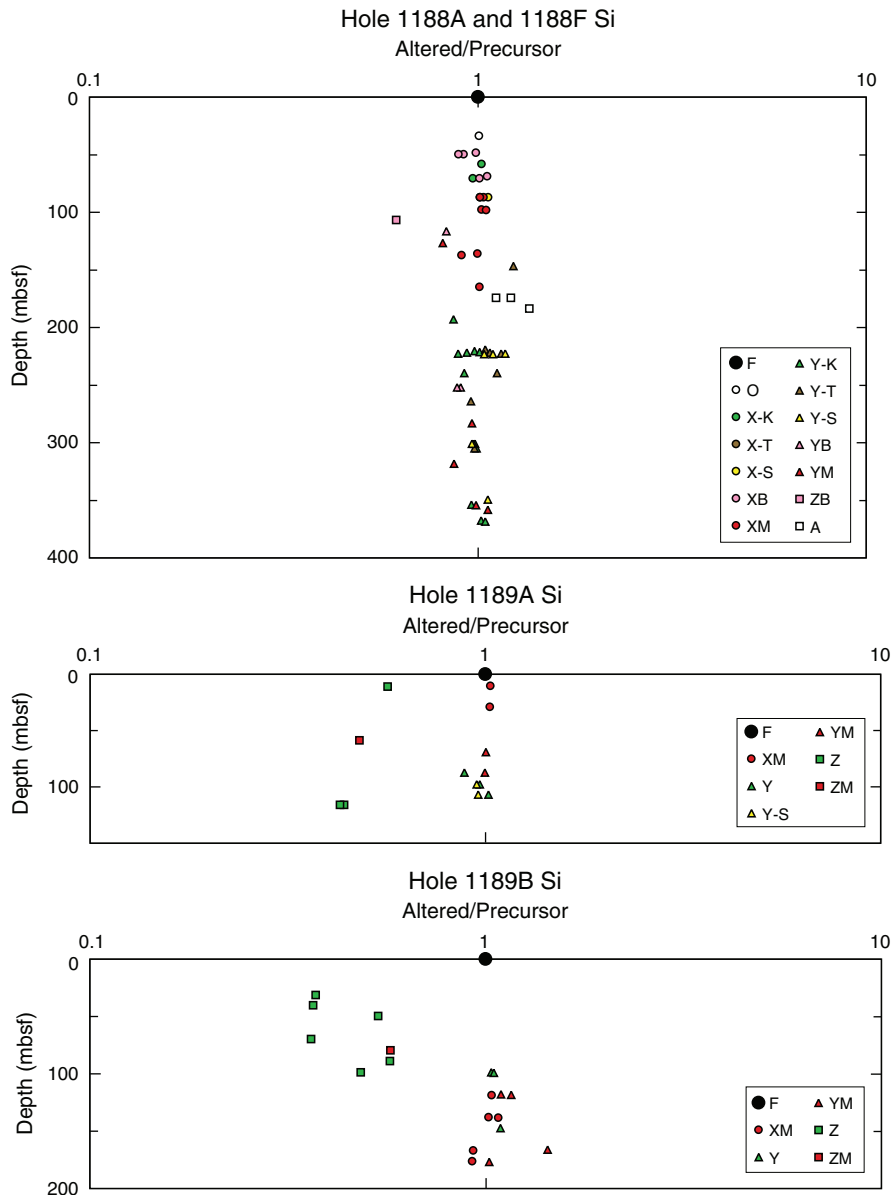


Figure AF3. Downhole profiles at Sites 1188 and 1189 for the ratio of Mg content in altered volcanic samples to that in their precursors (plotted logarithmically). Symbols denote the petrographic categories set out in Table T1, p. 62.

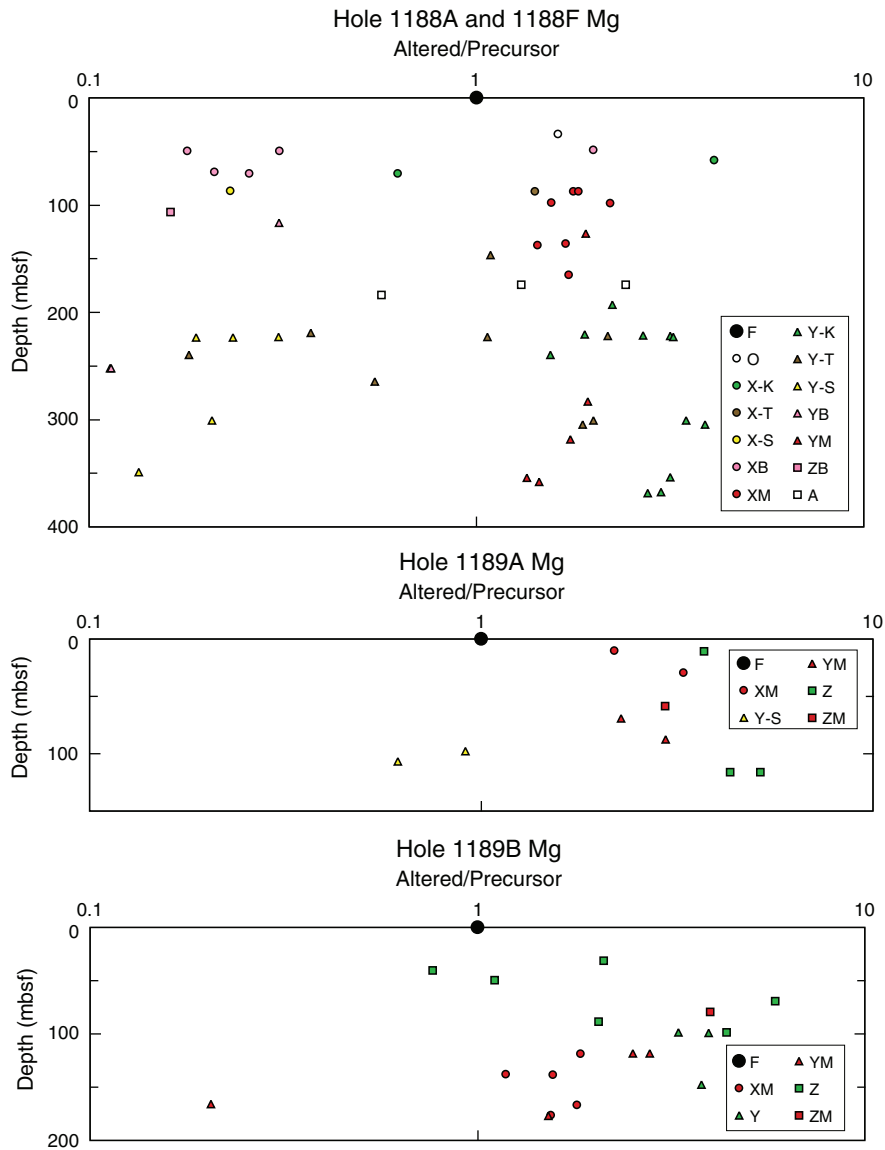


Figure AF4. Downhole profiles at Sites 1188 and 1189 for the ratio of K content in altered volcanic samples to that in their precursors (plotted logarithmically). Symbols denote petrographic categories set out in Table T1, p. 62.

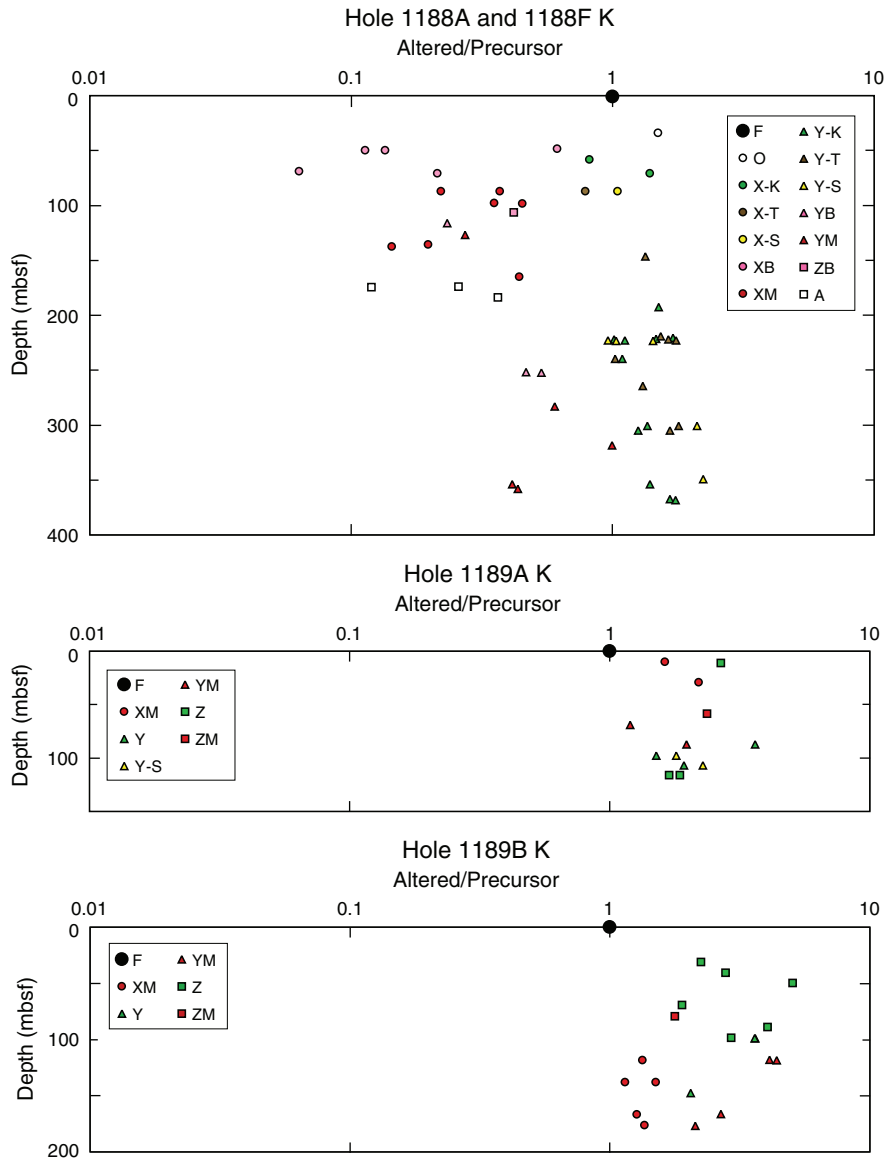


Figure AF5. Downhole profiles at Site 1188 for the ratios of (A) Cu, (B) Zn, and (C) Pb contents in altered volcanic samples to those in their precursors (plotted logarithmically). Symbols denote petrographic categories set out in Table T1, p. 62.

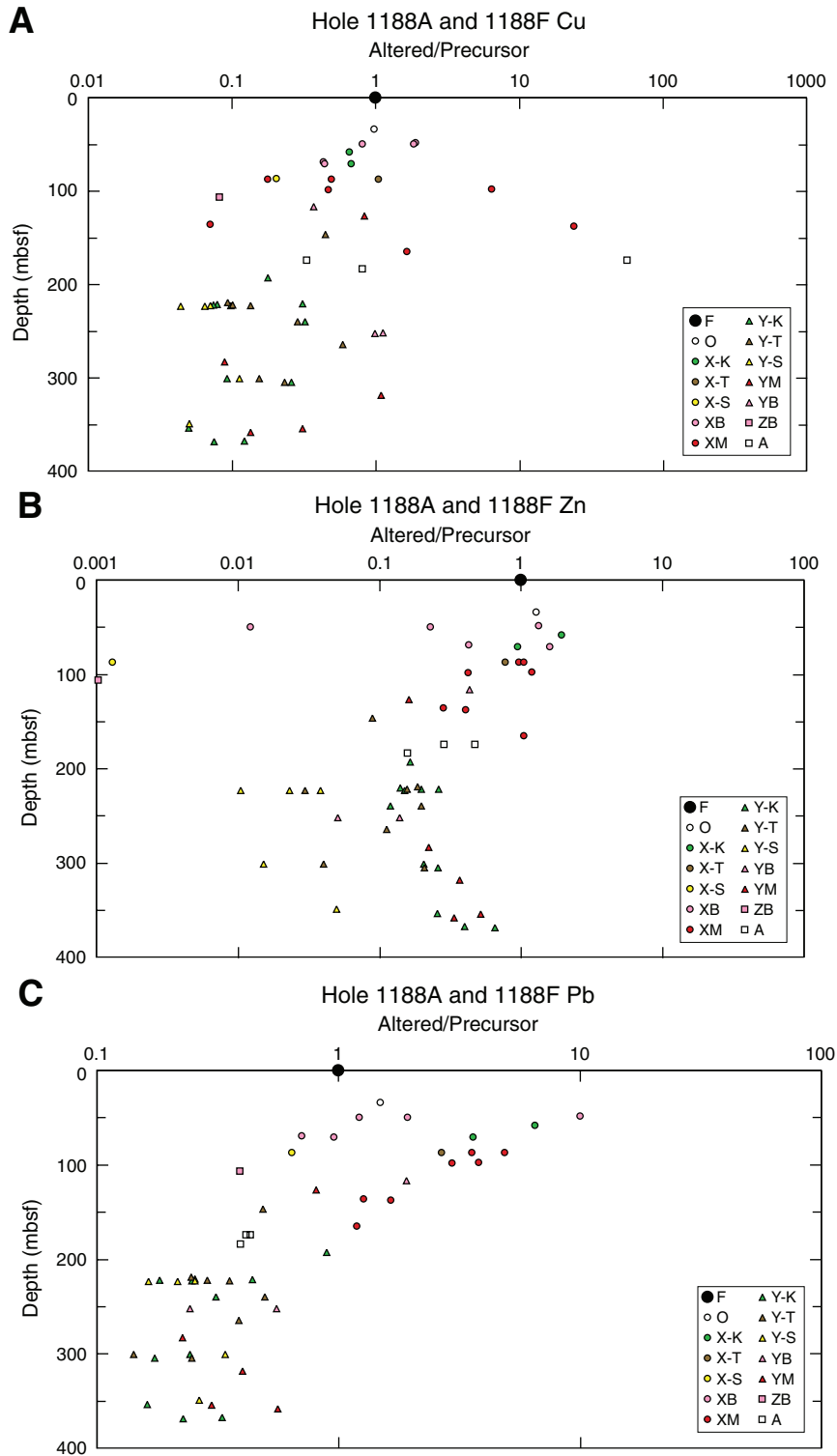


Table AT1. Algorithms for estimating precursor compositions of altered rocks, based on fractionation trends in fresh Pual Ridge lavas and the assumption of Ti and Zr immobility: $X = \text{Zr}$ (ppm)/ TiO_2 (wt%).

	Unit	Precursor composition (y)	Variance (%)
Oxide:			
SiO ₂	wt%	$y = 8.23 \ln(x) + 24.57$	1
TiO ₂	wt%	$y = 2.63 - 0.385 \ln(x)$	3
Al ₂ O ₃	wt%	$y = 20.54 - 1.23 \ln(x)$	1
FeO (total)	wt%	$y = 82.1x^{-0.557}$	5
MnO	wt%	$y = 0.75x^{-0.328}$	5
MgO	wt%	$y = 229x^{-1.031}$	24
CaO	wt%	$y = 124x^{-0.703}$	5
Na ₂ O	wt%	$y = 0.597 \ln(x) + 1.82$	3
K ₂ O	wt%	$y = 0.121x^{0.506}$	4
P ₂ O ₅	wt%	$y = 120x^{-1.30}$	11
Element:			
S (total)	wt%	$y = 10.0x^{-1.463}$	177
Li	ppm	$y = 4.64 \ln(x) - 10.9$	12
Be	ppm	$y = 0.321 \ln(x) - 0.55$	13
Sc	ppm	$y = 174x^{0.515}$	7
V	ppm	$y = (5E^{+06})x^{-2.32}$	34
Cr	ppm	$y = 7.72x^{0.047}$	148
Co	ppm	$y = 63.3 - 10.8 \ln(x)$	51
Ni	ppm	$y = 38.4x^{-0.325}$	103
Cu	ppm	$y = 275x^{-0.482}$	23
Zn	ppm	$y = 190x^{-0.167}$	5
Ga	ppm	$y = 41.5x^{-0.196}$	15
Ge	ppm	$y = 34.5 - 5.25 \ln(x)$	76
As	ppm	$y = 2.27x^{0.154}$	55
Rb	ppm	$y = 10.6 \ln(x) - 32.8$	11
Sr	ppm	$y = 2491x^{-0.420}$	3
Y	ppm	$y = 10.8x^{0.191}$	4
Zr	ppm	$y = 44.0 \ln(x) - 116$	3
Mo	ppm	$y = 0.728 \ln(x) - 2.0$	20
Ag	ppm	$y = 9.0 - 1.44 \ln(x)$	51
Cd	ppm	$y = 0.042 \ln(x) + 0.20$	44
In	ppb	$y = 71x^{0.017}$	19
Sb	ppb	$y = 1364 - 213 \ln(x)$	86
Te	ppb	$y = 4.70 \ln(x) - 8.5$	177
Cs	ppm	$y = 0.042x^{0.563}$	10
Ba	ppm	$y = 33.2x^{0.437}$	6
La	ppm	$y = 4.083 \ln(x) - 9.09$	9
Ce	ppm	$y = 8.339 \ln(x) - 16.05$	8
Pr	ppm	$y = 1.115 \ln(x) - 1.76$	11
Nd	ppm	$y = 3.66 \ln(x) - 1.77$	8
Sm	ppm	$y = 0.730 \ln(x) + 0.61$	7
Eu	ppm	$y = 0.0545 \ln(x) + 1.16$	10
Gd	ppm	$y = 0.621 \ln(x) + 1.69$	8
Tb	ppm	$y = 0.146 \ln(x) + 0.15$	12
Dy	ppm	$y = 0.745 \ln(x) + 1.59$	8
Ho	ppm	$y = 0.215 \ln(x) + 0.15$	13
Er	ppm	$y = 0.6401 \ln(x) + 0.28$	8
Tm	ppm	$y = 0.138 \ln(x) - 0.13$	13
Yb	ppm	$y = 0.889 \ln(x) - 0.84$	7
Lu	ppm	$y = 0.219 \ln(x) - 0.45$	12
Tl	ppb	$y = 24.0x^{0.447}$	22
Pb	ppm	$y = 1.14x^{0.309}$	15
Bi	ppb	$y = 21.2x^{0.260}$	90
Th	ppb	$y = 524 \ln(x) - 1448$	12
U	ppb	$y = 329 \ln(x) - 990$	12

CHAPTER NOTE

- N1. Arnold, J., Bartetzko, A., Iturrino, G., and Paulick, H., submitted. Application of logging-while-drilling data for the reconstruction of volcanic facies in a hydrothermally altered, submarine dacite lava sequence—Ocean Drilling Program Leg 193. *Mar. Geophys. Res.*